MASTERARBEIT | MASTER'S THESIS

Titel | Title

Development of a mass spectrometric technique to measure protein turnover

verfasst von | submitted by

Thomas Iellici BSc

angestrebter akademischer Grad | in partial fulfilment of the requirements for the degree of

Master of Science (MSc)

Wien | Vienna, 2025

Studienkennzahl lt. Studienblatt | Degree programme code as it appears on the student record sheet:	UA 066 862
Studienrichtung lt. Studienblatt | Degree programme as it appears on the student record sheet:	Masterstudium Chemie
Betreut von | Supervisor:	Ass.-Prof. Dr. Samuel Matthias Meier-Menches Privatdoz. BSc MSc

Contents

List of Figures

List of Tables

Abstract

The proteome-wide assessment of protein turnover can be achieved by the measurement of protein abundance levels over time. Such information can be valuable to the understanding of drug modes of action. The goal of this work was to develop a reliable method to assess the protein turnover in cells on a proteome-wide scale. The method is used to measure changes in protein degradation rates that occur upon treatment with Proteolysis targeting chimeras (PROTACs). PROTACs are heterobifunctional molecules that can specifically degrade proteins in cells and tissues. PROTACs make use of the ubiquitin proteasome system to degrade proteins, which is the main physiological degradation mechanism for proteins. Protein degradation induced by PROTACs is commonly demonstrated by means of endpoint perturbation experiments. Such experimental approaches, however, lack the ability to differentiate between the PROTAC induced share to the protein degradation and the physiological degradation over time. We hypothesized that PROTAC treatments would affect half-lives of a significant number of proteins.

Consequently, we identified a cell culture model system in a metabolic steady state, that displayed an adequate expression of proteins that were crucial for the PROTAC mode of action. Phorbol myristate acetate (PMA) differentiated HL-60 leukemia cells were selected as a steady state model system. The steady state model system allows the measurement of protein degradation without the need to account for potential confounding factors, such as non-uniform cell cycle distributions or cell cycle dependent changes in protein expression patterns. Methodical parameters, including the length of the chromatographic gradient, the database search parameters and the treatment concentrations, were adapted to the model system and optimized for a robust protein half-life determination. A 140-minute chromatographic gradient and a one-unique peptide database search strategy were employed to maximize the number of protein identifications. A timeseries-based experimental design based on the Cycloheximide chase method was successfully employed for this work, since it allowed to identify the effect of PROTAC treatments on protein half-lives. A 10 µM concentration of Cycloheximide was used to inhibit *de-novo* protein synthesis in the model system to assess the baseline protein degradation rates. The PROTAC effects on protein degradation rates were assessed in a separate experiment under inhibited protein synthesis. The decrease in protein abundance over time was then chased over the course of up to eight hours after the treatment. A proteasomal inhibition with Bortezomib was also performed in order to verify PROTAC-induced target degradation.

In this work we successfully developed an *in vitro* method that allows the assessment of proteome-wide protein degradation. It marks the first occasion where PROTAC activity was investigated by the measurement of protein degradation. The efficient degradation of literature-known target proteins was confirmed for the fully optimized ACBI2 PROTAC. The proteasomal inhibition with Bortezomib did not prevent the degradation of the reported ACBI2 PROTAC target proteins SMARCA2 and PBRM1. The experimental, gold-based metallo-PROTAC was not found to degrade the expected target protein TXNRD1. A strict protein filtering threshold over the experimental timepoints revealed that the median half-lives of proteins in the control condition (44 IDs, 15 hours) was higher than in the Cycloheximide condition (133 IDs, 11.53 hours); as well as the combined Cycloheximide, ACBI2 PROTAC treatment condition (320 IDs, 13.32 hours) and the combined Cycloheximide, gold PROTAC treatment (166 IDs, 10.54 hours). The employed setup mainly selected protein IDs with half-lives in the *sub*-20-hour range. The setup also allowed the detection of PROTAC specific effects on protein half-lives for protein IDs shared between the Cycloheximide and the combined Cycloheximide, PROTAC treatment conditions. The gold PROTAC treatment led to shorter half-lives in 78% of shared entries, whereas the ACBI2 PROTAC treatment reduced half-lives in 71% of protein IDs shared with the Cycloheximide condition. This confirms our hypothesis that PROTACs exert an effect on a much wider pool of proteins than expected. This finding represents a further step to better understand the mode of action of PROTACs.

Zusammenfassung

Die Messung der Proteinabundanz in Zellen mittels Proteomischer Techniken ermöglicht die Proteomweite Bestimmung von Protein Halbwertszeiten. Das Ziel dieser Arbeit war es, eine Methode zu entwickeln, die eine robuste und reproduzible Bestimmung von Halbwertszeiten erlaubt. Die Methode wird angewendet, um Proteom-weite Veränderungen in der Protein Abbaurate zu bestimmen, die aufgrund einer Behandlung mit Proteolysis targeting chimeras (PROTACs) auftreten. PROTACs sind heterobifunktionelle Moleküle, die sehr spezifisch Proteine in Zellen und Geweben abbauen. Dabei nutzen PROTACs das körpereigene Ubiquitin-Proteasom System aus, das generell für den Großteil des Proteinabbaus im Körper verantwortlich ist. Der durch PROTACs induzierte Protein Abbau wird meistens durch Endpunkt Perturbationsexperimente bewiesen. Diese Art von Experimenten ermöglicht es jedoch nicht, den durch die PROTAC Behandlung verursachten Anteil am Proteinabbau vom Körpereigenen Anteil zu unterscheiden. Die Grundvermutung lautet, dass PROTACs die Halbwertszeiten einer großen Anzahl von Proteinen beeinflussen.

Um die Vermutung überprüfen zu können, wurde zuerst ein Zellkultur Modellsystem in einem metabolischen Gleichgewichtszustand ausgewählt, das alle für die PROTAC Funktion notwendigen Proteine in ausreichender Abundanz exprimiert. Mit Phorbol myristat acetat (PMA) differenzierte HL-60 Leukämie Zellen wurden als Modellsystem ausgewählt. Der metabolische Gleichgewichtszustand ermöglicht die Messung des Proteinabbaus, ohne dass Faktoren wie eine nicht einheitliche Verteilung des Zellzyklus oder Zellzyklus abhängige Änderungen der Proteinexpression beachtet werden müssen. Methodische Parameter, wie die Länge des chromatographischen Gradienten, die Datenbank Suchparameter und die Behandlungskonzentrationen, wurden an das ausgewählte Modellsystem angepasst und für die Protein Halbwertszeit Bestimmung optimiert. Ein 140 Minuten langer Gradient, sowie ein auf einem einzigartigen Peptid basierten Datenbank Suchparameter wurden im Rahmen der Versuche angewendet, um die Anzahl der identifizierten Proteine zu maximieren. Ein auf Zeitreihen basierender Versuch hat es ermöglicht, den Einfluss zwei verschiedener PROTAC Behandlungen auf Protein Halbwertszeiten zu identifizieren. Im Rahmen der Zeitreihen wurde die Cycloheximid chase Methode erfolgreich angewandt, wobei gleichzeitig mit der PROTAC Behandlung eine Inhibition der Protein Neusynthese mittels einer 10 μM Cycloheximid Konzentration erfolgte. Der Abfall der Proteinabundanz nach der Behandlung wurde über acht Stunden verfolgt. Die baseline Protein Abbaurate im Modellsystem wurde in einem weiteren Experiment mit ausschließlicher Cycloheximid Behandlung ermittelt. Weiters wurde das Proteasom mit Bortezomib inhibiert, um den PROTAC induzierten Abbau von Zielproteinen zu verifizieren.

Im Rahmen dieser Arbeit wurde eine *in vitro* Methode zur Messung von Proteom-weiten Protein Halbwertszeiten erfolgreich entwickelt. Weiters wurde zum Ersten Mal die Aktivität von PROTACs mittels Messung des Protein Abbaus gemessen. Der effiziente Abbau von den, aus Literatur bekannten, SMARCA2 und PBRM1 Zielproteinen konnte für die ACBI2 PROTAC bestätigt werden. Die Inhibition des Proteasoms mittels Bortezomib hatte keinen Einfluss auf den Abbau der Zielproteine der PROTAC. Die experimentelle, Gold basierte metallo-PROTAC konnte das erwartete Zielprotein TXNRD1 nicht abbauen. Ein stringentes Filtern der experimentell nachgewiesenen Proteine hat gezeigt, dass der Median der Protein Halbwertszeiten im Kontrollzustand (44 IDs, 15 Stunden) höher war als mit Cycloheximid Behandlung (133 IDs, 11.53 Stunden). Weiters waren die Median Halbwertszeiten sowohl bei gleichzeitiger Cycloheximid, ACBI2 PROTAC Behandlung (320 IDs, 13.32 Stunden) als auch bei simultaner Cycloheximid, Gold PROTAC Behandlung (166 IDs, 10.54 Stunden) geringer als im Kontrollzustand. Das Experiment ermöglichte die Identifizierung von Proteinen mit experimentellen Halbwertszeiten unter 20 Stunden. Zudem ermöglichte das Experiment PROTAC spezifische Auswirkungen auf die Halbwertszeit von jenen Proteinen zu ermitteln, die sowohl in Cycloheximid als auch in Cycloheximid PROTAC Zuständen identifiziert wurden. Die Gold PROTAC Behandlung führte zu geringeren Halbwertszeiten bei 78% der Proteine deren Halbwertszeit in beiden Bedingungen identifiziert wurden. Die ACBI2 PROTAC Behandlung führte zu niedrigeren Halbwertszeiten in

71% der Proteine, die in beiden Bedingungen identifiziert wurden. Dies beweist, dass PROTACs einen Effekt auf einen weitaus größeren Pool an Proteinen ausüben als eigentlich erwartet. Diese Erkenntnis stellt einen weiteren wichtigen Baustein zum besseren Verständnis des Wirkmechanismus dieser Verbindungen dar.

1 Introduction

1.1 Protein turnover

Protein turnover refers to the continuous process of synthesis and degradation of proteins to keep a functional proteome over time. Proteins need to be removed from the existing protein pool because they might have been damaged over time or might only be needed for a limited amount of time. Defective protein turnover processes that lead to a disruption of protein homeostasis are associated with aging and, in more severe cases, with diseases. Protein turnover rates are very different and can range from minutes to more than 70 years in mammalians.[1–3] There are several literature-known methods to assess protein turnover and identify protein half-lives *in vitro*. The term protein turnover is not used very consistently in literature, but it is generally known as the time that is necessary to degrade and re-synthesize 50% of the protein pool inside the cell.[4] Hence, protein half-lives of single proteins are used to refer to turnover rates of the corresponding proteins.

Protein degradation can be experimentally measured over time and therefore be used to calculate protein turnover. Protein levels in cells and organisms can decrease over time *via* degradation, but also by the dilution of the protein pool by cell divisions during proliferation. The latter process can be assumed to be minor in differentiated mammalian cells.[5]

Proteins are predominately degraded *via* the ubiquitin proteasome system, whose function is briefly described in section 1.1.1. Protein degradation can, to a smaller extent, also take place in the lysosome or *via* autophagy.[6]

1.1.1 Ubiquitin- proteasome system

Protein degradation *via* the ubiquitin proteasome system is tightly regulated and involves several enzymes. The C-terminal carboxyl group of the 76 amino acid long ubiquitin is activated by an ATP hydrolysis step. The activated ubiquitin is transferred to the E1 ubiquitin activating enzyme, followed by a transfer from the E1 to the E2 ubiquitin-conjugating enzyme *via* a transthiolation reaction. An E3 ubiquitin–protein ligase then proceeds to transfer the ubiquitin to a Lysine residue of the target protein. The ubiquitylation of the Lysines is therefore classified as a post translational modification. Ubiquitin technically has seven Lysine side chains that can be used for adding further ubiquitins to the first ubiquitin. All Lysines are used to extend the ubiquitin chain. A poly-ubiquitylation on Lysine 48 primes the target protein for destruction by the 26S proteasome.[7,8] The proteasome proceeds to degrade the targeted protein to short peptides. The ubiquitin units from the poly-ubiquitin chain are then recycled for further use.[7]

1.2 Methods to assess protein turnover

The first steps that were undertaken to assess protein turnover *in vitro* heavily relied on radioactive ^{35}S labeling of Cysteine residues in pulse-chase experiments. To do so, cells were cultured in medium containing ^{35}S-Cysteine for a certain period of time (pulse), subsequently the medium was switched for medium containing the physiological ^{32}S-Cysteine. The protein degradation rate was then assessed by measurement of the ^{35}S signal over time (chase).[9] Although radiolabeling has seen the rise of several methods employing fluorescent proteins in bleach chase assays[5] or as fluorescent switches and/or fluorescent timers[10] to determine protein half-lives, it has retained its relevance in research as proven by a fairly recent protocol employing ^{3}H-Phenylalanine for protein degradation studies.[11] The main disadvantage of the mentioned methods is the fact that they require specialized environments due to the radioactivity and more generally, several antibodies to specifically detect proteins of interest on immunoblots. These methods are, however, not suitable to assess proteome-wide protein turnover rates.[9] Proteome-wide turnover assessments are theoretically possible with LC-MS/MS compatible methods such as Stable Isotope Labeling by/with Amino Acids in Cell Culture (section 1.2.1), the Cycloheximide chase assay 1.2.2 and Bioorthogonal Noncanonical Amino Acid Tagging (1.2.3).

1.2.1 Stable isotope labeling by/with amino acids in cell culture

As the name suggests Stable isotope labeling by/with amino acids in cell culture (SILAC) makes use of stable isotopes to label proteins and/or metabolites depending on the scope of the experiment. The main difference to the metabolic labeling of over-expressed proteins in e.g. *E.coli* with ^{15}N precursors, which are designed to be metabolized by specific pathways with irreversible steps in order to achieve the expected labeling,[12] proteomics approaches mainly resort to $^{13}C_6$-Lysine and $^{15}N_4$-Arginine amino acids for the incorporation into proteins.[4,9,13,14]

SILAC experiments are carried out in a pulse-chase manner. Cells are grown for a certain period of time (= pulse) in culture medium containing the isotopically labeled amino acids, but not the non-labeled ^{12}C and ^{14}N equivalents. The labeled amino acids are incorporated into newly-synthesized proteins during the pulse period. Following the pulse, the culture medium is swapped for fresh medium containing the unlabeled amino acids. Non-labeled amino acids are then incorporated into newly-synthesized proteins from that point onward, "chasing away"[4] the isotopically labeled counterpart. The cells are sampled at different timepoints following the medium change, which allows to measure both the degradation of "heavy" proteins containing the $^{13}C_6$-Lysine and $^{15}N_4$-Arginine and the synthesis of unlabeled "light" proteins.[4,13,14] The order of incubation can also be changed to a first incubation in "light" followed by "heavy" amino acids without issues in form of so-called label-swap experiments, to control for eventually occurring effects of the incorporation of "heavy" amino acids.[15] The use of $^{13}C_6$-Lysine and $^{15}N_4$-Arginine is particularly advantageous when coupled to digestion processes employing Trypsin as a protease, since it will ensure that almost every peptide resulting from the digestion contains at least one heavy-labeled amino acid.[4] This is of relevance as the isotopic envelopes of "heavy" and "light" peptides are shifted in the mass spectrum, which allows the simultaneous measurement of both species.[4,9]

SILAC is a very versatile method that allows to measure both protein synthesis and degradation rates at the same time, combined with sequential enrichment procedures it was also employed to assess the effect of post translational modifications in regard to their effect on protein turnover.[16]

1.2.2 Cycloheximide chase

Cycloheximide (figure 1) is a natural product that was first isolated from bacteria and global translation inhibitor in eukaryotes.[17,18] It has been used in several occasions to aid the measurement of protein degradation. Generally, Cycloheximide is pulsed to inhibit *de-novo* protein synthesis in cells.[19,20] Cycloheximide is reported to bind to the eukaryotic ribosome´s E-site at the same time as the deacylated tRNA is bound there. This prevents the translocation, where the ribosome would move along to the next codon, therefore inhibiting the *de-novo* synthesis of proteins. Protein abundance is then bound to decrease over time as protein degradation proceeds at a normal rate while protein synthesis is inhibited by Cycloheximide. The reduction of the protein levels are followed in the chase period by sampling the model system at several timepoints after the Cycloheximide addition. Protein half-lives of the resulting samples can be elucidated by means of immunoblots[20] and alternatively with more potent proteome-wide protein half-live assessments via LC-MS/MS.[19]

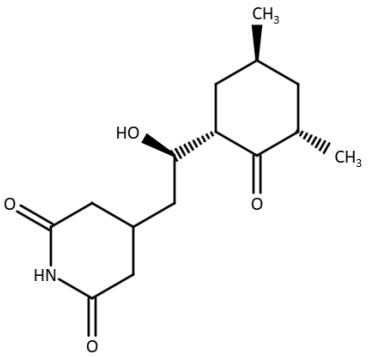

Figure 1: Chemical structure of Cycloheximide, a global translational inhibitor used to assess protein degradation in Cycloheximide chase experiments.

Cycloheximide chase experiments are straightforward to design and work especially well for proteins with short half-lives, as incubation periods beyond eight hours might induce cytotoxic effects to the model system.[9] There is a report that suggest that the Cycloheximide treatment does affect the degradation

rates of of a subset of proteins due to the activation of the serine/threonine kinase AKT, which is known to activate a downstream MDM2 E3 ligase. The half-lives of MDM2 substrate proteins might therefore be affected by the Cycloheximide treatment.[21]

1.2.3 Bioorthogonal Non-canonical Amino Acid Tagging

Bioorthogonal Non-canonical Amino Acid Tagging (BONCAT) experiments are, like the previously presented methods, based on a pulse-chase design. Methionine (l-Methionine) is replaced by an Azidohomoalanine (l-Azidohomoalanine) surrogate in the culture medium during the pulse phase.[22–24] Azidohomoalanine is then incorporated into newly synthesized proteins, the replacement of the canonical L-Methionine with the surrogate was not reported to be toxic to cell culture model systems and did not lead to increased protein synthesis and/or degradation as well as misfolding over short periods of time.[23] Azidohomoalanine was reported to be a suitable Methionine surrogate compared to other alternatives containing an azido moiety in *E.coli*.[25]

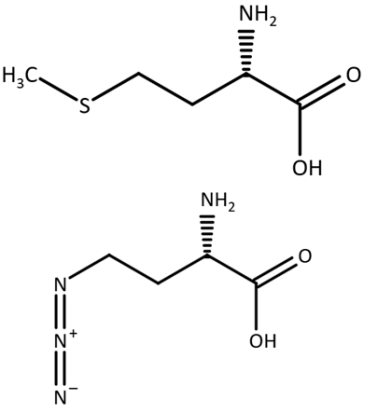

Figure 2: Chemical structures of L-Methionine (above) and its surrogate L-Azidohomoalanine (below) which is employed in BONCAT experiments.

Newly-synthesized proteins during the pulse phase contain azido moiety tags, which can be used to specifically react these proteins with alkyne modified beads alongside a copper catalyst, therefore immobilizing the proteins on the beads by means of Click chemistry.[4,23,24,26] The BONCAT affinity purification can also be combined with SILAC to get deeper insights into the proteome.[22,24] The major advantage of the affinity purification of tagged proteins is the creation of a less complex subproteome on the beads, which can aid the detection of lower abundant proteins that might not be detected in a more standard proteomics approach.[23] BONCAT is used to increase the depth of the analyzed proteome when used in combination with SILAC.[24]

1.2.4 Assumptions for protein half-life calculation

The model system employed in this work required to exhibit certain characteristics in order to allow the accurate quantification of the protein turnover. Protein turnover quantification in published literature is mainly performed using proliferating cell culture models. This makes turnover quantification complicated as myriads of proteins continuously undergo physiological synthesis and degradation processes in cell-cycle dependent manner. Hence, turnover quantification in those systems required non-linear curve fittings of experimental data and (complex) mathematical models to also account for the influence of the increasing biomass over time as such experiments are generally carried out from eight hours upwards. Oftentimes a steady state is assumed in proliferating model systems by presuming that the protein abundance remains equal during the course of the whole experiment.[13,16] A steady state condition can be achieved by differentiating cells with chemical agents or by allowing cells to fully cover the culture flask bottom area, which causes contact inhibition and thus a steady state. A cell culture model system in a steady state has the advantage that cells mainly produce housekeeping proteins and that no changes in protein expression patterns, which might occur in different cell cycle stages, are expected.

Several research papers successfully calculated protein and/or corresponding peptide half-lives assuming a first-order exponential decay over time as described in the reviews by Eldeeb et al.[9] and Toyama et al.[1]. McShane et al. analyzed protein degradation kinetics by means of BONCAT (method explained in section 1.2.3) and reported that around 50% of the detected proteins underwent exponential degradation, while 10% were classified as proteins undergoing non-exponential degradation based on the fit to their underlying model.[22] A first-order exponen-

tial decay model was therefore assumed for the proteins in the CHX chase experiments performed during this thesis. The same assumption was made by Li et al., who combined a CHX chase experiment with TMT labelling to identify short-lived proteins.[19] These experimental setups allowed a drastically simplified half-life calculation compared to SILAC-TMT experiments,[13,16] which need to account for the incorporation of labelled amino acids and amino acid recycling over the course of the experiment.

The processes of protein synthesis and degradation can be expressed by mathematical functions. The term for protein synthesis can be described with formula (1), where k_{Syn} is the synthesis rate constant for a protein and $Prot_{LFQ}$ is the measured protein LFQ value.

$$\frac{d\ (Prot_{LFQ})}{dt} = k_{Syn} \tag{1}$$

The protein degradation is hereby assumed to take place *via* a first order exponential decay during the experiment. Formula (2) is generally known from the half-life calculation of radioisotopes. k_{deg} represents the protein degradation rate. The derivation of the formula can be seen below.[4,6]

$$Prot_{LFQ}(t) = (Prot_{LFQ})_0 \cdot e^{-k_{deg}t} \tag{2}$$

Protein synthesis and degradation are assumed to be constant in a steady state condition, hence the combination of equation (1) and (2) yields (3).

$$\frac{d\ (Prot_{LFQ})}{dt} = k_{Syn} - Prot_{LFQ} \cdot k_{deg} = 0 \Longrightarrow Prot_{LFQ} = \frac{k_{Syn}}{k_{deg}} \tag{3}$$

As described in section 1.2 protein half-lives are used to refer to protein turnover rates.[4] The half-life calculation were therefore performed based on formula (4).

$$t_{\frac{1}{2}} = \frac{\ln(2)}{k_{deg}} \tag{4}$$

The actual protein half-lives in the CHX chase experiments would be calculated from the slope of a semi-ln plot occurring when plotting the ln(LFQ) values on the y-axis against the experimental timepoints on the x-axis. The slope of said plot represents k_{deg}. A semi-ln plot for an exemplary protein, as well as the half-lives for the experimental conditions calculated based on the slope, is shown on the right hand side of figure 10.

1.3 Targeted protein degradation

Targeted protein degradation strategies rely on the physiological protein degradation pathways inside the cells with the goal to specifically degrade target proteins that are tied to certain diseases and their progression.[27–29]

Targeted protein degradation (TPD) approaches can be classified into three sub-groups. One category makes use of the ubiquitin proteasome system. This group comprises, among others, the most famous TPD approach, Proteolysis-Targeting Chimeras (PROTACs). A second TPD subclass leverages protein degrdadation *via* lysosomal pathways with lysosome-targeting chimeras (LYTACs) and autophagy-targeting chimeras (AUTACs). Finally, monomeric degraders like molecular glues can also be employed to specifically degrade proteins *in vitro* and *in vivo*.[30]

Strategies like genome editing *via* e.g. small interfering RNAs or the creation of CRISPR-Cas9 knock-outs can also be used prevent or reduce the translation of disease causing proteins.[29,31]

This relatively new modality to specifically degrade proteins strongly differs from the mode of action of more commonly known small molecule inhibitor drugs. Small molecule drugs generally work by binding to catalytic or regulatory sites of the target protein, thereby inhibiting protein function. This is defined as an occupancy-driven mode of action because the small molecule

is required to bind to the active site, which is problematic if a disease causing protein does have no or too shallow binding pockets for the drug to bind, rendering the protein undruggable. PROTACs do not incur in these issues as they rely on a event-driven pharmacology that is described more in depth in section 1.4.2.[29]

1.4 Proteolysis-Targeting Chimeras (PROTACs)

PROTACs are classified as so-called heterobifunctional molecules and were first reported by Sakamoto et al. in 2001.[32]

1.4.1 Structure

PROTACs consist of three different moieties. One scaffold acts as a ligand that can bind an E3 ubiquitin ligase enzyme, whereas a second structure acts as a targeting moiety that can bind to the protein of interest (POI) that needs to be degraded. The two functional ligands are ultimately connected with each other by a linker.[31,33,34] The generalized structure of a PROTAC is illustrated in figure 3.

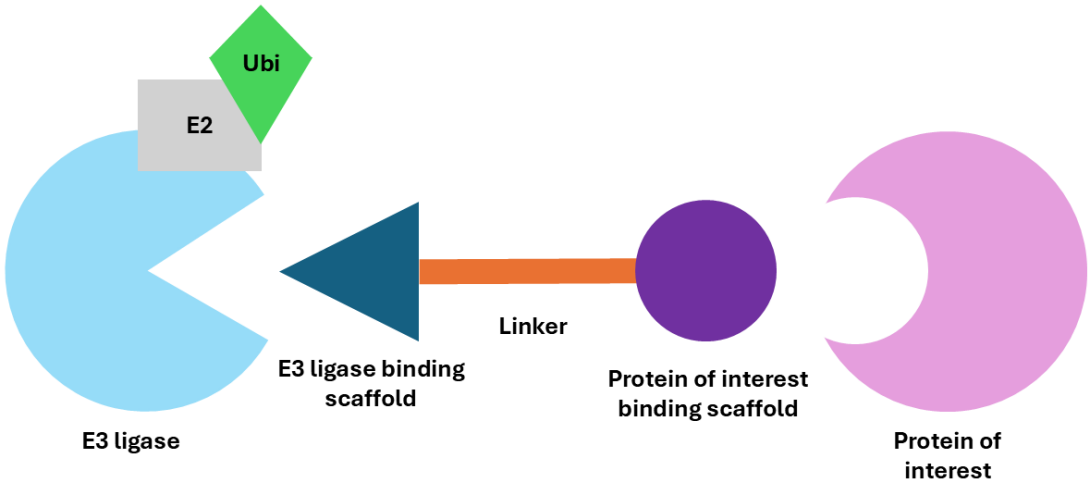

Figure 3: Illustration showing the PROTAC moieties and the targets. The E3 ligase targeting moiety is shown as a blue triangle, the E3 ligase itself is shown in light blue. The E3 ligase carries an E2 ubiquitin-conjugating enzyme with a bound Ubiquitin, which will be transferred to the protein of interest (pink) when the POI has been successfully brought in close proximity to the E3 ligase by the POI binding scaffold (purple). The linker connecting the two moieties is shown in orange.

Unsurprisingly, the effectiveness of PROTACs is influenced by all three constituents.

Oftentimes PROTACs are synthesized with scaffolds that were originally developed as a potential traditional small molecule drugs to target a certain disease causing protein then repurposed as POI targeting structures.[33] Several hundred isoforms of ubiquitin ligases are known to be present in the human proteome. Only a very small subset was reported to be targeted by published PROTAC molecules. PROTACs mainly employ MDM2, VHL and CRBN E3 ligases targeting domains as they were found able to effectively recruit E3 ligases in different cell lines, while showing a high affinity to the ligases in a wide pH and concentration range.[31,35] Achieving such properties is not easy, PROTACs targeting CRBN were reported to be quickly degraded in cell culture media,[36] researchers have therefore tried to optimize the structures of Cereblon targeting PROTACs to prevent excessive hydrolysis in media.[37] The length and the flexibility of the linker employed to connect the two functional moieties together is crucial for the PROTAC function. Linkers and their structures vary greatly as they may consist of simple alkyl or polyethylene glycol chains or more complex alkine, triazole and piperazine moieties.[31,35]

1.4.2 Mode of action

PROTACs take advantage of the ubiquitin proteasome system (section 1.1.1) to degrade the protein of interest. Briefly, the PROTAC recruits both the POI and the E3 ligase and brings them in close proximity to each other. The induced proximity between the E3 ligase and the POI trigger the former to transfer the Ubiquitin from the E2 unit to the POI. A poly-ubiquitin chain of three to four units then primes the POI for degradation by the 26S proteasome.[31,33–35] The most crucial step in the PROTAC mode of action is the formation of a ternary complex between PROTAC, POI and ligase. The sole vicinity of POI and ligase is not sufficient to trigger the ubiquitination.[33] The linker length, flexibility as well as the attachment positions to the active moieties can not only strongly influence the ternary complex formation, but also the stability and the cellular uptake of the PROTAC.[28] The E3 ligase affinity to the PROTAC strongly decreases after successful POI degradation leading to a release of the drug from the PROTAC binding site of the E3 ligase. The PROTAC is not degraded by this process and can proceed with the degradation of the next POI.[34,35]

1.4.3 Advantages of PROTACs

Because of their catalytic and irreversible mode of action PROTACs could be administered at very low concentrations. A very important advantage over traditional small molecule drugs is that the POI binding domain on the PROTAC does not require a very high affinity to the POI. The affinity needs to be sufficiently high to selectively recruit the POI from the complex protein matrix inside the cell.[31,34] It is the ternary complex formation between ligase, PROTAC and POI that provides the decisive advantage of PROTAC selectivity over traditional small molecule drugs. Only the combination of the correct POI and E3 ligase will, in a best-case scenario, be able to form the ternary complex that leads to ubiquitination of the POI. It is the very exclusive formation of the ternary complex that provides PROTACs with their selectivity.[31,34]

1.4.4 Disadvantages of PROTACs

PROTACs and their effects do not follow the classical dose-response relationship, the associated consequences are yet to be fully uncovered. High toxicities have been reported for PROTACs in clinical trials due to the effects of fully degrading a protein of interest that have scaffolding roles in cells. Long-term effects of PROTAC treatments and especially their toxicity seems to be still unclear.[33] Proteomics approaches can allow researchers to better understand the mechanisms of action, target protein specificity, as well as potential off-target effects that might come as a byproduct of the degradation of whole target proteins.[28] Proteomics can generally aid the development of PROTACs as both the E3 ligase and the protein target need to be present in an adequate abundance in the tissue and sub-cellular compartment where the degradation should take place.[28] Off-target protein degradation effects in tissues with sub-optimal protein abundances have already been reported.[33] While the ternary complex formation is of great importance for the selectivity of PROTACs, it renders predictions of whether a POI can effectively be degraded *in vitro* or *in vivo* difficult. The ternary complex formation between PROTAC, E3 ligase and POI can be kinetically slow and is difficult to model *in-silico*.[33,35] Because of the larger structure compared to more traditional small molecule drugs PROTACs are generally reported to have a low permeability which is not optimal for oral administration routes.[33]

1.4.5 ACBI2 PROTAC

The ACBI2 PROTAC was thoroughly optimized to selectively degrade SMARCA2, but not SMARCA4 by Kofink et al. (refer to section 1.5.2.a for a brief description of both proteins).[38] The PROTAC was also found to selectively degrade the PBRM1 protein (refer to section 1.5.2.b for a brief overview of the protein).[38] The compound itself was developed from ACBI1, a PROTAC predecessor which was found to degrade all three of the aforementioned proteins in cell culture experiments.[39] The PROTAC contains a VHL E3 ligase targeting moiety, highlighted by the orange box in figure 4. The scaffold designed to target SMARCA2 is highlighted by the dark blue box. ACBI2 was kindly provided by Boehringer Ingelheim *via* its open innovation platform opnMe, available at `https://www.opnme.com`.

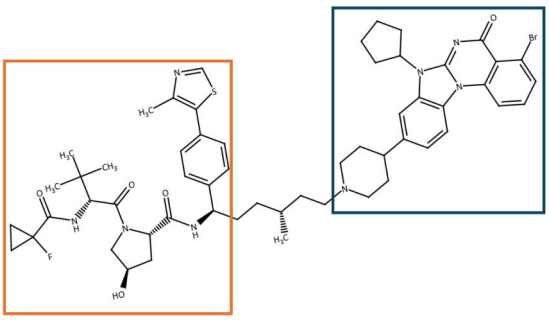

Figure 4: Chemical structure of the ACBI2 PROTAC. The structure highlighted by the orange frame is the VHL binding moiety, the SMARCA2 targeting scaffold is highlighted by the dark blue frame. Both moieties are connected by the linker.

Due to the well described effects and the optimized nature of the compound, it was used as the reference PROTAC in the experiments, whose effects on cancer cell lines have already been extensively studied and would therefore help to validate the experimental design to measure the protein turnover.

1.4.6 Gold PROTAC

The gold PROTAC employed in the experiments of this thesis was shown to specifically inhibit Thioredoxin reductase 1 (TXNRD1). A brief description of the protein is provided in section 1.5.2.c. The scaffold highlighted by the orange box in figure 5 has previously been described by Skos et al. to covalently bind to TXNRD1 in *in vitro* studies.[40] The selective TXNRD1 binding mechanism was exploited and the gold containing scaffold was used as the PROTAC warhead. The compound can therefore be classified as a covalent PROTAC. A thalidomide scaffold, highlighted by the dark blue box in figure 5, was chosen as a Cereblon E3 ligase targeting moiety for the PROTAC due to the well-known interaction between the two molecules.[41]

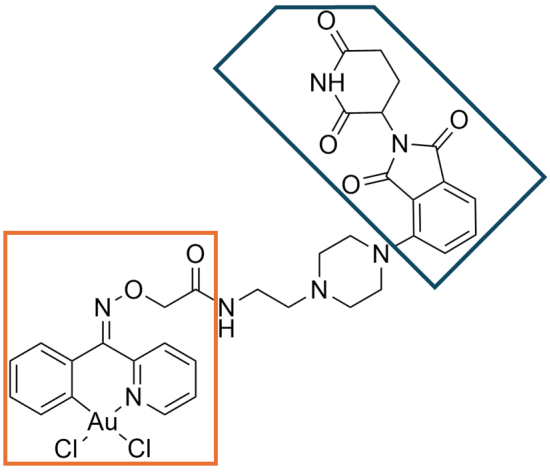

Figure 5: Chemical structure of the gold PROTAC. The structure highlighted by the orange frame is the TXNRD1 binding moiety. The CRBN targeting thalidomide scaffold is highlighted by the dark blue frame. Both moieties are connected by a piperazine containing linker.

The use of metal ions in PROTAC design is uncommon as PROTACs generally rely on fully-organic structures. The first PROTAC containing a metal center was termed metallo-PROTAC and was only reported as recent as of 2023. The platinum(II)-based PROTAC with a Cereblon ligand was reported to successfully degrade Thioredoxin 1 as well as Thioredoxin reductase 1 in a multiple myeloma cell line, which emphasizes the general applicability of metallo-PROTACs to cell culture model systems.[42]

A selective degradation of TXNRD1 *via* a PROTAC mode of action was therefore expected for the compound in figure 5 and would be tested for the first time in cell culture experiments in the context of this work. The presence of expreimentally relevant proteins at adequate expression levels and a sufficient cellular uptake are crucial for the mode of action of both PROTACs.

1.5 Experimentally relevant proteins

A panel of experimentally relevant proteins was selected, sub-categorized and ranked by importance for the experiments. The model system choice for the main experiments was guided by the presence or absence of these proteins. The presence of the two E3 ligase recruiters VHL and CRBN (section 1.5.1) was the most important criterion for the selection of the experimental model system, as the PROTACs would not be able to work without those specific proteins. The model system choice would also be determined by the presence of proteins that were reported to be specifically degraded by the PROTACs (section 1.5.2), the presence of those proteins was desired so as to be able to confirm the reported claims. The presence and the expression levels of several more proteins that were identified to be relevant for the PROTAC mode of action (section 1.5.3) were not deemed as crucial for the model system choice and therefore ranked in the less important category.

1.5.1 E3 ligases/ligase recruiters

1.5.1.a Von Hippel-Lindau disease tumor suppressor

Von Hippel-Lindau disease tumor suppressor (VHL, UniProt ID: P40337) was described to build a VBC-CUL-2 complex with Cullin-2 and elongins B and C that showed E3 ubiquitin ligase activity.[43] Cullins have the ability to bind RBX1, who is an important constituent of ubiquitin ligases as it was shown to bind E2 ligases. E2 ligases can then, if activated, transfer ubiquitin to target proteins.[43,44]

1.5.1.b Protein cereblon

Protein Cereblon (CRBN, UniProt ID: Q96SW2) was reported to be a substrate of the cullin-RING ubiquitin ligase 4 complex, which among other things consists of the RBX1, DDB1 and CUL4 proteins that are also briefly described in section 1.5.3.[45] Cereblon can interact in a 1:1 ratio with DDB1 which is part of the E3 ubiquitin ligase complex, additionally it was shown that the complex did show E3 ligase activity with CRBN bound to it, meaning that it can act as a subunit of the complex.[41] The gold PROTAC was designed with a Cereblon seeking scaffold which allows the PROTAC to recruit the E3 ligase complex and bring it to close proximity to the protein of interest.

1.5.2 PROTAC targets

1.5.2.a Probable global transcription activator SNF2L2

The ACBI2 PROTAC was found to selectively degrade the Probable global transcription activator SNF2L2 (SMARCA2, UniProt ID: P51531) while not affecting its Transcription activator BRG1 (SMARCA4, UniProt ID: P51532) paralogue.[38] Both proteins were reported to be relatively often mutated in tumors.[46] Both proteins are DNA-dependent ATPases and can both (not at the same time) be subunits of the SWI/SNF chromatin remodeling complex, where they are able to control the replication of DNA and control transcription processes.[47] A study performed by Hoffman et al. showed that the reduction of SMARCA2 levels in tumor cells reduced growth in most cells with SMARCA4 mutations. This makes SMARCA2 containing complexes a good target for therapeutic approaches that selectively degrade SMARCA2 in cancer cells with known SMARCA4 mutations.[47] Both ACBI1 and ACBI2 PROTACS were successful in exploiting the effects of a selective SMARCA2 degradation to induce apoptosis and, more generally, negatively impact the proliferation of cell lines that rely on SMARCA4 activity.[38,39]

1.5.2.b Protein polybromo-1

As the name suggests the Protein polybromo-1 encoded by the PBRM1 gene consists of six bromodomains which are responsible for the proteins ability to bind to Acetyllysine residues on histone tails.[48] It is part of the so-called PBAF chromatin-remodeling complex, which plays an important role in several processes like transcription, DNA repair and was reported to impact cell differentiation and proliferation.[48,49] PBRM1 is a crucial for the function of the whole complex because it can regulate genetic functions by influencing the interaction between DNA and histone and change the chromatin structure when needed.[49] While ACBI2 was not designed to specifically degrade PBRM1, the protein was often found to be mutated in renal tumors and can therefore be counted as a relevant protein for cancer progression.[48]

1.5.2.c Thioredoxin reductase 1, cytoplasmic

The Thioredoxin reductase 1 (TXNRD1, UniProt ID: Q16881) is an enzyme that plays an important role in the regulation of redox reactions inside cells.[50,51] TXNRD1 is mainly located in the cytoplasm, whereas the TXNRD2 isoform is mainly located in mitochondria.[51] The Selenocysteine residue present in the C-terminal end of the sequence was shown to be essential for the catalytic activity of the enzyme, which mainly consists in the reduction of the disulfide bonds in the active site of Thioredoxin (TXN) with the help of NADPH.[50,51] TXNRD is often found to be over-expressed in several human tumors making it an interesting target for anticancer treatments. The inhibition of the Selenocysteine containing enzyme active site *via* coordination of metallodrugs was shown to induce pro-apoptotic effects through the induction of oxidative stress.[40,50] The most prominent representative of TXNRD1 targeting metallodrugs is the gold(I) based Auranofin.[51] Gold(III) containing metallodrugs have also been shown to effectively inhibit TXNRD1 by employing a different mechanism.[40]

1.5.3 Other relevant proteins

Several other proteins beside the previously mentioned ones are also involved in processes that are relevant for the processes. The DNA damage-binding protein 1 (DDB1, UniProt ID: Q16531) was reported to be one constituent of (DDB1-CUL4-X-box) complexes and to therefore be involved in the ubiquitination of proteins, priming them for proteasomal degradation, upon DNA damage. DDB1 is relevant for the substrate recognition in the complex.[52,53] Both Cullin-4 isoforms can also be included in the complex. The Cullin-4A (CUL4A, UniProt ID: Q13619) and Cullin-4B (CUL4B, UniProt ID: Q13620) proteins act as scaffolds of the ligase, additionally they are relevant to the ubiquitination process because they help to correctly position the E2 ligase to the substrate protein.[41,53] A further component of the DDB1-CUL4-X-box complex is the E3 ubiquitin-protein ligase RBX1 (RBX1, UniProt ID: P62877), which is also involved in the in the correct E2 ligase positioning by interacting with CUL4.[53]

As the name suggests the multidrug resistance-associated protein 1 (ABCC1, UniProt ID: P33527) is a transmembrane protein that is involved in the expulsion of drugs from the cytoplasm. The effects are well described for chemotherapeutic agents and might also have an effect on the PROTAC treatments, which could be rendered unsuccessful in model systems with very high abundances of the protein encoded by ABCC1.[54]

1.6 Cell line panel

The panel of cell lines that came to closer consideration for the experiments was chosen based on previous reports of CRBN and VHL expression in the cells.
The SUSA cell line (figure 6a) has been established in 1977 from a human patient with malignant testicular teratoma. The epithelial cells tend to grow as small patches over time. The SUSA cell line appeared to be identical to testicular teratoma stem cells due to their morphological similarity, however no conclusive proof was found to confirm the claim.[55] The SUSA cell line is cisplatin sensitive and has since been used in cancer research to e.g. aid the understanding of

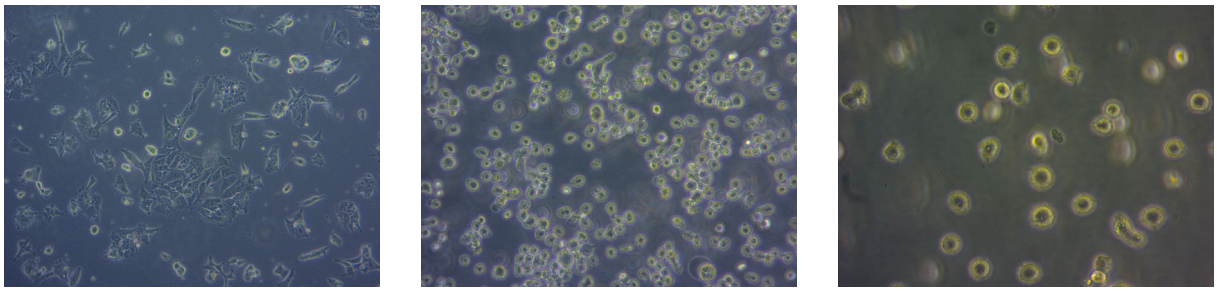

(a) SUSA cells at passage 5. 10x magnification.

(b) RPMI-8226 cells at passage 12. 10x magnification

(c) Non-differentiated HL-60 cells at passage 16. 20x magnification

Figure 6: The snapshots showing cells of the different cell lines at different passage numbers were acquired at different magnification levels.

why testis tumor cells are more sensitive to cisplatin treatment than other tumor types.[56]

The RPMI-8226 cell line (figure 6b) that was derived from the peripheral blood of a patient suffering from multiple myeloma in 1966 and was one of the first multiple myeloma cell lines to be established.[57,58] The cells are of semi-adherent nature, with a subset of the cells growing as adherent cells.

The HL-60 cell line (figure 6c) was derived from peripheral blood of an acute promyelocytic leukemia patient. It has been extensively used for research purposes since HL-60 cells, as opposed to many other leukemia cells, were able to sustain continuous growth in culture medium.[59] The cell line itself was first characterized as FAB-M3, which was later corrected to a French-American-British M2 classification as HL-60 cells showed a greater similarity to acute myeloblastic leukemia cells with granulocytic maturation.[60] HL-60 cells can be differentiated to four different types of cells of the myelomonocytic family. Differentiation of the cells can be induced *in vitro* by means of several agents, two of which were used in the context of this work. All-trans retinoic acid (ATRA) induces the differentiation to granulocytes,[59] whereas phorbol 12-myristate 13-acetate (PMA) differentiates HL-60 cells to macrophage like cells.[59,61,62] It is important to note that the differentiated HL-60 cells, regardless of the differentiating agent, do lack certain traits that their "normal" cell equivalents have.[59,61,62] Nonetheless, the cell line is often regarded as a good model system to investigate differentiation processes in leukemic cells.[59] HL-60 cells start to adhere to the culture flask as the differentiation progresses with time. Both ATRA and PMA lead to a terminal differentiation state in the HL-60 cells, which means that the cells loose their ability to proliferate,[59] hence leading to a steady state condition.

1.7 Mass spectrometry-based proteomics

Like other -omics technologies Proteomics can be broadly classified as an assay that theoretically allows the comprehensive identification and quantification of the majority of proteins within complex biological samples.[63,64] The analysis of sub-cellular protein expression, localization, protein turnover and the impact of post-translational modifications can lead to a deep understanding of biological functions and processes and how those might be impaired by disease.[63,64] The differences in protein concentration within cells spans upwards of seven orders of magnitude.[65] This very large dynamic range represents a hurdle even with modern LC-MS/MS systems which means that the proteomics, at the moment, is still far from allowing a comprehensive insight into the full proteome.[66]

1.7.1 Data dependent acquisition

Two methods of data acquisition can be used for -omics experiments employing mass spectrometers, data dependent acquisition (DDA) and data independent acquisition (DIA). In the former method the mass spectrometer acquires a full-MS1 scan in the m/z range defined by the experimenter. The spectrometer then chooses a certain number of precursor ions, generally the most intense, and proceeds to fragment those ions in the collision cell and acquires the MS2 spectra of the fragmented precursors. The number of fragmented precursor ions generally depends on the "top N" method employed, where N is the number of highest intensity precursor ions to be fragmented. Already fragmented precursors are placed on a exclusion list for a defined period of time, which ensures that not only very abundant precursors are fragmented during the analysis. A drawback of DDA methods in -omics experiments is that precursor ions with a low MS1 abundance might not be selected for fragmentation. A lack of MS2 spectra prevents the identification of the analyte precursor ions. On the opther hand, quantification relies on data from the MS1 spectrum. A more systematic data acquisition can, in principle, be achieved with DIA methods, that however come with their own challanges.[67,68]

1.7.2 Shotgun proteomics

Several approaches exist for proteomics experiments. The shotgun proteomics approach, also called bottom-up proteomics approach, is most commonly used for proteome profiling experiments and for protein turnover investigations. The workflow of such an experiment is briefly described below.

Proteomics samples from cell culture experiments are either obtained by cellular lysis with chaotrope containing buffers followed by a sample heating step or *via* sub-cellular fractionation and subsequent protein precipitation in ice-cold Ethanol. The protein amount present in each sample is then quantified, followed by a protein digestion step with a normalized protein amount. The resulting mixture of peptides then undergoes LC-MS/MS measurement. The different peptides inside the sample are then identified by matching the experimental MS2 spectra of the peptides that were generated by gas-phase fragmentation with the theoretical peptide fragmentation patterns calculated from a protein database. The identified peptides are then used to determine the proteins that were present in the samples.[63]

1.7.3 Label-free quantification

The quantification of proteins is of great interest because changes in protein abundance between two conditions, e.g. healthy vs. diseased patient or two conditions in perturbation experiments, can give a deep insight into disease associated processes or might hint to future targets in drug discovery. The importance of robust protein quantification methods in proteomics approaches is therefore undeniable. Relative protein quantification can be achieved by either spectral counting or *via* intensity.

The former method assumes that the actual abundance of the specific protein present in the sample can be correlated with the peptide spectrum-match frequency. This is because peptides "belonging" to more abundant proteins theoretically should be selected for fragmentation with a higher probability than peptides from lower abundant proteins. The relationship between the number of identified peptides and the protein amount has been successfully used for label free-quantification approaches, but has been contested because it assumes a linearity of MS response for all proteins even though different physicochemical properties of peptides are known to affect ionization efficiencies.[63,66,69]

Label free quantification *via* intensity works best with spectrometers with high mass resolution as the method relies on the calculation of the area under the curve (AUC) of peptide extracted ion chromatograms. The computational requirement of this method is higher as the employed software does need to match mass accuracy and, among others, peptide retention

times across many samples to correctly calculate the intensities of peptide ions for the calculation of protein abundance.[63,66,69] The development of a suitable normalization strategy was key to the widespread use this method sees in the majority of today's proteomics workflows. The normalization method assumes that the majority of proteins in the proteome is stable in different conditions. The "delayed normalization" developed by Cox et al. uses the stable proteome as a relative standard to define normalization coefficients for the LC-MS/MS measurement of each sample. The normalization coefficients for each run are determined by employing a Levenberg–Marquardt algorithm that minimizes the differential regulation of the stable proteome between samples.[69]

1.8 Mass spectrometry

Mass spectrometry is a technique that allows the measurement of the mass to charge (m/z) ratio of ionized analytes in a vacuum. The analytes can span a wide range of molecular weights and mass spectrometry can be used to both identify and quantify those analytes.

Analyses are carried out in a mass spectrometer which consists, among others, of three key components. An ion source, a mass analyzer and a detector. The ion source which provides the ionized analytes to be measured, an example for such an ion source would be the nano-ESI source described in section 1.8.1. The mass analyzer then proceeds to separate the ionized peptide ions based on their m/z ratios. The detector subsequently measures the m/z values of the ions that reach it over the course of the measurement.[70]

1.8.1 Nano electrospray ionisation

Proteomics nano-LC systems are coupled with nano electrospray ionisation (nano-ESI) sources, which like conventional ESI, generally yields multiply charged peptide ions and is classified as a soft ionization method. Interestingly, nano-ESI is not just a down-scaled version of ESI that can handle lower flows and allows for a better sensitivity. Nano-ESI is reported to be less susceptible to salt concentrations and to maintain a better spraying stability with high-water-percentage solvents (see solvent A in section 3.3) than ESI sources.[71]

1.8.2 timsTOF Pro™

The timsTOF Pro™ was developed by Bruker Daltonics and is a quadrupole time-of-flight device (QTOF) that provides an additional dimension of separation by means of the trapped ion mobility spectrometry (TIMS) analyzer placed after the electrodynamic ion funnels at the beginning of the ion path inside the device. The instrument schematic for the timsTOF Pro™ can be seen in figure 7.

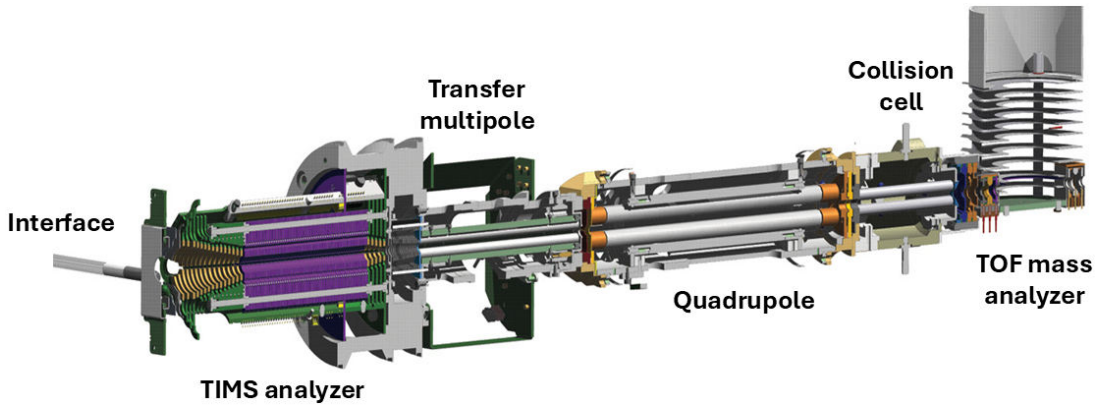

Figure 7: Instrument schematic of a timsTOF Pro QTOF mass spectrometer. The figure was adapted from Meier et al.[72]

Analyte ions are accumulated in the first section of the TIMS tube and are subsequently resolved based on their ion mobility in the second section of the TIMS analyzer before being progressively released to the quadrupole mass filter and the collision cell. The ion mobility separation in the TIMS analyzer is based on the charge of the ions and their collisional cross section. Depending on the scan mode ions reaching the collision cell are either left untouched for MS1 scans or are fragmented in the case of MS2 scans. Ions are then orthogonally diverted into the two-stage reflectron time-of-flight tube mass analyzer. TOF instruments have high scanning speeds and can therefore achieve the detection of a suitable number of peptide fragment ions for analyte identification in combination with the TIMS analyzer.[72–74]

1.9 Nano liquid chromatography

High throughput proteomics applications commonly utilize a nano liquid chromatography (nano-LC) coupled to the mass spectrometer because it significantly reduces sample complexity and can therefore aid the identification and quantification of lower abundant proteins in the samples. The most commonly employed LC stationary phases for proteomics are reversed phase (RP) silica-based C18 modified materials. Therefore, the separation is based on the interaction of the tryptic peptides, characterized by different hydrophobicities, with the reversed phase material and the hydrophilic mobile phase.[75,76] A C18 RP pre/trap column with bigger inner diameter and particle size than the actual analytical column is generally used in nano-LC setups for proteomics approaches to increase chromatographic resolution. Samples are first loaded on the pre-column at a high flow rate e.g. 10 $\mu L \cdot min^{-1}$ for the pre-column loading step vs. 300 $nL \cdot min^{-1}$ for the separation on the analytical column. This allows to load a bigger sample volume in a considerably lower amount of time. The hydrophobic peptides undergo a pre-concentration on the column because of their affinity to the C18 material, while salts and other hydrophilic components are flushed to waste. The peptides are then back-flushed onto the analytical column for the actual separation.[76,77] This setup allows for high-sensitivity measurements.[75–77]

2 Aims and objectives of this work

The main goal of this work is to establish a method that allows the measurement of protein turnover in a robust and reproducible way on a proteome-wide scale in order to better understand the PROTAC specificity and mode of action.

Protein turnover *per se* is a topic which is not new to the scientific community as showed the literature research for this project. The methods used to assess and measure turnover of proteins were oftentimes coupled with assays which are more likely to be assigned to the molecular biology community e.g. photo bleaching or fluorescent dye based assays as well as the use of immunoblotting.[9] While conceptually very interesting and sound methods, the aforementioned methods have the main disadvantage that they are generally limited to a small number of proteins whose turnover can be measured in the experiments. Turnover measurement methods suited for coupling with LC-MS/MS lend themselves as an option to analyze changes on the protein level allowing a deeper, proteome-wide insight of treatment effects.

Literature research was performed to find a method to assess protein turnover by means of a LC-MS/MS technique accessible by the available instrumental setup. A selection of suitable LC-MS/MS techniques that came into closer consideration for protein turnover assessment in this project were the Cycloheximide chase assay, BONCAT and SILAC, the latter possibly coupled with tandem mass tags. The method development itself comprised the selection of a suitable LC gradient length as well as the selection of the optimal database search parameters. Data processing would be performed in Python because of it´s ease of use and the ability to quickly test and adapt different filtering strategies to only account for robust protein half-life regulations. The LC-MS method parameters needed to be optimized before performing the actual protein turnover experiment(s) in order to be confident to detect relevant proteins in a robust manner.

Both the Cycloheximide chase assay and BONCAT were chosen for the experiments after careful literature analysis. The former because of the accessibility of Cycloheximide, the ease of use and the very low number of additional experimental steps, the latter because it allows the covalent immobilization of proteins containing Azidohomoalanine. This allows very strong washing steps leading to a less complex matrix during digestion, as well as increases the chance of binding and detection of lower abundant proteins due to the on-bead enrichment step. SILAC was not taken into further consideration because of the need of expensive isotopic labelling reagents and the loss of one SILAC channel upon Cycloheximide treatment of the cells, which was strictly necessary in order to inhibit *de-novo* protein synthesis.

The general assumption for the underlying work is that PROTACs may affect the half-lives of more than just a few proteins.

Figure 8 shows a graphical summary of the starting considerations of the project.

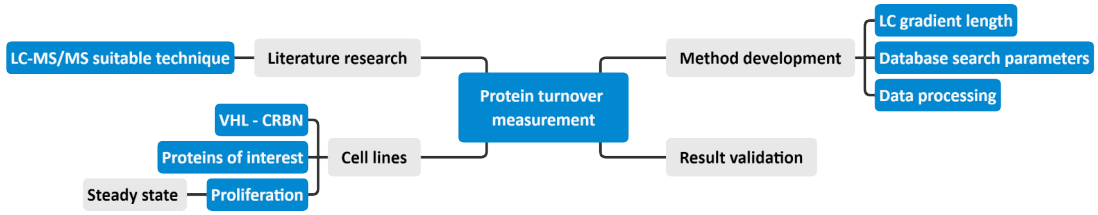

Figure 8: Graphical overview showcasing the necessary considerations and steps to be taken in this project. This figure was created using XMind.

The cancer cell line(s) used for the experiment needed to be carefully chosen as the expression of either the VHL or CRBN proteins is absolutely necessary for the mode of action the employed PROTACs. The presence or absence of certain other proteins of interest was important to a

smaller degree. Proteins of interest encompassed proteins that were known to literature to get degraded by the PROTAC and proteins that might aid the removal of the PROTAC from the cell, whose presence was unwanted. The proliferation state of the cells was also an important factor that needed consideration. Forcing the cancer cells into a steady state condition was assumed to reduce the number of proteins affected by the PROTAC and would simplify the data analysis. An additional advantage of a steady-state model system is that the PROTAC effects can be analyzed separate from the anabolism and the increase of biomass over the course of the experiment. Moreover, cells are not undergoing cell cycle changes in a steady state condition. Hence, no changes in cellular functionality are expected over the course of the experiment, which would go hand in hand with changes in protein expression patterns. The main problem of anabolism in protein turnover analysis is the non-uniformity of the cell cycle distribution in the large number of cells during the experiments. Proliferation would therefore be tracked by means of a Cellwatcher module to demonstrate a steady state in the selected model system.

Method development would be performed with a cell lysate that was additionally separated on a 1D SDS PAGE gel, as this allows for a pre-fractionation of proteins and a deeper insight into the cellular proteome. The pre-separation of the proteins on the gel is advantageous for protein detection, especially of less abundant proteins, as only a subset of the total proteins is competing for detection in the mass spectrometer. Both LC gradient lengths of 85 minutes and 140 minutes were compared by employing both gradients for the separation of the same samples. Key performance parameters for the gradient length selection were the number of protein detections as well as the detection of VHL-CRBN and the experimentally relevant proteins needed for the assembly of the protein of interest-PROTAC-E3 ligase complex.

Several candidate cell lines came to closer consideration for the project as available literature reported the expression of VHL and CRBN. SUSA, RPMI-8226 and the HL-60 cell lines underwent sub-cellular fractionation and the proteomes of the Cytoplasmic and Nuclear fraction were acquired using the previously optimized LC gradient length. The MaxQuant database search parameters would then be optimized on the dataset resulting from the proteome profiling experiments. Once a cell line was selected based on the presence of experimentally relevant proteins, compounds were tested for cytotoxicity and the treatment concentrations optimized to ensure sufficient responses in the employed model system. The experimental parameters like differentiation conditions and CHX concentrations would then be gradually optimized before performing the final experiment.

The decision tree that led to the design of the finalized experiment performed to assess protein half-lives is shown in figure 9.

The finalized CHX chase experiment would be designed in such a way as to differentiate between the proportion of the cells own share to natural protein degradation and the PROTAC contribution. More classic perturbation based proteomics approaches with an active and the corresponding inactive compound would not be able to differentiate between physiological protein degradation and the PROTAC effect on said degradation.

Once the effects of the different treatment concentrations on the selected cell line were understood, the main experiment was designed as a time-resolved experiment to follow protein degradation over time.

A separate value would be calculated for each protein at every given timepoint, the protein fraction remaining (PFR). LFQ values of all experimental timepoints would be normalized to the t_{0h} LFQ value of each protein, the resulting number was then multiplied by 100 to be expressed in percent. The PFR allows the assessment of time resolved protein abundance changes on a common scale for all proteins. The protein half-lives in the different experimental conditions will then be calculated based on a linear fit from a semi-ln plot. Time resolved experimental

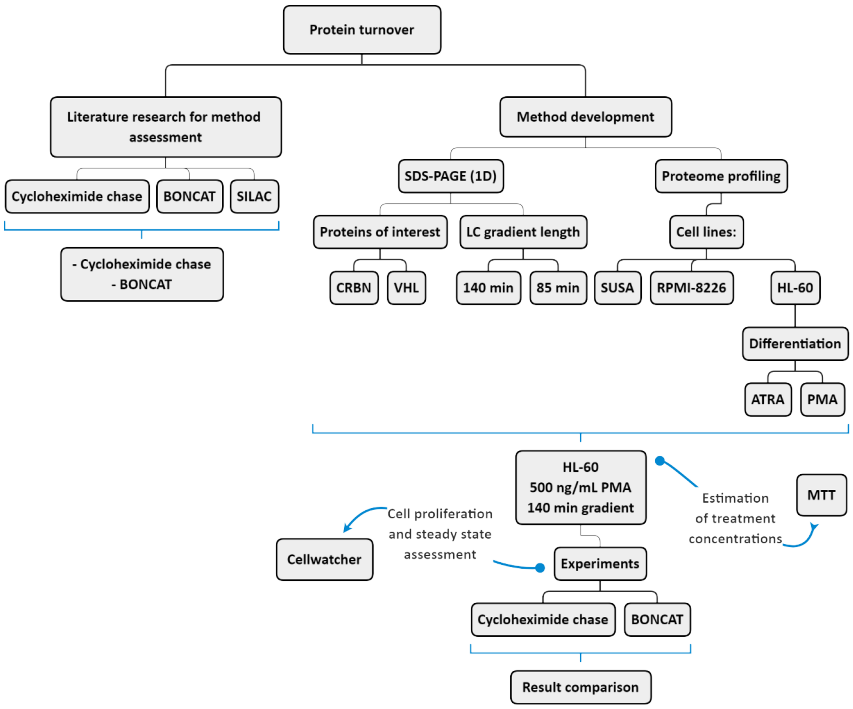

Figure 9: Overview showing the steps leading to the finalized experimental design for the project. This figure was created using XMind.

data would then be analyzed in a manner shown for an exemplary protein in figure 10.

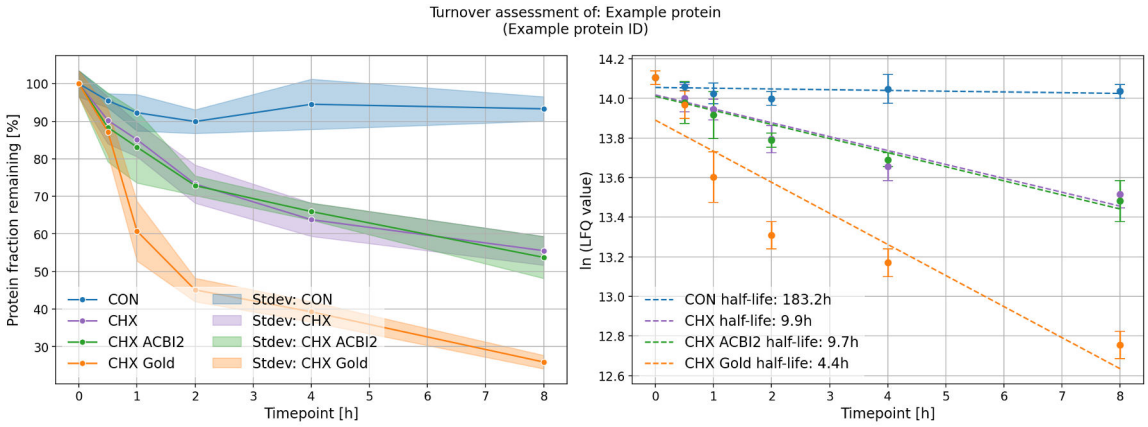

Figure 10: Time resolved protein abundance data for an exemplary protein is shown in the left hand side plot by employing the protein fraction remaining factor calculated from LFQ data. Different experimental conditions are highlighted with different colors. The right hand side plot shows the protein half-life calculation *via* a linear fit through experimental data.

As can be seen from figure 10 the final experiment consisted of four conditions. A Cycloheximide condition (CHX) timeseries and further three timeseries which would be worked-up in parallel. An untreated, solvent-matched, control timeseries (CON) and two timeseries where the ACBI2 and gold PROTACs will be added in addition to CHX.

The main expectation from these experiments is that the protein fraction remaining over time would practically be stable in the control condition (blue time course in figure 10) as protein synthesis and degradation should be in equilibrium in a steady state model system.

This changes for the other conditions, the PFR should decrease over time in the CHX and

CHX + PROTAC conditions due to the *de-novo* protein synthesis inhibition. The PFR value should decrease at a higher rate in CHX + PROTAC conditions of proteins affected by PROTAC degradation, which would also show itself in a lower half-life in the affected condition. Figure 10 shows two exemplary time courses of a protein in the different treatment conditions.

As would be expected both the CHX and CHX + PROTAC conditions show decreasing PFR values over time. The CHX + gold PROTAC condition in orange shows a significantly faster degradation than the other conditions which would indicate that the gold PROTAC exerts an effect on the exemplary protein. This would not be the case for the ACBI2 PROTAC as the PFR time course practically overlaps to the one of the CHX condition. These observation can also be made in the fitted half-lives.

In summary, we expect the investigations of protein degradation in a steady state cell culture model system to give deeper insight into specific system-wide effects of protein turnover rates upon PROTAC treatment that are independent of cell-cycle associated phenomena.

3 Materials and methods

3.1 Cell culture

Three different cancer cell lines were used for the proteomic profiling experiments. Both the testicular teratoma cell line SUSA and the multiple myeloma cell line RPMI-8226 were purchased from the American Type Culture Collection (ATCC). The acute myeloid leukemia cell line HL-60 (AML FAB-M2) was provided by M. Jakupec from the Faculty of Inorganic Chemistry of the University of Vienna, Austria. The adherent SUSA cells were cultured in RPMI-1640 medium with L-glutamine and sodium bicarbonate (Gibco) supplemented with qualified heat-inactivated 20% fetal bovine serum (FBS, Gibco) and 1% Penicillin-Streptomycin (P-S, 10000 units penicillin and 10 $mg \cdot mL^{-1}$ streptomycin, 0.1 µm filtered, Sigma-Aldrich) in standard T75 flasks with ventilated caps (SARSTEDT AG & Co. KG). Both the HL-60 suspension and semi-adherent RPMI-8226 cells were cultured in RPMI-1640 medium with sodium bicarbonate (Gibco) containing 10% qualified heat-inactivated FBS (Gibco) and 1% P-S (Sigma-Aldrich). HL-60 cells were cultured in suspension T75 flasks with ventilated caps (SARSTEDT AG & Co. KG) while standard T75 flasks were used with RPMI-8226 cells due to their semi-adherent nature. HL-60 cells used in the BONCAT experiment were cultured in methionine deficient RPMI-1640 medium (Gibco) supplemented with 10% FBS, 1% P-S and 59.86 µM L-Azidohomoalanine hydrochloride (Cayman Chemical). All cell-culture procedures were performed inside HERASAFE KS laminar flow cabinets (Thermo Fisher Scientific), cells were grown inside HERACELL 150i CO_2 incubators (Thermo Fisher Scientific) at 37 °C in a humidified environment with 5% CO_2 and 95% air.

3.1.1 General procedures

Cells were generally subcultured when reaching a confluency of around 90% inside the culture flask, confluency was checked every two days with a Primo Vert microscope equipped with an AxioCam ERc5s camera controlled *via* Zen 2011 (blue edition v.1.0.0.0) software (all ZEISS AG) from a desktop computer.

Suspension cells were transferred from the respective culture flasks to 15 mL polypropylene tubes (Falcon, Corning) for both subculturing and medium change procedures. The cell suspension was then centrifuged in a Megafuge16 R centrifuge (Thermo Fisher Scientific) at 1100 rpm, 23 °C for five minutes to pellet the cells. The supernatant containing the spent medium was discarded and the cell pellet resuspended in a small volume of fresh medium, generally one to two milliliters. A certain ratio of the resulting cell suspension was transferred back to the flask with fresh medium when a subculturing step was performed, the suspension was transferred back to the flask as a whole in case of a medium change.

The medium change procedure for adherent cells consisted of removing the spent culture medium and replacing it with fresh medium. The subculturing workflow for adherent cells involved additional steps, namely the removal of the spent medium prior to a careful washing step of the bottom of the flask with three milliliters of phosphate-buffered saline (PBS, composition specified in table 1). Two milliliters of 0.25% Trypsin-EDTA solution (Sigma-Aldrich) were added to the flask upon PBS removal. The flask was then incubated for approximately five minutes in the incubator until the cells were found to be quantitatively detached. A volume of 8 mL of fresh medium was then added to the resulting cell suspension, which was subsequently transferred to a 15 mL Falcon tube. The following steps for subculturing the cells were the same as described for suspension cells in the previous paragraph.

Cell counting was generally performed by mixing 50 µL of the resuspended cell pellet with 50 µL of 0.4% Trypan Blue solution (Sigma-Aldrich), 10 µL of the resulting solution were then pipetted on the clean sample slide of a Brightfield Cell Counter (DeNovix CellDrop BF). Separate methods were created on the device for each cell line, accounting for the different diameters,

Table 1: Composition of the PBS buffer pH=7.4

Compound	Concentration [mM]
NaCl	137
KCl	2.7
Na_2HPO_4	10
KH_2PO_4	1.8
Water	-

dilution factors as well as cell roundness. Exposure and focus pane of the device were checked prior to each cell count and adapted when necessary.

Several stock solutions of the compounds used throughout the experiments were prepared in DMSO. A 36.44 mM Bortezomib ($\geq$ 99.8%, Merck KGaA) stock solution was prepared in DMSO, as well as the 11.02 mM stock solution of a gold PROTAC synthesized by Lukas Skos. ACBI2 PROTAC, the corresponding negative control cisACBI2 as well as BI-3663 and its negative control BI-4206 were all ordered from the Boehringer Ingelheim opnMe plattform[78] and dissolved in DMSO. ACBI2 and cisACBI2 stocks were prepared at a 20 mM concentration, while BI-3663 and BI-4206 stocks respectively had a 10.66 mM and 9.42 mM concentration. A 42.60 mM stock of ±-Thalidomide ($\geq$ 98%, Sigma-Aldrich) was also prepared in DMSO. Additionally small-volume aliquots of a previously prepared 1 mg·mL^{-1} Phorbol 12-myristate 13-acetate (PMA, $\geq$ 99%, Sigma-Aldrch) were used in the experiments. An all-trans retinoic acid (ATRA, 97%, Thermo Fisher Scientific) stock with a 5 mM concentration was prepared in absolute ethanol (EtOH abs., $\geq$ 99.8%, Fisher Scientific). A 59.71 mM Cycloheximide (Merck KGaA) solution was also prepared in EtOH abs..

3.1.2 Preliminary HL-60 cell line differentiation experiments

Several experiments were performed in sixwell plates (SARSTEDT AG & Co. KG) with the HL-60 cell line to optimize the differentiation conditions for the experiments. The workflow was equal for all the differentiation experiments, 500,000 HL-60 cells in 2 mL of fresh culture medium supplied with the differentiating agent were seeded in the wells of the sixwell plates. Differentiation experiments were performed in twice, with cells at two different passage numbers, in triplicates with 0.1 µM ATRA, 1 µM ATRA, 100 ng·mL^{-1} PMA and 500 ng·mL^{-1} PMA. Differentiation efficacy was visually checked under the microscope by assessing the number of cells sticking to the well floor after supernantant removal and PBS washing.

3.1.3 MTT cytotoxicity assays

The colorimetric MTT (3-(4,5-dimethylthiazol-2-yl)-2,5-diphenyltetrazolium bromide; $\geq$ 97.5 %, Sigma-Aldrich) assay was employed to assess cancer cell viability after treatment with several dilutions of different compounds.[79] The assays were carried out in standard 96-wellplates (SARSTEDT AG & Co. KG) by pipetting 100 µL of water in the outermost wells. The equal volume of medium was transferred to six wells used as blank, while the rest of the wells was filled with 100 µL culture medium containing 10,000 HL-60 cells per well. All assays were performed in medium containing 100 ng·mL^{-1} of PMA, the plates were then incubated for 72h to allow the differentiation of HL-60 cells before the treatment. Six replicates for each concentration of the compound of interest were added to the wells in 100 µL of culture medium as treatment. The six blank and control replicates contained the equal amount of DMSO and/or Ethanol as the highest concentrated treatment wells without the compound. The plates were placed in the incubator for further 24h, subsequently 20 µL of a 5 mg·mL^{-1} MTT solution in PBS was added to every well. The plates were again placed in the incubator for 4h. The solution in the wells was

then quantitatively removed before the addition of 50 µL of DMSO in each well to dissolve the formazan crystals. The crystals arise due to the reduction of the water soluble tetrazolium dye to the insoluble formazan form by enzymes of the endoplasmic reticulum in living cells.[80] Each well´s extinction was measured at 570 nm in a Multiskan GO photometric plate reader controlled *via* SkanIt Software (v.3.2.0.35 Research Edition, both Thermo Fisher Scientific) from a desktop computer. The raw data was further processed in Microsoft Excel. Briefly, the averaged blank readout was subtracted from all extinctions, the average extinction of the control wells was then used to normalize the remaining results to the untreated cells giving the cell viability. The calculated viabilities were then transferred to GraphPad Prism version 6.07, where a non-linear fit over the data was performed by employing the "log(inhibitor) vs normalized response - Variable slope" setting.

MTT viability assays were performed on HL-60 cells differentiated with 100 ng $\cdot$ ml^{-1} PMA, with Cycloheximide concentrations between 0.0001 and 100 µM and with Bortezomib in a range between 0.001 to 100 nM. Cell-viability effects of ACBI2, cis-ACBI2 as well as gold PROTAC were tested with concentrations ranging from 0.005 up to 50,000 nM with a 42 nM CHX background concentration. The cytotoxicity of ACBI2 and Gold PROTACs was additionally tested in a combination treatment of 42 nM CHX and 1 nM Bortezomib in the same concentration ranges.

3.1.4 Cell line proteomic profiling

Proteomic profiling experiments were performed with the SUSA, RPMI-8226, non-differentiated HL-60 cells, as well as HL-60 cells differentiated with both 1 µM ATRA and 100 ng·mL^{-1} PMA. Six replicates of each of the mentioned cell lines and conditions were prepared by counting $2 \cdot 10^6$ of the respective cells. All cells besides the non-differentiated HL-60 cells, which were counted and worked up directly, were transferred into separate standard T25 culture flasks (SARSTEDT AG & Co. KG) in 5 mL medium for the profiling experiments. SUSA and RPMI-8226 cells were left to adhere to the flask for 24 hours in the incubator before the workup, while ATRA and PMA differentiated cells were incubated for 72 hours as shown in the exemplary workflow for PMA differentiated cells in figure 11. Due to the semi-adherent nature of RPMI-8226 cells, suspension RPMI-8226 cells and their adherent counterpart were fractionated and therefore also worked up separately. The work-up procedures for adherent and suspension cells are described in detail in section 3.2.2.

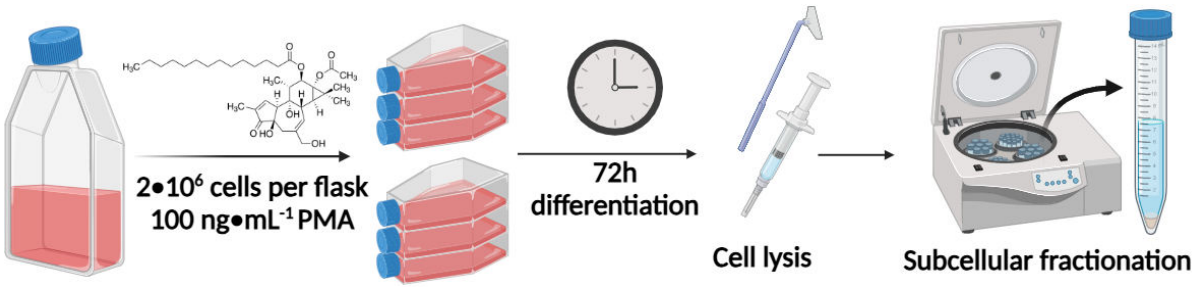

Figure 11: Overview of the subcellular fractionation workflow employed for separating the cytoplasmatic fraction from the nuclear fraction after cell lysis. The process shown in the figure shows the undertaken steps to differentiate $2 \cdot 10^6$ suspension HL-60 cells in 100 ng $\cdot$ mL^{-1} PMA containing medium over the course of 72h, followed by cell lysis and the subcellular fractionation. The same experiments were carried out using 1 µM ATRA. As described in this section, the exact workflow differed depending on the profiled cell line. Created in `https://BioRender.com`.

3.1.5 Preliminary timeseries experiment

The experiment was carried out in sixwell plates, 500,000 HL-60 cells were seeded in 1.8 mL of culture medium containing 100 ng·mL^{-1} PMA and incubated for 72 hours. Several plates were prepared and worked-up at different timepoints after treatment. The sampling timepoints were t_{0h}, t_{2h}, t_{4h}, $t_{7.5h}$, t_{24h}. Besides the t_{0h} plate, which solely consisted of a duplicate of solvent control wells. All other plates were made-up of 10 nM Cycloheximide treated wells in duplicate and a further duplicate of wells co-treated with 10 nM Cycloheximide and 100 nM ACBI2 beside the solvent control wells. The stated concentrations refer to the final compound concentration inside the sixwell. Both treatments and controls were added to the wells in 200 µL of culture medium after the incubation period.

3.1.6 Proteasomal inhibition with Bortezomib

One sixwell was prepared by seeding 500,000 HL-60 cells in 1.6 mL medium containing a 100 ng·mL^{-1} PMA concentration, followed by a 72h incubation. 200 µL of medium containing Bortezomib was added to the well volume to achieve a final concentration of 25 nM Bortezomib inside the well. The DMSO content of the Bortezomib treatment wells was matched by addition of the equal DMSO amount to the triplicate control wells. The plate was subsequently incubated for 2 hours before the addition of further 200 µL medium containing ACBI2 to achieve a final ACBI2 concentration inside the treatment wells of 1 nM. Again, DMSO content for he treatment wells was matched in the control wells. The plate was then incubated for further 4 hours before being worked up.

3.1.7 Optimization of Cycloheximide treatment concentrations

Further Cycloheximide concentrations were tested to optimize the *de-novo* protein synthesis inhibition for further experiments. The experiments were carried-out in triplicates. Cells were treated for 24 hours by adding 200 µL of Cycloheximide containing medium to achieve final in-well concentrations of 40 nM, 200 nM and 1 µM Cycloheximide. Control wells were "treated" with 200 µL of culture medium containing DMSO and EtOH abs. percentages of the corresponding treatments. The treatments were preceded by a 72 hour incubation of 0.5e^6 HL-60 cells in 1.8 mL of culture medium containing 100 ng·mL^{-1} PMA. Additionally, a treatment was performed over the course of 24 hours with a 10 µM Cycloheximide concentration on cells differentiated with 500 ng·mL^{-1} PMA. The triplicate solvent control cells were prepared correspondingly.

3.1.8 Finalized experimental design

The finalized experimental design is shown in figure 12. Briefly, HL-60 cells were counted and seeded in sixwells at a density of $0.5 \cdot 10^6$ cells per well in 1.8 mL fresh culture medium containing 500 ng $\cdot$ mL^{-1} and differentiated over the course of 72 hours. Cells were then treated with 200 µL fresh culture medium containing 10 µM CHX ("CHX" condition), 10 µM CHX and 1 nM ACBI2 PROTAC ("CHX + ACBI2 PROTAC" condition), 10 µM CHX and 60 µM gold PROTAC ("CHX + Gold PROTAC" condition) in triplicates. The control cells ("Control" condition) were treated with the corresponding DMSO and EtOH amounts as solvent control. Cells were worked-up after 0.5, 1, 2, 4 and 8 hours to allow a time-resolved analysis of the treatment effects. Control cells were additionally harvested directly at the beginning of the experiment (t_0 timepoint). An additional experiment was conducted in parallel by performing a four hour incubation with 25 nM Bortezomib, followed by the addition of 100 nM ACBI2 and a second four hour incubation step. All the conditions were worked-up in form of whole-cell lysates and subjected to in-solution digestion of the proteins.

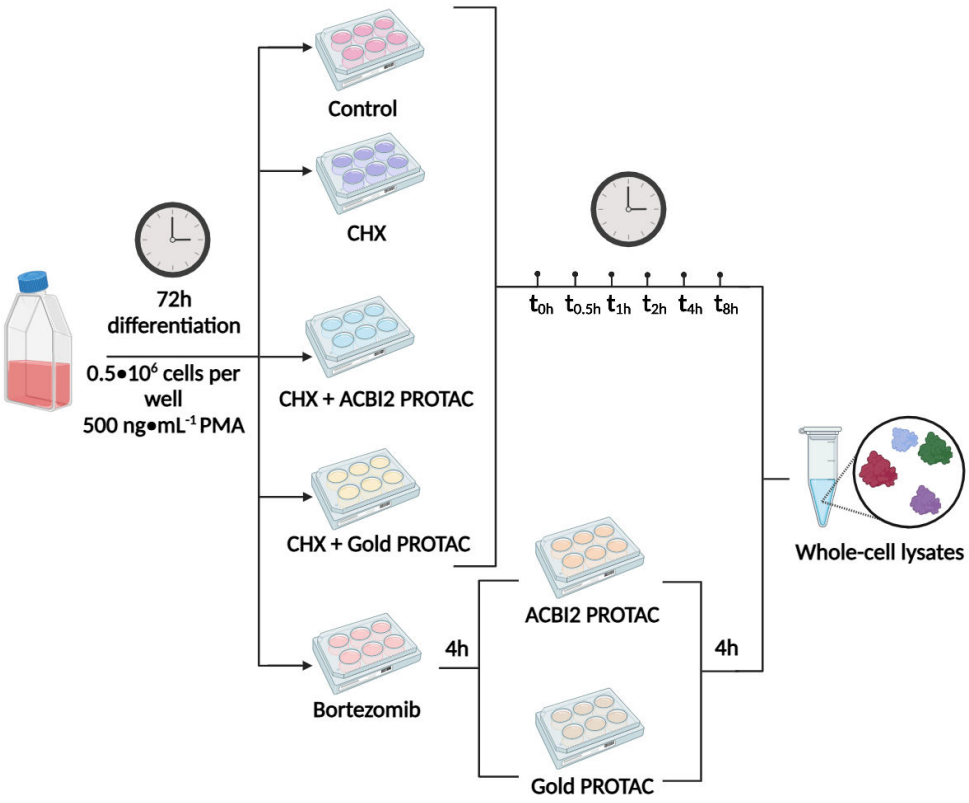

Figure 12: Graphical overview of the finalized experimental design employed to assess changes in protein turnover upon PROTAC treatment in PMA differentiated HL-60 cells. Created in `https://BioRender.com`.

3.1.9 Cell proliferation assessment *via* Cellwatcher

The effects of the PMA differentiation and the ACBI2 and Gold PROTAC treatments on HL-60 cell proliferation were continuously assessed by means of a Cellwatcher M (PHIO scientific GmbH). One sixwell plate was prepared by seeding HL-60 cells at a density of $0.5 \cdot 10^6$ cells per well in 1.8 mL medium containing 500 ng $\cdot$ mL^{-1} PMA. The sixwell plate was placed in the Cellwatcher module, where differentiation was allowed to proceed for 72 hours. The Cellwatcher assay was paused after 72 hours and the cells treated in duplicates to achieve final in-well concentrations of 10 µM CHX and 1 nM ACBI2 PROTAC, 10 µM CHX and 60 µM gold PROTAC as well as the corresponding solvent control condition. The treatments correspond to the treatments employed for the timeseries experiment described in section 3.1.8. The plate was returned to the Cellwatcher module before the assay was resumed. The plate was incubated for further 24 hours to assess whether the treatment would affect cellular proliferation.

A further experiment was performed to evaluate whether the L-Azidohomoalanine containing medium had an impact on HL-60 cell proliferation in the timeframe relevant for the BONCAT experiment. Three replicates of HL-60 cells were seeded at a density of $1 \cdot 10^6$ cells per well in 2 mL of standard RPMI-1640 medium containing 500 ng $\cdot$ mL^{-1} PMA. Further three replicates were seeded in the same manner in BONCAT RPMI-1640 medium on one sixwell plate, which was subsequently placed in the Cellwatcher module. Differentiation was then allowed to proceed for 72 hours inside the humidified incubator.

3.1.10 BONCAT experimental design

A brief graphical overview of the employed experimental design can be seen in figure 13. HL-60 cells were counted and the cell suspension containing $2 \cdot 10^6$ cells per replicate was separately centrifuged in 25 mL Falcon tubes at standard settings to pellet the cells and quantitatively

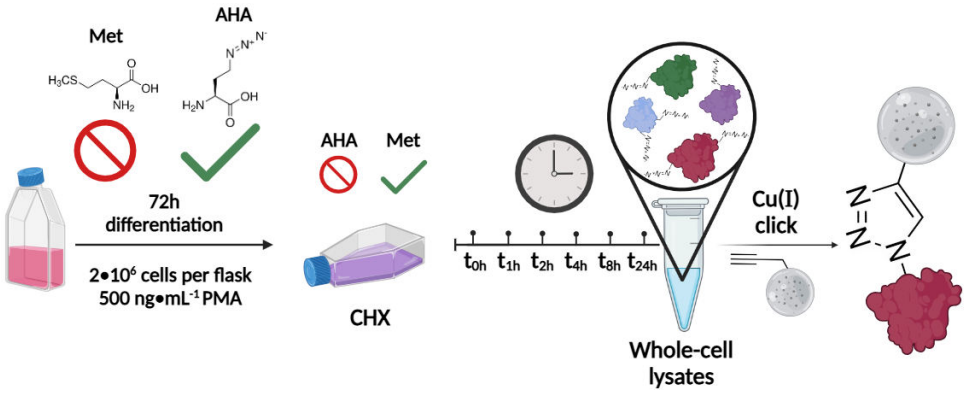

Figure 13: Graphical overview of the finalized BONCAT experimental design employed to assess the effects of CHX treatment in PMA differentiated HL-60 cells. Created in `https://BioRender.com`.

remove the supernatant standard RPMI-1640 medium. The cells were subsequently resuspended in 5 mL L-Azidohomoalanine (59.86 µM) containing RPMI-1640 medium with a 500 ng · mL^{-1} PMA concentration and seeded in T25 cell culture flasks. Cells were then allowed to differentiate over the course of 72 hours. The supernatant Azidohomoalanine RPMI-1640 medium was then removed and centrifuged to pellet not-fully differentiated cells. The pelleted cells were then resuspended in 5 mL standard RPMI-1640 medium containing 10 µM CHX and transferred back to the corresponding flask. Three biological replicates for each timepoint were worked-up on ice as whole cell lysates (section 3.2.1) 1, 2, 4, 8, 24 hours after addition of the CHX containing medium, while the t0 timepoint was processed immediately.

3.2 Sample preparation

Two different kinds of workup were used for the experiments. On the one hand, whole cell lysates were used for working up the preliminary timeseries (section 3.1.5, the Cycloheximide concentration optimization experiments and ACBI2 rescue experiments (both section 3.1.7, the final experiment (section 3.1.8) as well as the BONCAT timeseries (section 3.1.10). On the other hand, subcellular fractionation of the proteome was performed for the proteomic profiling experiments of the different cell lines (section 3.1.4).

3.2.1 Whole cell lysates

Once experiments were completed, the corresponding sixwell plates were placed on ice. The supernatant medium was removed and the wells washed twice with 2 mL of cold PBS buffer. The cells were scraped twice from the bottom of each wells using a scraper (SARSTEDT AG & Co. KG) and 60 µL of freshly prepared Sodium deoxycholate (SDC, composition specified in table 2 the first time and 50 µL the second time for the preliminary timeseries experiment. The volume of SDC used for the second scraping was reduced to 30 µL in all further experiments where whole cell lysates (WCLs) were made in sixwell format.

The cells present in T25 flasks in the BONCAT experiments were washed twice with 4 mL cold PBS after the supernatant was transferred to a 15 mL Falcon tube. Supernatant cells were pelleted at 1100 rpm for five minutes at room temperature and washed twice with 4 mL PBS. The cells attached to the bottom of the washed T25 flasks were scraped twice with 140 µL SDC buffer. The washed supernatant cells were resuspended in the 140 µL SDC of the second addition before pooling the two fractions of the same sample.

The resulting whole cell lysate solution was transferred to labelled Eppendorf tubes after each SDC addition and thorough scraping of the well. The resulting Eppendorf tubes were then shaken at 1400 rpm at 95 °C for five minutes in a preheated Thermomixer Comfort (Eppendorf

Table 2: Composition of the SDC lysis buffer

Compound	Concentration [mM]
Sodium deoxycholate $\geq$ 98%	102
TRIS (Tris(hydroxymethyl)-aminomethane)-HCl pH 8.5	100
Water	-

AG). Occurring condensate was then centrifuged using a tabletop centrifuge after the sample was allowed to cool down. Samples were thereafter stored at -20 ℃ until further processing.

3.2.2 Subcellular fractionation

All fractionation steps were performed on ice. The workflow for suspension cells and adherent cells slightly differed at the beginning of the workup.

The former were directly transferred after counting in the exact volume containing $2 \cdot 10^6$ cells to a 15 mL Falcon tube and centrifuged at 1100 rpm at 4 ℃ for five minutes to pellet the cells. The supernatant medium was then carefully removed, 1 mL of fractionation buffer (composition specified in table 3) containing a 1% of protease and phosphatase inhibior cocktail (PIC, Sigma-Aldrich) and 1% phenylmethylsulfonyl fluoride (PMSF, 100 mM in isopropanol, Sigma-Aldrich) were added on top of every cell pellet. The suspension cell pellet was resuspended with a 23G needle attached to a syringe by pipetting it up and down.

Table 3: Composition of the fractionation buffer

Compound	Concentration [mM]
1M HEPES (4-(2-hydroxyethyl)-1-piperazineethanesulfonic acid)/NaOH pH 7.4	10
5M NaCl	10
1M $MgCl_2$	3.5
2M EGTA (ethylene glycol-bis(β-aminoethyl ether)-N,N,N',N'-tetraacetic acid)	1
2M Sucrose	250
20% Triton X-100	0.5%
Water	-

The supernatant medium in T25 culture flasks with adherent cells and differentiated HL-60 cells was removed and the cells washed twice with 5 mL of cold PBS buffer. 1 mL of fractionation buffer containing 1% PIC and 1% PMSF was then pipetted into the flask, the cells were then scraped from the bottom of the flask using a cell scraper. The scraped suspension cells were then transferred to labelled 15 mL Falcon tubes using a 23G needle attached to a syringe.

The following steps were then performed with both the suspension cells as well as the scraped adherent cells inside the respective 15 mL Falcon tubes. The cells were lysed by applying shear stress by drawing the solution up in the syringe and then draw it down at a 45° angle directly onto the Falcon tube wall. A small volume of the resulting solution was then transferred to a slide for the first processed sample and checked under the microscope to assess whether the cell membrane was destroyed and only the nuclei were visible. The exact number of times necessary for a successful lysis was then adapted according to the microscope check and adopted for all further samples. The resulting solution was then centrifuged at 3500 rpm at 4 ℃ for five minutes to pellet the nuclei. The supernatant cytoplasm was then transferred to correspondingly labelled

15 mL Falcon tubes with 4 mL ice cold EtOH abs. to precipitate the proteins. The tubes were then vortexed, inverted, sealed and stored at -20 ℃ until further processing.

The Falcons containing the remaining pellet were dried with a paper tissue without touching the pellet itself. Subsequently 100 µL of TE-NaCl solution (see table 4 for the composition) were added to each pellet, which was resuspended during the addition where possible and incubated on ice for 10 minutes. The solution was then sonicated three times for one second at 80% power using an ultrasonic homogenizer (UW 2070, BANDELIN electronic GmbH & Co. KG). Thereafter 900 µL of TE-TritonX solution (composition specified in table 5) were added to each sample, which was followed by an incubation on ice for 15 minutes. The sample tubes were then centrifuged at 3500 rpm at 4 ℃ for five minutes before transferring the nuclear extract into labelled Falcon tubes with 4 mL EtOH abs., which were then handled as described in the previous paragraph.

Table 4: Composition of the TE-NaCl solution

Compound	Concentration [mM]
1M TRIS-HCl	10
0.5M EDTA (Ethylenediaminetetraacetic acid)	1
5M NaCl	500
Water	-

Table 5: Composition of TE-Triton X-100 solution

Compound	Concentration [mM]
1M TRIS-HCl	10
0.5M EDTA	1
10% Triton X-100	0.5%
Water	-

3.2.3 Protein quantification

Samples processed *via* the whole cell lysate method described in section 3.2.1 were removed from -20 ℃ storage and left to thaw. The tubes were then centrifuged for a short amount of time at high rpm on a tabletop centrifuge (accuSpin Micro 17, Fisher Scientific) prior to placing them into a preheated Thermoshaker and heated at 95 ℃ for five minutes at 1400 rpm. The tubes were again centrifuged at high rpm after letting them cool to remove condensate.

Fractionated samples in the 15 mL Falcon tubes were centrifuged at 5000 rpm for 30 minutes at 4 ℃ to pellet the proteins. The EtOH abs. supernatant was removed by inverting the tube, which was then placed with the top down to allow further Ethanol present in the tube to flow away. The tubes were subsequently placed into a vacuum exsiccator and the protein pellets completely dried. The cytoplasmic protein pellet was usually larger and was therefore resuspended in 70 µL of lysis buffer (LB, for composition see table 6), while the smaller nucleic fraction pellet was usually resuspended in 20 µL.

The pellets were generally resuspended by pipetting the solution up- and down several times after leaving the pellets at room temperature for 15 minutes for the buffer to ease the resuspension. The resuspended pellets were placed in an ultrasonic bath (SONREX DIGITAL 10 P, BANDELIN electronic GmbH & Co. KG) for 15 minutes at 100% power at 25 ℃ to further solubilize the proteins. The tubes were then centrifuged at 1000 rpm at 20 ℃ for five minutes before keeping them overnight at room temperature to allow a complete reconstitution.

Table 6: Composition of Protifi lysis buffer

Compound	Concentration [mM]
Urea	8000
1M TEAB (Triethylammonium bicarbonate buffer)	50
20% SDS (Sodium dodecyl sulfate)	0.2

Fractionated samples that were used for an In-gel digestion were processed a similar way as described in the previous paragraph with some minor modifications. A spatula tip of Urea (Honeywell Fluka) was added to the dried pellets prior to the addition of 30 µL of sample buffer (SB, composition can be seen in table 7) to resuspend both the cytoplasmic and nucleic protein pellet.

Table 7: Composition of In-gel digestion sample buffer

Compound	Concentration [mM]
Urea	7500
Thiourea	1500
CHAPS	65
20% SDS	0.05
DTT	100

The actual protein quantification needed for normalization of sample amounts for the protein digestion was performed by means of the Bicinchoninic acid (BCA) colorimetric assay.[81]

Ten-point calibration curves of bovine serum albumin (BSA, Carl Roth GmbH + Co. KG) in a concentration range from 0-9 $\mu g \cdot mL^{-1}$ were pipetted in 96-wellpates for the BCA assay. Then 1 µL of SDC for in-solution digestion or lysis buffer for fractionated samples was added to the calibration curve wells for matrix correction. Ultimately water was added to ensure identical volumes inside the wells. Sample-wells were prepared by pipetting 9 µL of water before the addition of 1 µL sample. The working reagent used for the photometric detection in the BCA assay was prepared by mixing BCA reagent A (composition can be seen in table 8) with BCA reagent B (200 mM $CuSO_4 \cdot 5H_2O$) in a 50:1 ratio. 200 µL of the working reagent were pipetted into every well.

The plate was then mixed at 800 rpm on a tabletop mixer for five minutes before incubation at 60 ℃ for 40 minutes. The extinction of the wells was then measured in a photometric plate reader at 562 nm in the case of the BCA assays. The Bradford assay plate extinction was measured at 595 nm. The raw data was then exported to Microsoft Excel 365 for further processing. Briefly, the measured extinction of the calibration curve wells was plotted against the known BSA concentration. The protein content in the samples was then calculated from the transformed linear regression equation of the BSA calibration curve. The protein concentration

Table 8: Composition of 100 mL reagent A for BCA assay pH 11.25

Compound	Concentration [mM]
Bicinchoninic acid	29
Sodium carbonate	188.7
Sodium tartrate	8.25
Sodium bicarbonate	113
Water	-

of Azidohomoalanine containing whole-cell lysates of the BONCAT experiment was assessed by pipetting 9 µL of sample into 1 µL of water, the resulting protein concentration was then corrected accordingly.

3.2.4 BONCAT enrichment

The protein concentration was very similar in the different BONCAT samples. The protein enrichment was therefore performed with the total sample volume without prior protein amount normalization, usually to 20 µg protein in all the other experiments. A Click-iT™ Protein enrichment kit (invitrogen by Thermo Fisher Scientific, ref C10416) was employed to enrich Azidohomoalanine containing proteins using a modified protocol compared to the one provided by the supplier.

Reaction additive 2 of the kit was dissolved in 2 mL of water shortly before performing the enrichment. The alkyne agarose bead resin slurry was resuspended by rotating the vial with 50 rpm on a programmable end-over-end mixer (RM Multi-1, Starlab International GmbH) for 20 minutes. The vial was thoroughly vortexed before a cut-off tip was used to transfer 100 µL of the bead slurry into 2 mL Eppendorf tubes. The beads were washed three times by with 1.8 mL water by consecutive vortexing, pelleting (1000 rcf, 5 minutes) and supernatant removal steps. An approximate volume of 150 µL of water above the pelleted beads was left in the tube after the last washing step.

The 2X catalyst solution was prepared by mixing and vortexing 8350 µL water, 1250 µL reaction additive 1, 200 µL of 100 mM $Cu(II)SO_4$. Finally, 200 µL of reaction additive 2 were added to the solution followed by a further vortexing step.

The whole-cell lysates were quantitatively transferred to the respecting Eppendorf tubes containing the washed bead slurry, followed by 500 µL of 2X catalyst solution. The tubes were fitted to the end-over-end rotator sample holder and rotated end-over-end in the dark at 50 rpm and room temperature for 18.5 hours.

The beads were then pelleted by centrifugation at 1000 rcf for five minutes. The resulting supernatant was then discarded. The beads with the immobilized L-Azidohomoalanine containing proteins were quantitatively transferred to a spin column (MobiSpinColumn "F", 10 µm filter pore size, small, MoBiTec GmbH) in four steps, each one with 500 µL water. The beads were washed further three times on-column with 300 µL water to ensure a complete removal of the copper sulfate solution. Five washing steps were then performed with SDC buffer, followed by further four washing steps using ABC buffer. All on-column washing steps were performed at 2000 rcf over the course of one minute at room temperature, the flowthrough was discarded after each centrifugation step. The beads were then centrifuged to dryness over the course of three minutes.

The dried beads were then transferred to 1.5 mL Eppendorf tubes by quantitatively scraping the beads from the spin column with an antistatic plastic spatula. The beads were then resuspended in 90 µL of SDC and subjected to the standard in-solution digestion procedure (section 3.2.5.b).

3.2.5 Protein digestion

Based on the results obtained from the protein quantification a volume containing 20 µg of proteins was transferred from each sample to a correspondingly labelled Eppendorf tube. This was done for all experiments with the sole exception of the BONCAT timeseries, as described in section 3.1.10. A two-fold approach was followed for the preliminary timeseries experiment, one digestion was done by normalizing to 20 µg of protein as described. For the second approach the necessary volumes to reach 20 µg of protein in the t_{0h} control samples were averaged and the calculated sample volume then transferred to labelled tubes for the digestion of all further samples. Protein digestion was therefore always performed with a fraction of the available sample, the

remaining sample volume was stored at -20 ℃.

3.2.5.a ProtiFi protocol

Cell-line proteomic profiling samples were digested using this protocol. Sample tubes containing 20 µg of protein were topped up to 50 µL with lysis buffer (composition in table 6) before the addition of 64 mM Dithiothreitol (DTT). The tubes were briefly vortexed and placed in a Thermoshaker at 95 ℃ where it was shaken at 300 rpm for ten minutes. The samples were then left to cool to room temperature and centrifuged shortly before the addition of 12.5 µL of 486 mM Iodoacetamide (IAA). The sample tubes were then placed in a thermoshaker and incubated in the dark for 30 minutes at 30 ℃ at 300 rpm. The tubes where left to cool to room temperature before a centrifugation step at 13,000 g for eight minutes. Thereafter 11.25 µL of 12% phosphoric acid were added to each sample, followed by 866 µL S-trap buffer (exact composition stated in table 9).

Table 9: Composition of Protifi S-Trap buffer

Compound	Formulation [%vol/vol]
Methanol	90
1M TEAB	10

The resulting solution from each sample was then quantitatively transferred to the corresponding S-Trap spin columns (C02-mini, ProtiFi LLC) in two 500 µL steps. The column was centrifuged at 1000 g for one minute and rotated 180° after each step. The column was washed four times by adding 400 µL of S-Trap buffer, centrifuging and rotating the column for each step. The spin column was then placed on top of a fresh tube. The digestion enzyme mix was then prepared and/or thawed depending on availability of already prepared aliquots. To do so, a fresh vial of MassSpec Grade Trypsin Lys-C mix (PROMEGA GmbH) containing 20 µg of enzyme was reconstituted in 100 µL reconstitution buffer (PROMEGA GmbH) or Trypsin buffer (composition specified in table 10) on ice.

Alternatively, already reconstituted 0.2 $\mu g \cdot \mu L^{-1}$ enzyme aliquots (maximum one additional freeze-thaw cycle) were used when available and thawed on ice. A mixture of 122.5 µL of digestion buffer (50 mM TEAB) and 2.5 µL of reconstituted enzyme per sample were prepared in a separate Eppendorf tube before pipetting 125 µL of the resulting solution onto the column. The column was gently tapped to ensure an even distribution of the solution on the filter. The columns were then capped and placed inside an incubator for two hours at 37 ℃. The digestion was performed at an enzyme to substrate ratio of 1:100. Subsequently 80 µL of digestion buffer were added to the column. The column was then centrifuged at 1000 g. Afterwards 80 µL of 0.2% formic acid (FA) were added to the column, which was again centrifuged. Additionally 80 µL of 50% acetonitrile, 0.2% FA solution were added to the columns before the last centrifugation step. The eluates were ultimately dried in a centrifugal vacuum concentrator (miVac DUO, Genevac) and stored at -20 ℃ until further processing.

Dried peptides were reconstituted in 5 µL of a 10 fmol $\cdot$ μL^{-1} synthetic standard peptide mix (in 30% formic acid) shortly before the measurement. Further 40 µL of loading solvent (97.95%

Table 10: Composition of trypsin buffer

Compound	Formulation
Acetic acid	0.05 %vol/vol
$CaCl_2$	2 mM
Water	-

water, 2% acetonitrile, 0.05% TFA) were then added to the solution before briefly vortexing the tube. The tubes were then placed in a centrifuge for five minutes at 10,000 g. The solution was then quantitatively transferred to LC-MS glass vial inserts for the measurements.

3.2.5.b In-solution digestion protocol

All samples that were worked-up with the whole cell lysate method were digested using this method. Sample tubes containing 20 µg of protein in the great majority of cases or the constant sample volume for timeseries experiments were topped-up to 90 µL with SDC lysis buffer. Subsequently, 10 µL of reduction/alkylation buffer (composition specified in table 11 were added to each sample before incubation in a Thermoshaker at 45 °C for five minutes at 1400 rpm. The samples were left to cool to room temperature before a short centrifugation step, 1 µL of Trypsin Lys-C was added to each sample after having reconstituted the enzyme or having thawed an aliquot on ice as described in section 3.2.5.a. The samples were then digested at 37 °C at 1400 rpm for 17-18 hours with an enzyme to protein ratio of 1:100.

Table 11: Composition of reduction/alkylation buffer

Compound	Concentration [mM]	Preparation
TCEP (Tris(2-carboxyethyl)phosphine hydrochloride)	200	500 µL of TCEP stock solution were mixed with 500 µL of freshly prepared 2-CAM stock solution. 940 µL of the resulting solution were then mixed with 60 µL of 5M NaOH. The pH was checked and adjusted to reach 7.5 - 8.
2-CAM (2-Chloroacetamide) $\geq$ 98%	800	
Water	-	
5M NaOH	-	

Following the incubation the samples were then nearly dried in a vacuum concentrator set to 40 °C for approximately 40 minutes.

The bead containing Eppendorf tubes of the BONCAT enrichment procedure were centrifuged for eight minutes at 3000 rcf to pellet the beads. The peptide-containing supernatant was quantitatively transferred to a fresh 1.5 mL Eppendorf tube. The beads were resuspended in 100 µL SDC buffer, followed by a second centrifugation. The supernatants were then pooled before undergoing concentration in the concentrator.

The appropriate amount of StageTips was prepared by stacking 2 mL waste Eppendorf tubes without a lid, centrifuge adapters and 200 µL pipet tips. Two disks of a polystyrenedivinylbenzene-reversed phase sulfonate material (Empore 2241 SDB-RPS, 12 µm particle size, 47mm; CDS Analytical LLC) were carefully inserted into each pipet tip to complete the StageTip. A 100 µL volume of SDB-RPS loading buffer (composition stated in table 12 was added to each sample, which was then repeatedly pipetted up- and down before being quantitatively transferred to the corresponding StageTip. The tips were then centrifuged at 1500 g for eight minutes to allow the whole solution to pass through the RPS material. Further 100 µL of loading buffer/wash buffer 1 were added to the StageTip before centrifugation followed by 100 µL of SDB-RPS wash buffer 2 (composition can be found in table 13) and a further centrifugation step.

Table 12: Composition of SDB-RPS loading buffer and wash buffer 1

Compound	Formulation [%vol/vol]
Isopropanol	99
Trifluoroacetic acid 99%	1

The waste tube was then switched out for a storage tube with a glass LC-MS inlet placed inside. The peptides were directly eluted into the inlet with the addition of 60 µL of SDB-RPS elution buffer (exact buffer composition can be found in table 14) followed by a centrifugation step at 1500 g for five minutes. The samples were then dried in the vacuum concentrator at 45 °C until LC-MS measurement.

The dried peptides were reconstituted by adding 5 µL of 10 fmol · μL^{-1} peptide standard mix as well as 40 µL of loading solvent to the glass inlet. Then, 400 µL of water were added into the storage tube. The storage tubes with the glass inlets inside were then placed into the ultrasonic bath for five minutes at room temperature at 20% power. The sample tubes were then centrifuged for seven minutes at 5000 g before transferring the inlet to a labelled glass vial for the measurement.

3.2.5.c In-gel digestion protocol

The samples were loaded on a previously cast 12% Acrylamide gel. The SDS-PAGE slab gel was cast in separate steps to give two sections for the for discontinuous electrophoretic separation of the proteins in the sample. The separating gel was cast from a solution with final concentrations of 12% Acrylamide/ Piperazine di-acrylamide (PDA), 375 mM 2M Tris-HCl pH=8.8, 0.1% Sodium dodecyl sulfate (SDS), 0.075% Tetramethylethylenediamine (TEMED) and 0.045% Ammonium persulfate (APS) in water. The solution was covered with a small volume of 90% Isopropanol during the 40 minute polymerization timeframe. The stacking gel was cast after removal of the Isporopanol layer on top of the separating gel. The stacking gel consisted of a solution with final concentrations of 4% Acrylamide/ PDA, 125 mM 2M Tris-HCl pH=6.8, 0.1% SDS, 0.1% TEMED and 0.05% APS in water. A sample comb with ten spacers was then inserted between the two glass slides and the gel left to polymerize for one hour.

The gel was then placed into an SDS-PAGE apparatus (Mini PROTEAN Tetra Cell, Bio-Rad Laboratories Inc.) which was then filled with Tris-Glycin buffer. The molecular weight marker (5 µL, Precision Plus Protein Dual Color Standards, Bio-Rad Laboratories Inc.) was pipetted into one lane. Subsequently 5 µL of 5xSDS sample buffer were pipetted into every other lane. Both 62.4 µg proteins of the Cytoplasm and Nuclear fraction were loaded into separate lanes of the gel and topped up to a volume of 25 µL with sample buffer (composition stated in table 7). The rest of the lanes were filled with 25 µL of sample buffer and used as blanks. A maximum current of 40 mA and a maximum voltage of 250 V was set on the control unit (PowerPac Universal, Bio-Rad Laboratories Inc.) before starting the electrophoresis. The SDS-PAGE was run until a separation of the samples over a distance of 1.5 cm was achieved, the gel was then removed from the apparatus and placed in a fixing solution (50% Methanol, 10% Acetic acid in water) for 30 minutes.

This and all the following steps were performed at room temperature while slowly shaking the gel on a plate mixer. The gel was washed for 10 minutes in 50% Methanol followed by two five minute steps in water. Sensitization was performed by transferring the gel into a 0.02% Sodium Thiosulfate solution for one minute, which was then followed by two brief rinsing steps in water. The gel was then stained in a 0.1% Silver Nitrate solution over the course of 10 minutes, briefly rinsed with water and developed in a 3% Sodium Carbonate, 0.05% Formaldehyde solution over the course of 15 seconds. The gel was again rinsed in water and then placed into a 1% Acetic acid solution until further processing.

Table 13: Composition of SDB-RPS wash buffer 2

Compound	Formulation [%vol/vol]
Water	94.8
Acetonitrile	5
Trifluoroacetic acid 99%	0.2

The lanes containing the Cytoplasm and Nuclear fractions were removed from the rest of the gel. The two gel pieces were then respectively horizontally cut seven times, therefore achieving eight different bands of similar sizes which contained proteins with cascading molecular weights. Each one of the bands was then vertically cut four times, the pieces belonging to one band were then transferred to one correspondingly labelled Eppendorf tube. Assuming an even distribution of the loaded 62.4 µg of proteins, each band contained a protein amount of 7.8 µg. Figure 14 shows the approximate positions of the cuts on the silver stained SDS-PAGE gel.

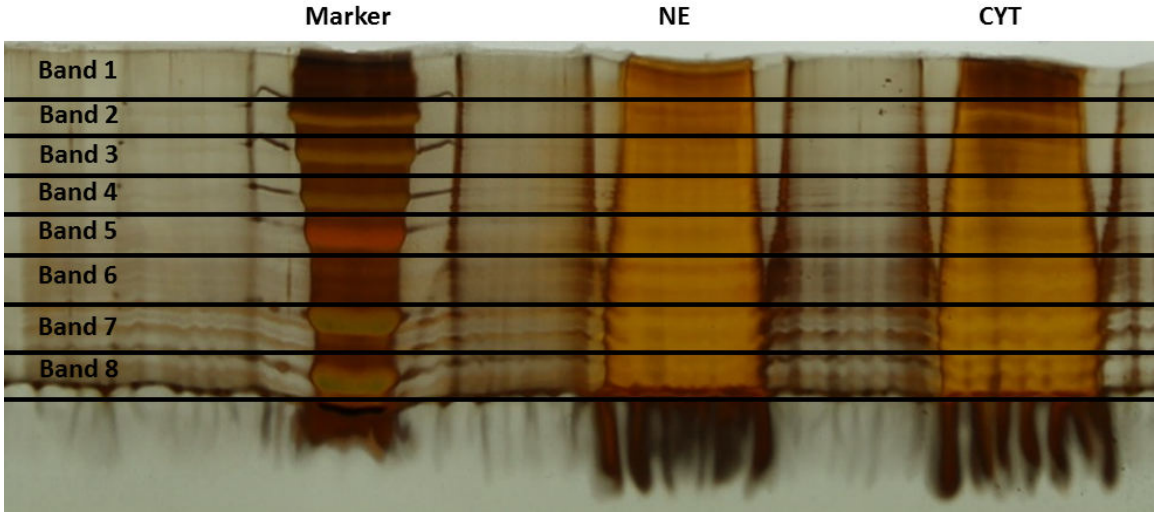

Figure 14: The figure shows the silver stained SDS-PAGE gel with the superimposed horizontal black lines show the cutting positions which lead to the eight separate bands for both the CYT and NE lane. The average molecular weight of the proteins found in each lane should decrease with increasing band number. Therefore band 1 should contain the highest molecular weight proteins while band 8 should contain the lowest based on the separation achieved in discontinuous electrophoresis.

The gel pieces inside each Eppendorf tube were then destained in 200 µL of a 15 mM Potassium ferricyanide ($K_3[Fe(CN)_6]$), 50 mM Sodium Thiosulfate solution by vortexing the tubes until the gel pieces were transparent. The supernatant was discarded and the gel pieces were then respectively washed four times in total by shaking the tubes for ten minutes at 1200 rpm at room temperature. The first washing step was in 400 µL of 25 mM Ammonium bicarbonate (ABC) solution, followed by 400 µL Acetonitrile after supernatant removal. These two steps were then repeated for a second time.

Thiol groups in each sample were reduced in 200 µL of a 20 mM Dithiothreitol (DTT), 25 mM ABC solution by shaking the tubes at 56 °C, 1100 rpm for 30 minutes on a Thermoshaker. The supernatant was then discarded and the gel pieces washed twice with ABC followed by Acetonitrile as described in the previous paragraph.

Alkylation was performed by adding 200 µL of a 50 mM IAA, 25 mM ABC solution to the gel pieces and incubating the tubes in the dark at 37 °C, 1100 rpm for 30 minutes. The samples were allowed to cool down and the gel pieces were washed as previously described. The gel pieces were then dried to completion in the centrifugal concentrator for 20 minutes at 40 °C.

Table 14: Composition of SDB-RPS elution buffer

Compound	Formulation [%vol/vol]
Water	39.8
Acetonitrile	59.7
NH_4OH	0.5

The digestion was performed by adding Trypsin/LysC in a 1:20 enzyme to protein ratio to each band in 10 µL of 25 mM ABC buffer. The enzyme was either reconstituted or an aliquot was thawed on ice as described in section 3.2.5.a. After 15 minutes further 20 µL of ABC solution were further added to the gel pieces. The samples were then incubated overnight at 37 °C for 17 hours. The samples were then allowed to cool down to room temperature, briefly centrifuged and cooled down to 4 °C. Trypsin/LysC was then added for a second digestion in a 1:40 enzyme to protein ratio. The samples were then incubated at 37 °C for four hours.

The supernatant containing the peptides of each tube was subsequently transferred to a correspondingly labelled sample tube. The peptides inside the gel pieces were extracted three times with 40 µL of 25 mM ABC on a Thermoshaker for 15 minutes at 1200 rpm. The supernatant was transferred to the corresponding sample tube after each washing step. A further extraction step was performed with 5% formic acid, the workflow was the same as described for the ABC buffer. The solution containing the peptides was then dried to completion in the centrifugal concentrator.

The dried samples were resuspended in 4 µL of 10 fmol $\cdot$ μL^{-1} synthetic standard peptide mix and 30 µL loading solvent shortly before measurement. The tubes were centrifuged for five minutes at 10,000 g before the solution was quantitatively transferred to LC-MS glass inlets. Samples of different bands were additionally pooled after a first LC-MS/MS measurement run to evaluate pooling effects.

3.3 Nano liquid chromatography parameters

The chromatographic separation was performed on a Dionex UltiMate™ 3000 RSLCnano system (Thermo Fisher Scientific). A 5 µL volume of the reconstituted samples were loaded onto a pre-column (Acclaim™ PepMap™ C18 100, Thermo Fisher Scientific) making use of solvent A (99.9% water, 0.1% formic acid) at a flow rate of 10 $\mu L \cdot min^{-1}$. Peptides were then eluted from the pre-column to the analytical column (Aurora series emitter column, 1.6 µm C18, 25 cm $\cdot$ 75 µm, IonOpticks) by applying a gradient ranging from 12% to 42% solvent B (79.9% acetonitrile, 20% water, 0.1% FA) over the course of 90 minutes at a flow rate of 300 $nL \cdot min^{-1}$. The applied method resulted in a total runtime of 140 minutes with inclusion of equilibration and washing phases. In-gel samples also underwent a second chromatographic separation where a 41 minute long gradient was applied starting from 12% up to 40% mobile phase B, which led to a total runtime of 85 minutes with washing and equilibration steps.

3.4 Mass spectrometer instrument parameters

The MS/MS analysis of all samples was performed on a timsTOF Pro (Bruker Daltonics) mass spectrometer running in parallel accumulation- serial fragmentation (PASEF) and data dependent acquisition (DDA) mode. A m/z scan range from 100 to 1700 was set to acquire both MS1 and MS2 spectra. An inverse reduced ion mobility (1/k0) scan ranging from 0.6 to 1.6 $Vs \cdot cm^2$ contributed to a total ramp time of 100 ms to achieve trapped ion mobility separation. The total cycle time was 1.16 s accounting for 10 PASEF MS/MS scans per cycle.

3.5 Data processing

The acquired data was processed using MaxQuant v 1.6.17.0 with the Andromeda search engine[82] to allow for the label-free quantification and identification of proteins and searched against the SwissProt "*homo sapiens*" database (14.12.2019 with 20380 canonical entries). False discovery rates for peptide-spectrum match (PSM) and protein were set to 0.01, the "Match between runs" setting was enabled with a matching time window of 0.7 and an alignment time window of 20 minutes. Further criteria included a MS/MS mass tolerance of 40 ppm and a maximum of two missed cleavages. A minimal requirement for protein identification was set to one unique peptide, after a two-peptide searches were not further pursued after preliminary data evaluation in combined proteome profiling results. Carbamidomethylation of Cysteine was set as fixed

modification while Methionine oxidation and the acetylation of the protein N-terminus were included in the search as variable modifications.

Perseus (version 1.6.14.0)[83] was used for data processing. Proteins only identified by site, common contaminants as well as proteins matching reversed sequences were filtered out. LFQ-values of remaining entries were $\log_2(x)$ transformed before further processing, which differed between experiments.

Proteins in the proteome profiling experiment datasets had to be identified in at least 70% of the samples to be kept in the matrix for further analysis.

Datasets of preliminary experiments with a smaller sample size were reduced in a less stringent manner by filtering out proteins that were not present at least once in one analysis group.

The SDS-PAGE data matrix was filtered to contain at least one valid entry in total.

Data resulting from the finalized timerseries experimental design, as well as the BONCAT timeseries was filtered to contain at least one valid entry in total inside Perseus.

Entries with missing values were then computationally replaced with values from a normal distribution (downshift: 1.8, width: 0.3) to eliminate NaN values for PCAs and the performance of two-sided t-tests with a s0 of 0.1 and a false discovery rate of 0.05 for volcano plot creation.

Data matrices prior and after replacement of missing values were exported from Perseus and imported to Python 3.11.5 for further filtering steps, analysis and plotting. The Pandas[84] package was used for the bulk of data processing, while the Matplotlib[85] and Seaborn[86] packages were employed for plotting of the data.

4 Results and discussion

4.1 Selection of the liquid chromatography gradient length

It is generally known that mechanistically relevant proteins might be present at very low abundances inside the cells, which therefore will not necessarily be detected. Employing SDS-PAGE pre-fractionation of samples allows a deeper insight into the (sub-)cellular proteome of a cell line compared to non-fractionated samples because the proteins are separated into several bands. This helps the detection of lower abundant proteins in data dependent acquisition modes as less high abundant proteins will be present in each sample.

The non-differentiated HL-60 cell model system was chosen for a deep proteome investigation because of an increased probability that also lower abundant experimentally relevant proteins are found this way. The generated gel-band samples were then used to optimize methodological parameters like the liquid chromatography gradient length to allow a robust detection of proteins in all further experiments.

The 85 minute liquid chromatography gradient led to an overall detection of 5357 proteins in the gel bands of the undifferentiated HL-60 cells, while an overall number of 6488 proteins were detected by employing the longer 140 minute gradient separation on the same gel band samples. A very lenient filtering strategy was employed after the standard filtering procedure for this dataset because of the lack of replicates. In order to be kept in the dataset proteins needed to be identified in at least one gel band, regardless of the subcellular fraction. The protein identifications from both gradients were compared by means of a Venn diagram in figure 15. The Venn diagram shows a substantially higher number of proteins that were only identified in the 140 minute gradient.

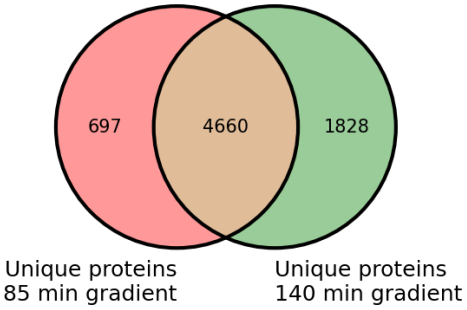

Figure 15: Venn diagram showing the number of shared and unique proteins that were identified by applying two different LC gradients, with a total length of both 85 and 140 minutes, on the same samples. The numbers displayed in the diagram show the overall number of identified proteins in all eight bands of both cytoplasmic and nuclear fractions of non-differentiated HL-60 cells.

A heatmap representing the SDS-PAGE gel was created to visualize the proteomics results of the 140 minute gradient (figure 16). All proteins detected in each band were plotted as horizontal bars in decreasing molecular weight order, the different shades of blue of the horizontal bars represent the corresponding $\log_2$ transformed LFQ value of each single protein. Experimentally relevant proteins were highlighted by the use of specific colors in every band they were detected in order to qualitatively evaluate whether the separation on the SDS-PAGE gel was successful. The band numbering corresponds to figure 14 where higher molecular weight proteins are located in the first bands.

Figure 16 shows the enrichment of a subset of proteins with a certain molecular weight in each gelband, as was expected by performing the on-gel discontinuous electrophoresis of the proteins. Lower and/or higher molecular weight proteins compared to the majority of the enriched protein fraction were also identified in the different bands. This was expected due to the utopic nature of the "perfect" molecular weight separation, especially over a very short on-gel separation distance. The number of proteins detected in band number eight is higher compared to other bands, probably because the separation on the gel was only allowed to proceed for

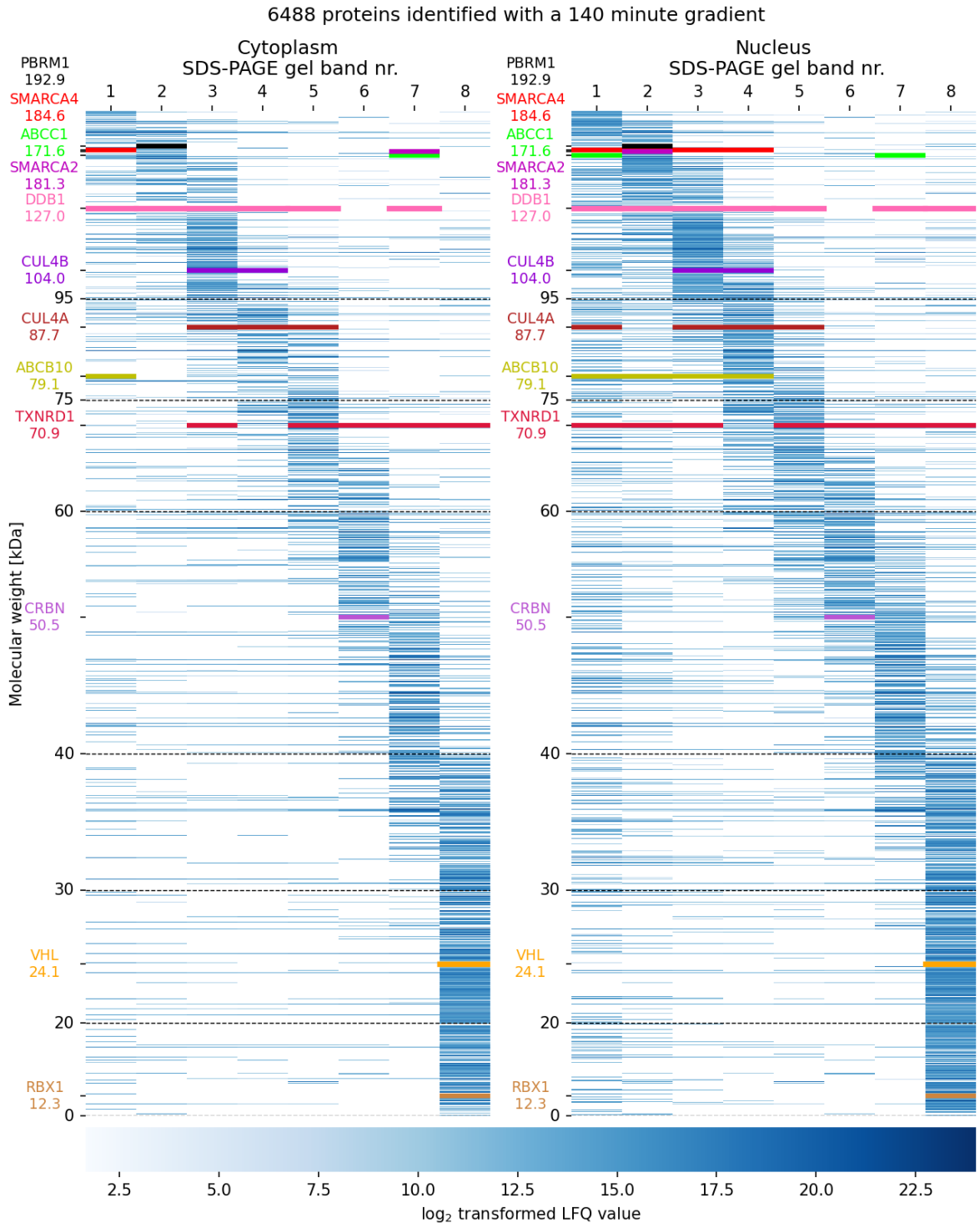

Figure 16: Separate visualization of the SDS-PAGE gel-band proteomics results for the cytoplasmic and nuclear fraction of non-differentiated HL-60 cells. The heatmap represents all the identified proteins in form of horizontal bars, the different hues of blue display the corresponding $\log_2$ transformed LFQ intensity measured using the 140 minute LC gradient. Experimentally relevant proteins were color coded. ABCC11 was not detected.

approximately 1.5 cm. This implies that especially low molecular weight proteins were not able to fully separate. An acceptably good on-gel separation to maximize the number of identified proteins was however never the actual goal of the experiment.

Overall, the SDS-PAGE separation of the proteins appeared to be successful. Bands in which experimentally relevant proteins were detected, correctly fit the molecular weight reported in the corresponding UniProt entries. It is noticeable that some proteins were detected in more than one gel-band, represented by the columns in the figure. For example DDB1 and TXNRD1 were both detected in the majority of the gel bands, even though this should not be the case. This might be attributable to e.g. endoprotease activity, which might have cut the protein to smaller subunits. Correspondingly, these lower molecular weight fragments will then be detected in lower molecular weight bands. Alternatively, full-length proteins can be cut to control their localization within the cell. TXNRD1 is a homodimeric, which might dissociate into subunits with lower molecular weight upon separation in the gel. CUL4B was detected in two adjacent bands, this shows that the arbitrary position when cutting the gel will inevitably lead to cases where the protein band is cut "in half" and shared between two gelbands. These factors would allow the identification of said protein in several bands, aided by the very low limit of detection and quantification of mass spectrometry.

The longer gradient led to the identification of a higher number of proteins (6488 vs. 5357), which was expected due to the superior peptide separation that can be achieved over the course of 140 minutes compared to the shorter gradient. The reduced number of co-eluting peptides aids the detection of a higher number of proteins. Correspondingly, all experimentally relevant proteins were detected in the longer 140 minute gradient, while SMARCA2 and PBRM1 were not detected in the shorter 85 minute gradient.

A quantitative comparison of the two gradients was attempted based on the number of identified unique and non-unique peptides for experimentally relevant proteins in table 15a, while table 15b highlights the performance differences over the 4660 protein IDs shared between both LC gradients.

Table 15: A quantitative comparison of peptide numbers detected by employing the 85 minute and the 140 minute liquid chromatography gradient on the gel band samples of non-differentiated HL-60 cells is shown in the following tables. The proteins SMARCA2 and PBRM1 were not detected in the shorter 85 min gradient, ABCC11 was not detected in either gradient. Table 15a strictly focuses on the experimentally relevant proteins described in section 1.5, whereas table 15b shows calculated summary statistics of unique and non-unique peptides detected for all the 4660 proteins shared between the two LC gradients.

(a) Quantitative comparison of unique and non-unique peptide numbers detected employing the two LC gradients for experimentally relevant proteins. The longer 140 minute gradient enables the detection of a higher number of both non-unique as well as unique peptides compared to the shorter 85 minute gradient, with the sole exception of the unique peptide number of TXNRD1.

	85 min LC gradient		140 min LC gradient	
Gene Name	Nr. peptides	Nr. unique peptides	Nr. peptides	Nr. unique peptides
ABCB10	19	18	22	21
ABCC1	29	28	31	31
CRBN	8	8	12	12
CUL4A	49	38	49	38
CUL4B	31	20	38	27
DDB1	50	50	52	52
PBRM1	-	-	51	50
RBX1	2	2	3	3
SMARCA2	-	-	34	17
SMARCA4	33	18	39	22
TXNRD1	23	22	25	1
VHL	2	2	3	3

(b) Summary statistics comparison of the 4660 proteins shared between the two gradients. While it is clear that non-integer peptide numbers of peptides do not exist, this table affirms the observations from table 15a. Hence confirming the increased performance of the longer chromatography gradient in unique and non-unique peptide detection compared to the shorter 85 minute gradient on an overall protein level.

85 min LC gradient		140 min LC gradient	
Nr. peptides	Nr. unique peptides	Nr. peptides	Nr. unique peptides
13.7 ± 12.6	12.4 ± 11.9	16.1 ± 13.3	14.7 ± 12.7

Overall, the 140 minute gradient showed a higher performance for the SDS-PAGE gelbands than the shorter 85 minute gradient, even though the latter would generally allow for a higher sample throughput. The higher number of overall identified proteins, as well as the higher number of unique and non-unique peptides, are a great advantage of the longer gradient. This increases the chance to detect relevant proteins in proteome profiling experiments, allowing for the selection of the best-suited cell line for turnover experiments. This is especially relevant because the actual protein turnover experiments will feature a more complex peptide matrix due to the missing SDS-PAGE pre-fractionation step preceding the liquid chromatography. Hence, the 140 minute gradient was selected for performing the liquid chromatographic separation for all further samples.

4.2 Cell line proteome profiling

4.2.1 Selection of MaxQuant search parameters

Beside the optimal length of the liquid chromatography gradient, which was selected by means of the SDS-PAGE gelband data in the previous section 4.1. MaxQuant parameters employed for the database search are a further methodological parameter that needs to be taken into account in the workflow optimization. There are several settings that can be tweaked before performing MaxQuant searches. One factor significantly impacting the search stringency is the number of peptides needed for protein identification. A less stringent search performed necessitates at least one peptide that is unique to the protein for protein identification. This type of search is named "One peptide search" in this work and will generally yield a higher number of identified proteins. The "Two peptide search" refers to a more stringent MaxQuant search which necessitates at least one peptide that is unique to the protein, as well as a second peptide for protein identification. This type of search yields higher confidence protein IDs, but might be too stringent for the identification of certain experimentally relevant proteins. The selection of a suitable search parameter therefore is another important methodological parameter that needs to be carefully chosen for the main experiment.

The effects of the two MaxQuant search parameters were tested on the raw data of the proteomic profiling experiments that was obtained by employing the previously selected 140 minute LC gradient. Raw data from both CYT and NE fractions of SUSA, RPMI-8226 (susp. and adh.), HL-60, HL-60 + PMA, HL60 + ATRA profiling experiments was searched with both the "One peptide search" and "Two peptide search" parameters. The former search required at least two peptides, one of which had to be unique to the protein, while the latter required at least one unique peptide for protein identification. An additional filtering step was employed on both resulting data matrices. Proteins needed to be present in at least 70% of samples in one profiling group, e.g. SUSA CYT to be kept in the data matrices used for further analysis.

The number of proteins identified by the two separate MaxQuant searches are shown in the Venn diagram of figure 17. Unsurprisingly, the less stringent search led to the identification of more proteins from the same raw data compared to the more stringent two peptide search.

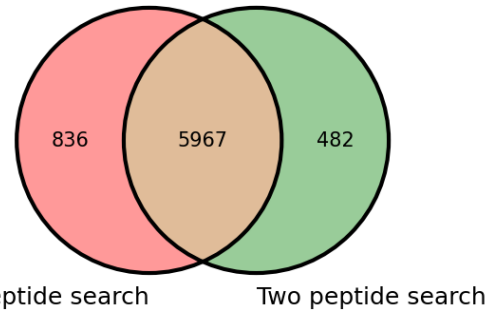

Figure 17: Venn diagram showing the overall number of unique and shared proteins identified in all profiled cell lines and subcellular fractions by employing the two different search parameters. Raw data generated with the 140 minute LC gradient from SUSA, RPMI-8226 (susp. and adh.), HL-60, HL-60 + PMA, HL60 + ATRA profiling was searched by employing both "One peptide search" and "Two peptide search" parameters. Minimum requirement for protein IDs in the datasets was the presence in at least 70% of samples in one cell line and fraction.

The $\log_2$ transformed LFQ intensities were then compared between the two MaxQuant searches. A barplot representing the experimentally relevant proteins for the PMA differentiated HL-60 cell dataset is shown in figure 18 as an example for the overall patterns seen when analyzing all further datasets. As can be seen from the figure, intensity values are slightly higher throughout almost all relevant proteins when performing a less strict one peptide search.

In order to get a deeper insight into the data quality yielded by two MaxQuant searches the two original data matrices containing the $\log_2$ transformed LFQ values were reduced to the

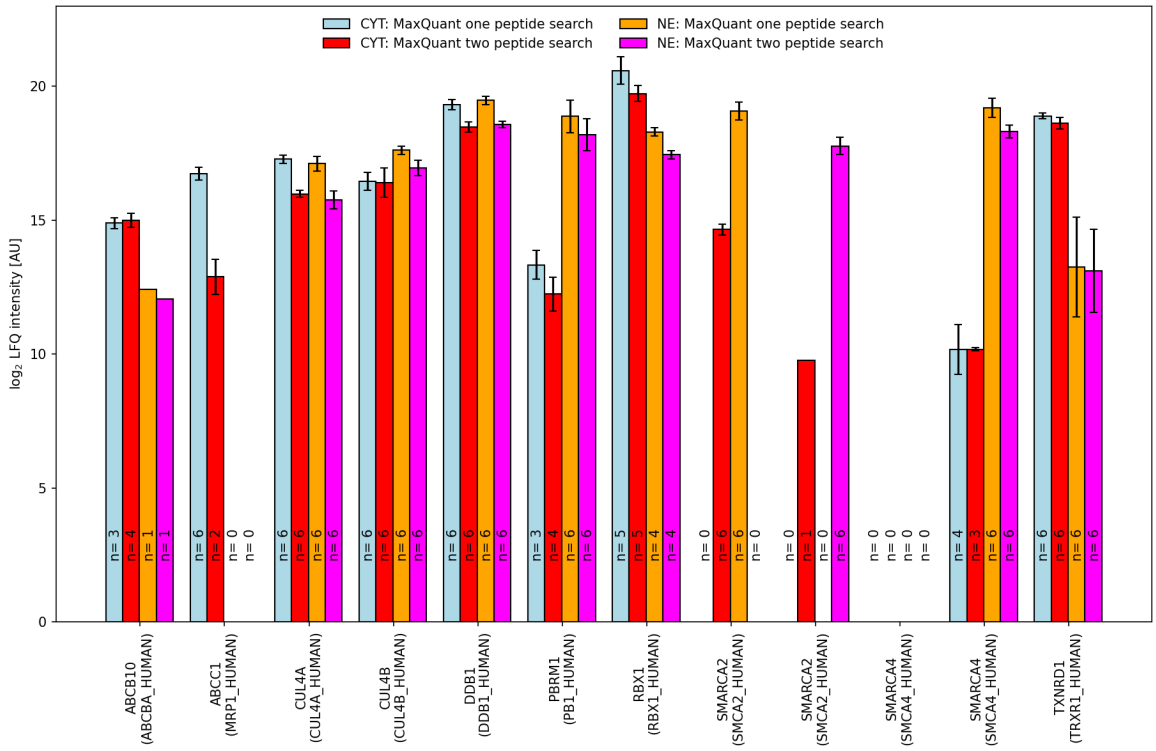

Figure 18: Barplot showing $\log_2$ transformed data of selected experimentally relevant proteins that were identified in the PMA differentiated HL-60 cell data to illustrate the difference of $\log_2$ transformed LFQ intensities between the two MaxQuant searches. The presence of two separate SMARCA2 and SMARCA4 groups is related to the detection of the full-length protein, respectively the left of the two groups, and a shorter isoform of the protein. Full-length SMARCA4 was not detected in PMA differentiated HL-60 cells unlike in other cell-lines, hence the four n=0 entries. CRBN and VHL were not present in the final matrices used for plotting as they were filtered out when applying the 70% "in at least one group" filter step.

5967 shared protein IDs (see figure 17) between
the two searches and transformed to the non-logarithmic scale. Then, coefficients of variation (CVs) were calculated for every protein that was present in at least three of six replicates of each condition (e.g. CYT, One peptide search, HL-60 + PMA). The CV calculation was then repeated for all other conditions with the filtering threshold increased to five out of six replicates.

The CV values were then visualized in form of a scatter plot by plotting the CVs of the one and two peptide MaxQuant searches against each other. Additionally, a violin plot was made from the three out of six replicate filtering threshold CV distribution to assess the CV density distribution.

The resulting scatter plots for the three out of six and five out of six replicate filtering thresholds for the PMA differentiated HL-60 cells are shown in figure 19. The dashed black lines present in the figures shows the x=y line, which would represent the perfect equality of CVs between the two different MaxQuant searches. The green lines, on the other hand, represent the fitted linear function over the actual protein CV distribution in the cytoplasmic fraction.

The linear fits over the shared protein distribution, shown in green in both figure 19a and figure 19b are skewed toward the right of the x=y line, which reveals that the less stringent one peptide search leads to increased CV values compared to the two peptide search. Unsurprisingly, the slope of the fit gradually nears the "perfect" value of one, when the minimum replicate number for inclusion in the final matrix is increased as can be seen from the increase in slope steepness from the three out of six (0.79) to five out of six (0.86) filtering threshold. These observations were also made with the data from all other profiling experiments.

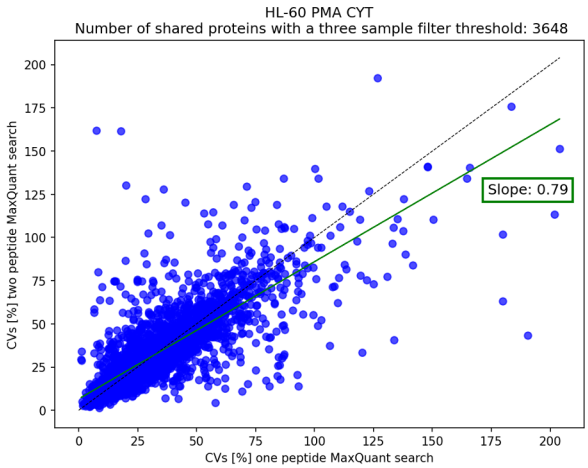

(a) CV value distribution in the cytoplasmic fraction with a filtering threshold of at least three out of six replicates.

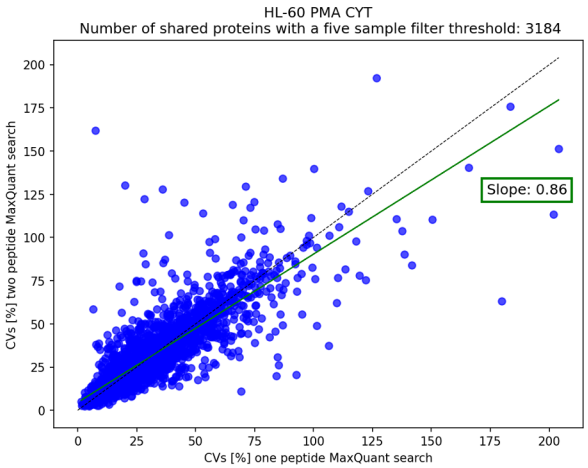

(b) CV value distribution in the cytoplasmic fraction with a filtering threshold of at least five out of six replicates.

Figure 19: Scatter plots visualizing the CV value distribution in the cytoplasmic fraction of PMA differentiated HL-60 cells with two different filtering thresholds. Prior to the application of the filtering threshold the data matrices from the one peptide and two peptide MaxQuant search were reduced to exclusively contain common entries and transformed to non-logarithmic scale LFQ values. As expected, the increased filtering stringency reduces the number of proteins present in the data matrix of shared proteins.

The density distribution of the CV values for the two MaxQuant searches for the three out of six replicate filtering threshold appears to be similar at first sight with the majority of shared proteins showing CVs of around 15%, the median CV value however is lower in the one peptide MaxQuant search as can be seen from the white line in the boxplot of the corresponding dataset.

Unexpectedly, figure 20 shows that the median CV value is lower with the one peptide MaxQuant search parameters, which is quite counterintuitive, especially because the scatter plots in figure 19 suggest that the two peptide MaxQuant search parameters are better suited for searching raw data as they yield lover overall CV values. From this point onward, all further MaxQuant searches were performed with the minimal protein identification threshold of one unique peptide, specifically to increase the number of protein detections, accepting the drawback of a slightly reduced overall LFQ data quality compared to the two peptide search parameters.

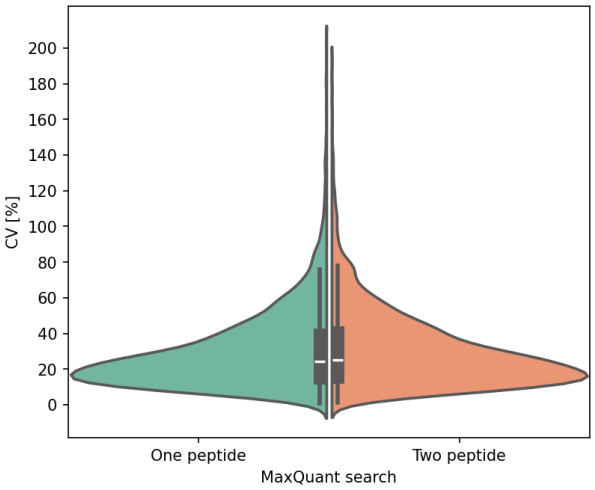

Figure 20: Violin plot of the CV value density distribution for the two MaxQuant searches with the non-logarithmic LFQ data from PMA differentiated HL-60 cells after keeping only proteins present in at least three out of six replicates. The median CV is lower for the one peptide MaxQuant search compared with the median of the two peptide search.

4.2.2 Data quality verification of the acquired proteomes

Based on the knowledge gained from section 4.2.1 the proteome profiling samples were further analyzed by employing the data from the less strict MaxQuant search requiring one unique peptide for protein identification. The data from the profiling experiments searched using the less strict parameters underwent a filtering step that required proteins to be present in 70% of samples of at least one group, e.g. RPMI-8226 CYT, to be retained in the data matrix used for further analysis.

The similarity between samples in the proteomic profiling experiments was then calculated from the filtered data matrix and depicted as a correlation heatmap shown in figure 21. Samples of the same cell line, condition and subcellular fraction are expected to show high correlation among different replicates, as this indicates a low variability introduced by cell culture, sample preparation and LC-MS/MS measurements.

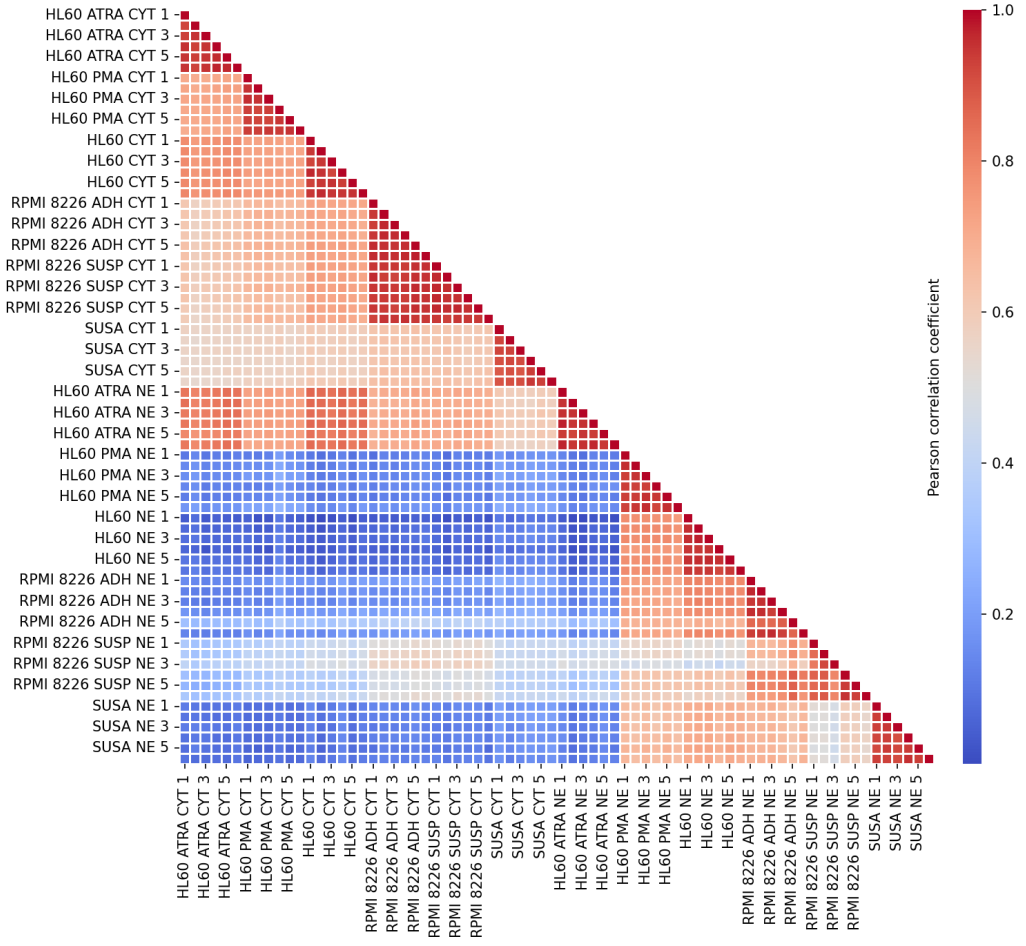

Figure 21: Correlation heatmap containing all cell lines and conditions that underwent the proteome profiling workflow described in section 3.1.4. The peptides resulting from protein digestion were separated by employing the 140 minute LC gradient and searched in MaxQuant requiring one unique peptide for protein identification. The resulting data matrix was additionally filtered to contain only proteins that were present in 70% of replicates of at least one group. Each box in the correlation heatmap contains the color-coded equivalent of the calculated Pearson correlation coefficient between two samples that were generated in the proteomic profiling experiments. This allows to visualize patterns of similarity in the samples. Sample combinations with red-ish boxes are characterized by a higher similarity than combinations with boxes with a blue-ish hue.

Samples belonging to the same "group", e.g. SUSA CYT are, as would be expected, all characterized by very high similarities within the group. This suggests a good reproducibility of differentiation of HL-60 cells with both ATRA and PMA as well as successful and reproducible lysis and workups for all samples. Upon closer inspection one can see that HL-60 ATRA NE samples have a higher similarity to cytoplasm samples of other cell lines and differentiation states, than to other nuclear samples. This surprising similarity can also be seen in the principal component analysis shown in figure 22. All further NE samples do not show this behavior.

The six replicates of the sample nuclear fractions can be located on the right hand side of figure 22´s coordinate system. Replicates of ATRA differentiated HL-60 cells represent the exception as they are positioned in proximity of cytoplasmic fractions. Possibly this effect is linked to the ATRA differentiation, which would however be unexpected as it does not fit the pattern found in the other profiling experiments. The premature lysis of the nucleus by the shearing forces can definitely be excluded, as the CYT and NE fractions would have to be equal, which they are not.

Generally, the three HL-60 conditions showed high levels of similarity, while still being distinguishable from each other in the PCA. Unsurprisingly, as they were cultured in the same flask and separately processed, the same can be written about adherent and suspension RPMI-8226 replicates.

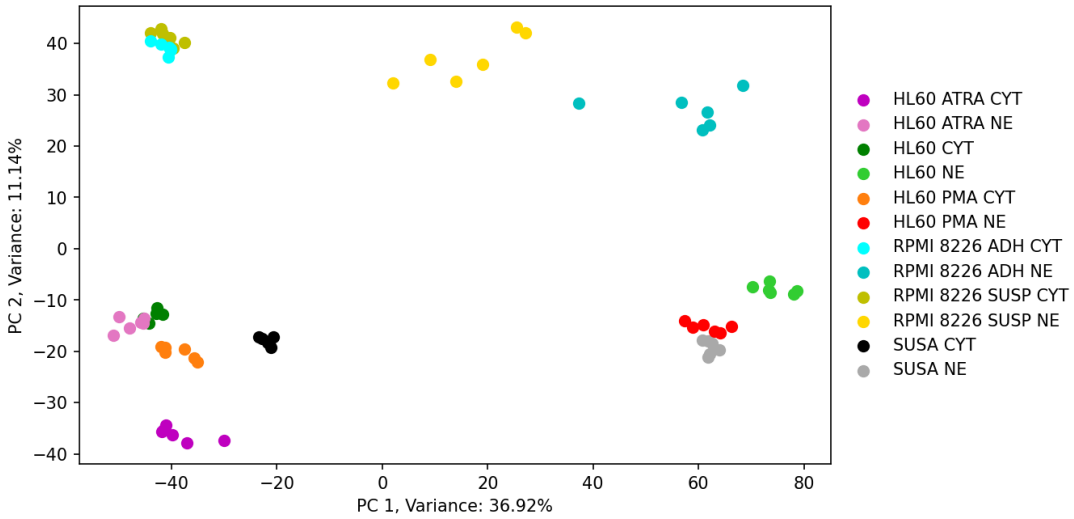

Figure 22: Principal component analysis of the proteome profiling data matrix used to generate the correlation heatmap. Each dot in the PCA represents one proteomic profiling sample, samples that are more similar to each other are clustered together. Replicates from the cytoplasmic fraction cluster in the left hand side of the coordinate system, whereas the nuclear fraction replicates do cluster on the right hand side. The nuclear fraction of ATRA differentiated HL-60 cells represents an exception as it clusters on the left hand side, therefore showing a greater similarity to cytoplasmic fractions of other samples.

Overall, all six replicates of the different groups cluster tightly, hinting toward a low experimental variability introduced throughout all the sample preparation steps. Additionally, the overall separation of CYT and NE samples in the PCA show that the employed subcellular fractionation protocol worked well in separating the cytoplasmic from the nuclear proteins. Hence, it can be concluded that the acquired proteomic profiling data is well suited for further analysis and for planning of future experiments where the knowledge of the cell-line proteome might be needed.

4.2.3 Proof of presence of experimentally relevant proteins

The main goal of the proteomic profiling of the cell lines and the two differentiation states of HL-60 cells was to understand which one of the profiled condition was best suited for the protein turnover measurements with the two available PROTACs. As described in the introduction (section 1.5), the presence of VHL and CRBN was an absolute necessity for the selection of a suitable model system because of the PROTAC mode of action. A further criterion for model system selection was the presence of proteins that are of relevance for PROTAC function as they take part in the ligase formation process or are known drug exporters. Additionally, the presence of literature known targets of the employed PROTACs was also deemed relevant in the selection of the cell line and differentiation state.

The visual comparison of the presence or absence of proteins is aided by profile plots like the one shown in figure 23. At first it was attempted to use the data also used for the creation of the correlation heatmap and PCA from section 4.2.2, which was suboptimal because CRBN and VHL were found in only two samples. Hence, a further search was performed in MaxQuant to yield the data matrix used for the profile plots. Two gel bands from section 4.1 containing the highest number of peptides for CRBN and VHL were identified and the raw data added to the raw data of all the profiling samples. A combined MaxQuant search was run by employing the "match between runs" feature to allow the identification of CRBN and VHL in a higher number of samples. The resulting data matrix was additionally filtered to contain only proteins that were present in 70% of replicates of at least one group. This additional filtering step was too stringent for CRBN and VHL, which is why the profile plot shown in figure 23a came from unfiltered data.

It appears that proteins with higher intensity are detected in the great majority of the samples (e.g. RBX, CUL4A, CUL4B), whereas proteins with lower $\log_2$ LFQ intensities tend to be detected less robustly throughout replicates and conditions. This might be attributed to the nature of data acquisition. More highly abundant proteins potentially yield more peptides during the digestion compared to less abundant proteins, leading to an increased probability of peptide fragmentation and thereafter identification in the different replicates and samples. Interesting patterns can be seen when looking at the SMARCA2, SMARCA4 and PBRM1 profiles. The acquired experimental data fits the reported subcellular location as they appear to be largely located in the nucleus. The mentioned proteins were also detected in Cytoplasmic fractions, but in generally much lower intensities compared to the nucleic fractions.

Both CRBN and VHL were detected in a small number of samples before applying a 70% "in at least one group" filtering. VHL was detected in the Cytoplasm of four PMA differentiated HL-60 cell replicates as well as one HL-60 CYT and adherent RPMI-8226 CYT replicate in the data matrix before filtering. CRBN was identified once in a HL-60 PMA CYT replicate, twice in HL-60 CYT, four times in HL-60 ATRA NE and once in HL-60 NE replicates. All in all, the lacking protein pre-fractionation on the SDS-PAGE gel and the consequently more complex peptide matrix renders the robust detection of VHL and CRBN very difficult in the proteomic profiling experiments.

As can be seen in figure 16 CRBN was exclusively detected in gel band 6, while VHL was only detected in gel band 8. In these two bands both proteins were detected with a high number of unique and non-unique peptides. The number of detected proteins was calculated for both bands and CYT and NE condition. Average and standard deviation of LFQ values of the identified proteins were calculated for both bands and conditions. Subsequently, the number of identified proteins was averaged for the profiled model systems, each consisting of six proteome profiling replicates. Standard deviation and average $\log_2$ LFQ values were calculated for every protein over the six replicates. The resulting $\log_2$ LFQ value averages and standard deviations were then averaged to allow an overall comparison. Only valid values were taken into account for the calculations.

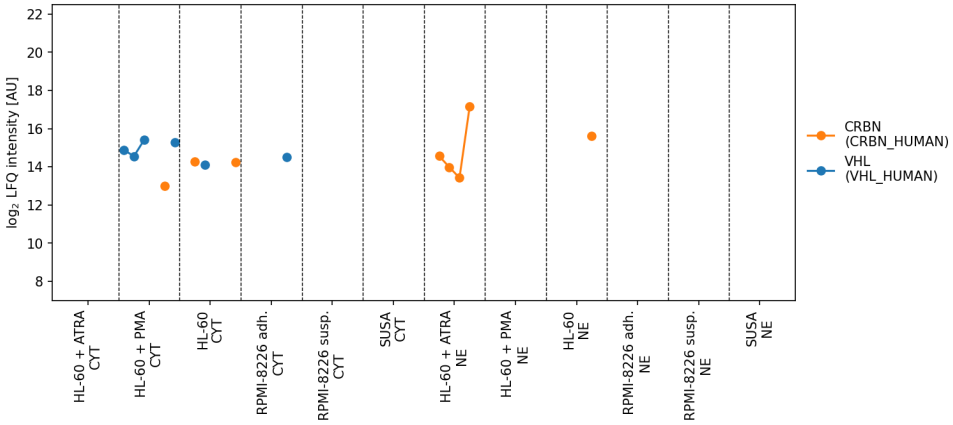

(a) Profile plot showing the presence of CRBN and VHL in the profiled conditions. The profile plot was created from the original data matrix because the additional 70% "in at least one group" filtering step applied to the matrix for the other two profile plots removed the two proteins from the matrix because these two proteins were below the applied filtering threshold.

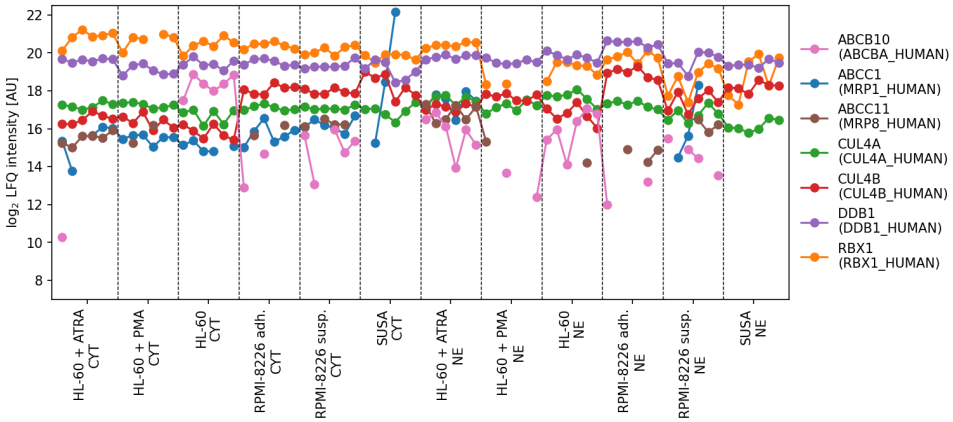

(b) Profile plot showing several proteins that are necessary for a successful PROTAC function, as well as known drug exporters.

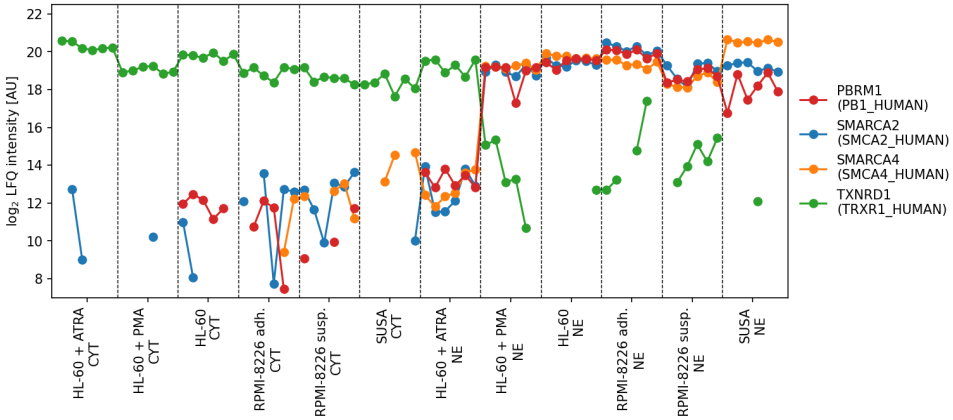

(c) Profile plot showcasing the $\log_2$ LFQ intensities of literature known PROTAC targets of the employed ACBI2 and gold PROTACs.

Figure 23: Profile plots showing the presence and absence of different proteins of interest in the subcellular fractions of the corresponding model systems. The MaxQuant search requiring one unique peptide for protein identification was run with two gel band samples with the enabled "match between runs" feature to boost CRBN and VHL identification in the profiling samples.

The differences between the average number of detected proteins and the overview $\log_2$ LFQ values between the gel band samples and the proteome profiling samples were used in an attempt to depict the increased matrix complexity present in the profiling samples due to the lacking pre-fractionation of the samples on the gel. The calculated values can be seen in table 16.

Table 16: The difference in the number of detected proteins and the overall $\log_2$ LFQ values is hereby used as proxy measure for increased matrix complexity in proteome profiling samples compared to gel band samples. Contrary to the gel bands, which consisted of only one replicate, profiling samples consisted of six replicates for each subcellular fraction and profiled model system. The raw proteome profiling matrix was filtered with the same settings as the gelband matrix (at least one entry in total) to ensure equal filtering conditions in both datasets. The resulting values are shown below.

	Gel Band 6		Gel Band 8	
Sample	CYT	NE	CYT	NE
Avg. $\log_2$ LFQ value	13.29 ± 3.19	13.15 ± 3.22	14.33 ± 3.09	14.21 ± 3.17
Avg. nr. detected proteins	1127	1292	1992	2155
	HL-60 ATRA		HL-60 PMA	
Sample	CYT	NE	CYT	NE
Avg. $\log_2$ LFQ value	16.39 ± 0.48	16.36 ± 0.42	16.64 ± 0.48	16.43 ± 0.54
Avg. nr. detected proteins	3502	4795.3	3508.2	2923
	HL-60		SUSA	
Sample	CYT	NE	CYT	NE
Avg. $\log_2$ LFQ value	16.40 ± 0.48	16.35 ± 0.49	16.40 ± 0.54	16.54 ± 0.56
Avg. nr. detected proteins	4583.8	3096	3230.5	3096
	RPMI-8226 ADH		RPMI-8226 SUSP	
Sample	CYT	NE	CYT	NE
Avg. $\log_2$ LFQ value	16.44 ± 0.48	16.30 ± 0.63	16.31 ± 0.43	16.36 ± 0.75
Avg. nr. detected proteins	4104.7	3618.5	4211	4124.8

Table 16 shows a drastically smaller number of identified proteins in the two gel bands compared to all proteome profiling samples. However, the total number of proteins detected in the eight CYT bands was 4987, while 5343 proteins were detected in the eight NE bands. Again, duplicate etc. identifications were not counted. Overall protein detection numbers are in similar orders of magnitude. The SDS-PAGE gel was run with a HL-60 lysate, that was worked-up in

parallel to the corresponding proteome profiling samples. This shows that the number of protein identifications can be drastically increased by reducing matrix complexity prior to the protein digestion. The differences in the average $\log_2$ values within the proteome profiling samples was very low, the difference between the proteome profiling samples and the gel-band samples on the other hand is noteworthy. There are differences of around three units in $\log_2$ space, which translates into approximately eight fold differences in the average LFQ values detected in the samples. Because of this higher background proteome noise is inevitably higher which renders the identification of low abundant proteins like CRBN and VHL quite difficult as there is a smaller chance that they are fragmented during the experiment.

Protein pre-fractionation on the SDS-PAGE gel proved to be a advantageous as it significantly aided protein detection. A shortcoming of the in-gel digestion protocol, however, is the very high number of steps that needed to be performed until the samples were ready for measurement. The major drawback which negated the use of this technique for all further experiments was the four/eight fold number of samples (depending on the number of bands) for each condition and replicate, which would have disproportionately increased the measurement time.

As a compromise, the MaxQuant search leading to the final data matrix was performed with gelband samples from section 4.1 and the enabled "match between runs" feature. Performing the MaxQuant search with the gelbands therefore aided the detection of VHL and CRBN, as well as probably many other proteins in the proteome profiling samples. Searches without the gelbands at an early stage of the profiling experiments yielded no detection of the VHL and CRBN proteins. The greatest challenge for the robust detection of the two proteins is their low abundance. The $\log_2$ LFQ values of the two proteins in the HL-60 gelbands were found to be between 13.6 and 14.4.

Proteomic profiling experiments showed that the crucial VHL and CRBN proteins could only be found in RPMI-8226 as well as HL-60 cells, therefore the SUSA cell line was removed from further consideration as cell line for the turnover experiments. The RPMI-8226 and the non-differentiated HL-60 cell lines were also excluded from further analyses because both could not be forced into a steady state condition. The steady state condition is crucial for the turnover experiment, as it reduces the number of proteins that are continuously degraded and newly synthesized by the cells. Only proteins that are strictly necessary for the cell survival are synthesized as proliferation has come to a halt. The differentiation of HL-60 cells with ATRA and PMA leads to a steady state, hence both differentiation methods were further analyzed.

4.3 Differentiation of HL-60 cells

The effects of HL-60 cell differentiation can be seen both as morphological changes in cell shape as well as on the protein level. The images in figure 24 show the experimentally achieved differentiation results.

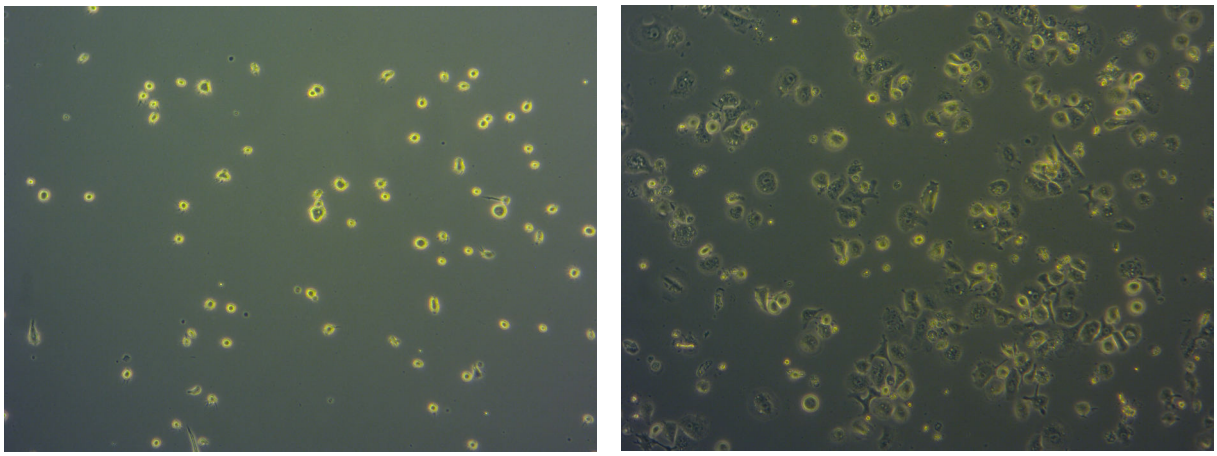

(a) Small number of adherent HL-60 cells after a 72 hour differentiation period with 1 µM ATRA. The picture was acquired with four-fold magnification.

(b) Picture showing 500 $ng \cdot mL^{-1}$ PMA treated HL-60 cells after a 72 hours differentiation timeframe. The picture was acquired with ten-fold magnification.

Figure 24: The differentiated cells were washed twice with PBS prior to the picture acquisition. The pictures show great differences in the number of cells that were adhering to the culture flask. Both chemicals induced morphological changes in HL-60 cells compared to the very round and regularly shaped undifferentiated cells pictured in figure 6c. ATRA differentiated cells mainly displayed a loss of regular shape. The PMA differentiation additionally led to the formation of little-arm-like structures protruding from the cells.

Although HL-60 cells treated with 1 µM ATRA showed some morphological signs of differentiation, the most important feature of a successful differentiation, the transformation from suspension to adherent cells was not observed. These differentiation experiments were performed four times, twice with an older ATRA aliquot and twice with a freshly prepared stock from a newly bought aliquot. Only a minor number of cells appeared to stick to the culture flask, these could could however be returned to suspension by carefully tapping the flask. No explanation could be found for this behavior.

The comparison of the HL-60 proteomes in the three experimentally analyzed differentiation states allows the understanding of the underlying molecular mechanisms that allow the progression of the differentiation. Volcano plots are well suited to highlight differences between those states. Figures 25a and 25b show the comparison between the cytoplasmic and nuclear fraction of ATRA differentiated HL-60 cells, with the corresponding fraction of non-differentiated HL-60 cells (HL-60 CON) by means of a two-sided t-test. Significant and not significant protein regulations were then highlighted accordingly. Figures 25c and 25d show the comparison between PMA differentiated HL-60 cells and the corresponding fraction in non-differentiated HL-60 cells. In a previous work by Meier-Menches et al.[87] HL-60 cell differentiation markers were identified, those differentiation markers were specifically highlighted in the volcano plots by means of black arrows and the gene names.

What stands out in the volcano plots in figure 25 is the fact that practically all differentiation markers, with the sole exception of ACSL1 in the CYT fraction, were up-regulated in ATRA differentiated HL-60 cells. These results on the proteome level were quite unexpected, since the

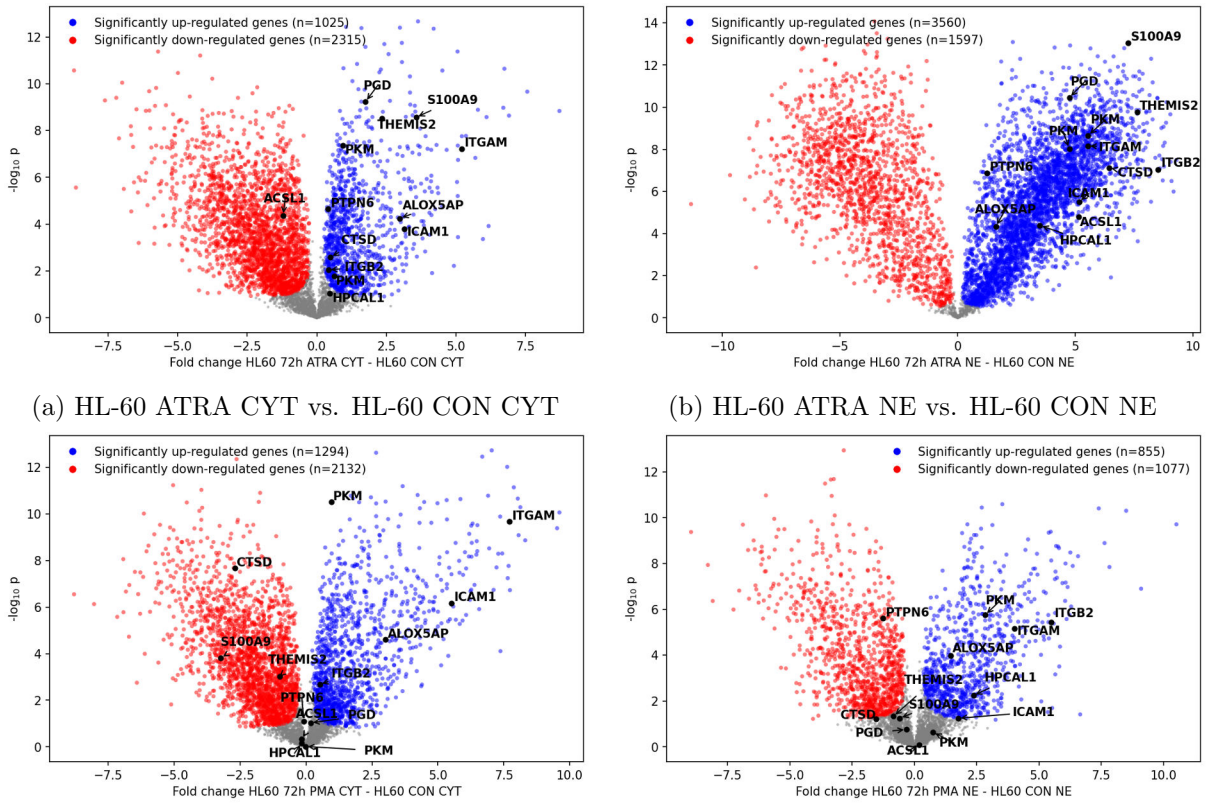

(a) HL-60 ATRA CYT vs. HL-60 CON CYT

(b) HL-60 ATRA NE vs. HL-60 CON NE

(c) HL-60 PMA CYT vs. HL-60 CON CYT

(d) HL-60 PMA NE vs. HL-60 CON NE

Figure 25: Volcano plots highlighting the differentiation effects of PMA and ATRA in HL-60 cells on the subcellular level. Red dots represent significantly down-regulated proteins while blue dots show the significantly up-regulated proteins in differentiated HL-60 cells when compared to the non-differentiated HL-60 control cells. The HL-60 differentiation markers described by literature are highlighted in black.

ATRA treated cells were not exhibiting the expected behavior of differentiating into adherent cells. 100 $ng \cdot ml^{-1}$ PMA treated cells were sticking to the culture flasks, even though the differentiation markers were found to be both up- and down-regulated.

The ATRA differentiation was no longer pursued from that point onward, because of the mentioned issue. Further differentiation experiments were performed with 500 $ng \cdot ml^{-1}$ PMA in order to assess whether the higher concentration would increase the number of cells sticking to the culture flasks. The higher PMA concentration proved to be more effective in differentiating HL-60 cells compared to the lower concentration. Hence, all further differentiations were performed with 500 $ng \cdot ml^{-1}$ PMA in culture medium.

4.4 MTT cytotoxicity assays

Having decided on the model system for the turnover experiments, MTT cytotoxicity assays were performed in order to select suitable treatment concentrations for the different compounds. The results of the cytotoxicity assays performed on the PMA differentiated HL-60 cells are shown in figure 26.

Sub EC_{50} concentrations of Cycloheximide, Bortezomib and ACBI2 were therefore chosen for preliminary experiments, based on these results. Preliminary experiments were performed with 10 nM in-well Cycloheximide concentrations and 10 nM Cycloheximide + 100 nM ACBI2 co-treatments, in both cases well below the EC_{50} values of 1.17 μM and 2.94 μM respectively. For preliminary proteasomal inhibition experiments a 25 nM Bortezomib concentration, which is relatively close to the EC_{50} concentration of 38.72 nm, was chosen to incubate the cells for two hours, followed by a second four hour incubation step with 1 nM ACBI2.

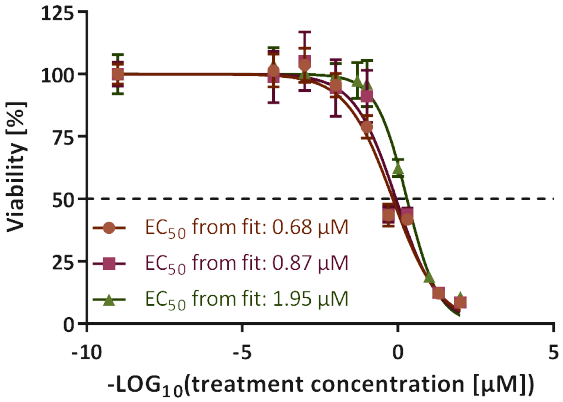

(a) Cycloheximide

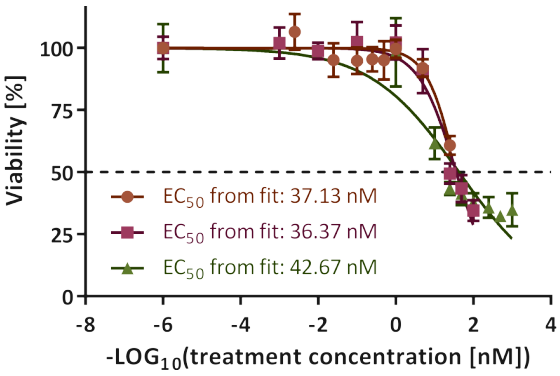

(b) Bortezomib

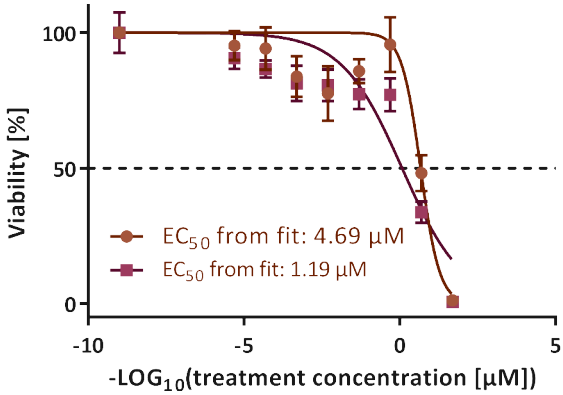

(c) ACBI2 PROTAC + 42 nM CHX

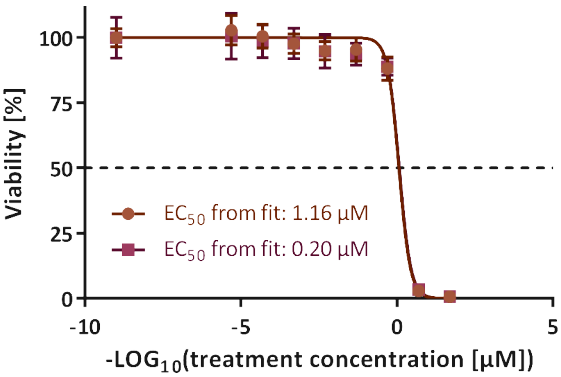

(d) Cis ACBI2 + 42 nM CHX

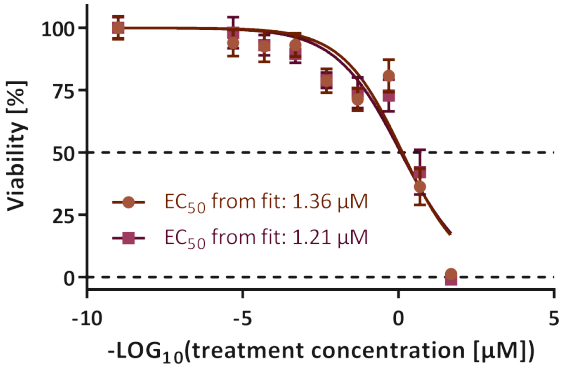

(e) ACBI2 PROTAC + 42 nM CHX + 1 nM Bortezomib

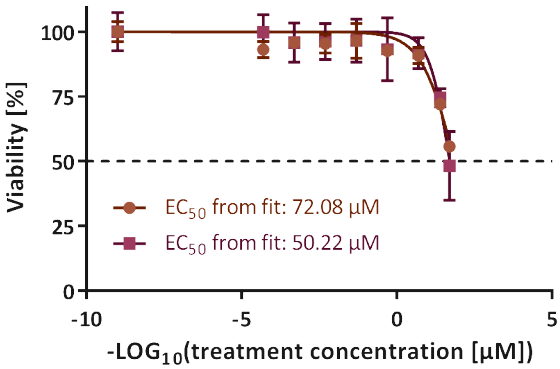

(f) Gold PROTAC + 42 nM CHX

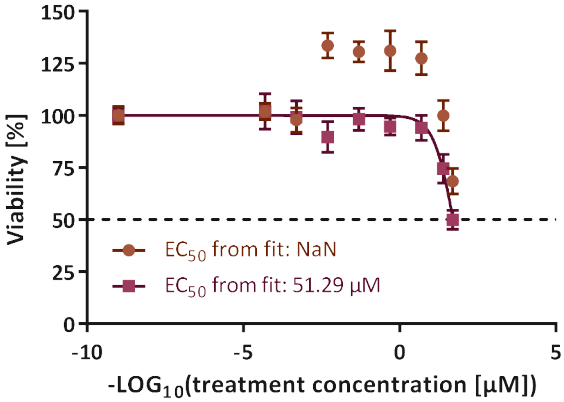

(g) Gold PROTAC + 42 nM CHX + 1 nM Bortezomib

Figure 26: Combined EC_{50} plots displaying the results of the MTT cytotoxicity assays.

4.5 Step-wise model system optimization

4.5.1 Preliminary timeseries experiment

The preliminary timeseries experiment performed to better understand the employed model system showed that the 10 nM Cycloheximide treatment concentration was not nearly sufficient for *de-novo* protein synthesis inhibition. The remaining protein fraction after an incubation period of 24 hours was above 95% for all proteins that were detected over the course of all timepoints in the Cycloheximide treated samples. A number of proteins was only missing in wells treated with 100 nM ACBI2, hinting toward a successful degradation of proteins over the course of the chosen timeframe.

Overall, the preliminary experiment showed that higher Cycloheximide concentrations were needed to allow *de-novo* protein synthesis inhibition to a sufficient degree. The ACBI2 treatment concentration was retained for further experiments, since successful degradation of certain proteins was detected. Sampling timepoints were changed from t_{0h}, t_{2h}, t_{4h}, $t_{7.5h}$, t_{24h} to shorter intervals, especially at the beginning in order to detect more quickly degraded proteins. Hence t_{0h}, $t_{0.5h}$, t_{1h}, t_{2h}, t_{4h}, t_{8h} timepoints were chosen for the main experiment.

4.5.2 Proteasomal inhibition with Bortezomib

No effects of Bortezomib were seen in wells treated with 25 nM Bortezomib over the course of 2 hours prior to a 4 hour 1 nM ACBI2 treatment. It was decided to increase the incubation time from 2 hours to 4 hours.

4.5.3 Optimization of Cycloheximide treatment concentrations

Several Cycloheximide (CHX) concentrations were tested on PMA differentiated HL-60 cells ranging from 40 nM, 200 nM up to 1 µM over the course of 24 hours to ensure a sufficient inhibition of *de-novo* protein synthesis. The effect on the proteome was visualized by means of volcano plots as they allow the comparison of the proteome of CHX treated PMA differentiated HL-60 cells with non-treated PMA differentiated HL-60 cells as the control group. Two volcano plots showing the proteome-wide regulations of 40 nM CHX and 1 µM CHX can be seen in figure 27a and 27b respectively.

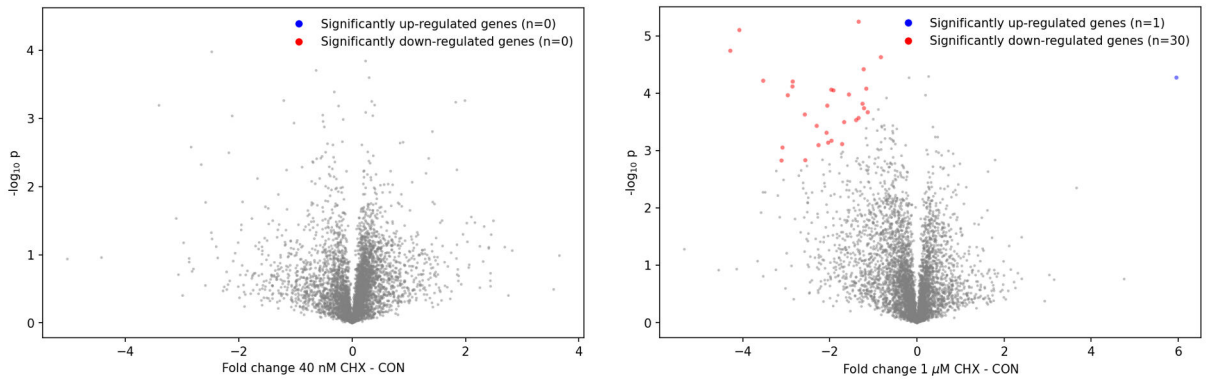

(a) 40 nM CHX vs CON

(b) 1 µM CHX vs CON

Figure 27: Volcano plots showing the proteome regulations induced by both 40 nM and 1 µM CHX treatments on PMA differentiated HL-60 cells.

As can be seen in figure 27 no significant regulation occurs with a 40 nM treatment, while only very few were induced upon 1 µM CHX treatment. The volcano plot for the 200 nM CHX treatment is not shown as it showed less regulations than the 1 µM CHX treatment. The almost non-existing protein synthesis inhibition detected in the preliminary timeseries experiment with

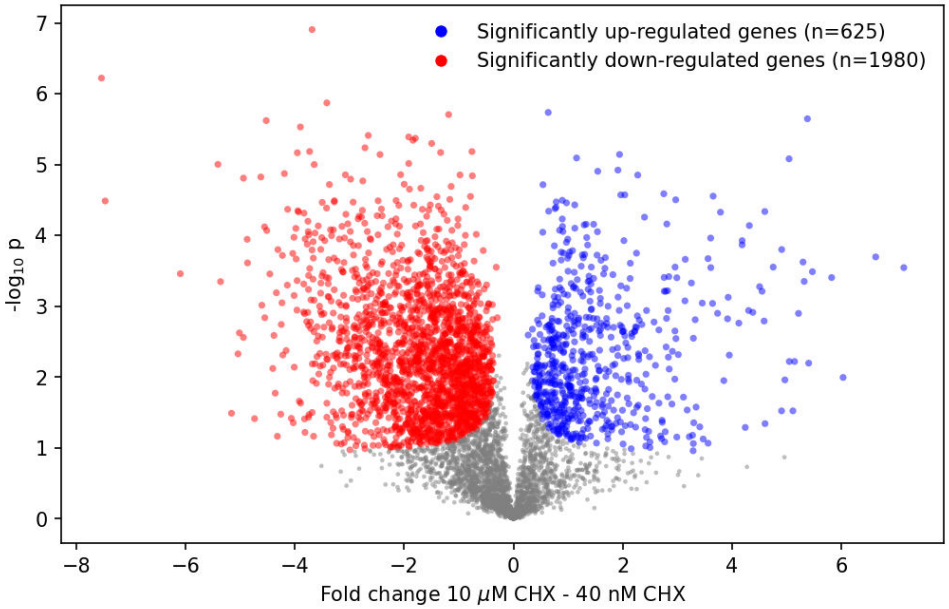

Figure 28: Volcano plot showing the proteome-wide regulations occurring upon *de-novo* protein synthesis inhibition over the course of 24 hours with a 10 µM CHX treatment compared to a 40 nM CHX treatment in PMA differentiated HL-60 cells.

only a 10 nM Cycloheximide treatment concentration (section 4.5.1) can therefore definitely be attributed to an insufficient Cycloheximide concentration.

This hinted toward the fact that a higher Cycloheximide was needed to actually inhibit protein synthesis in the PMA differentiated cells. Hence, a further treatment was performed with 10 µM CHX. The inhibited *de-novo* synthesis of proteins should present itself as a massive down-regulation of proteins compared to control cells or lower concentration CHX treatments, therefore a mostly left facing volcano plot was expected upon successful inhibition of protein synthesis. Figure 28 shows the volcano plot resulting from the comparison of the 10 µM CHX to the 40 nM CHX inhibition over the course of 24 hours.

The 10 µM CHX treatment led to the strong down-regulation of almost 2000 proteins. The, due to the nature of the experiment, unexpected up-regulation of proteins in the volcano plot can be explained by the normalized protein amount used for the digestion. Some proteins inside the highest concentrated CHX sample had to be present in higher amounts compared to the lower concentration CHX sample, otherwise it would have been impossible to reach 20 µg for the digestion if all proteins had only been down-regulated.

Overall, the 10 µM CHX treatment appeared to inhibit *de-novo* protein synthesis in a sufficient manner. The main turnover experiment and the BOCNCAT experiment was therefore performed with a 10 µM CHX concentration.

4.6 PHIO Cellwatcher assays

The Cellwatcher module was used to continuously monitor the confluence during the 72 hour differentiation timeframe of the $0.5 \cdot 10^6$ HL-60 cells induced by 500 $ng \cdot ml^{-1}$ PMA in the culture medium. After 72 hours the assay was stopped and the cells treated with CHX + ACBI2 PROTAC, CHX + gold PROTAC and solvent matched with DMSO to the CHX + Gold PROTAC condition as control condition. The employed CHX, ACBI2 and gold PROTAC concentrations were equal to the actual timeseries experiment described in section 3.1.8. Briefly, a 10 µM CHX concentration was paired with either a 1 nM ACBI2 PROTAC or 60 µM gold PROTAC for the assay. The assay was then resumed for further 24 hours. The results from the continuous confluence tracking can be seen in figure 29.

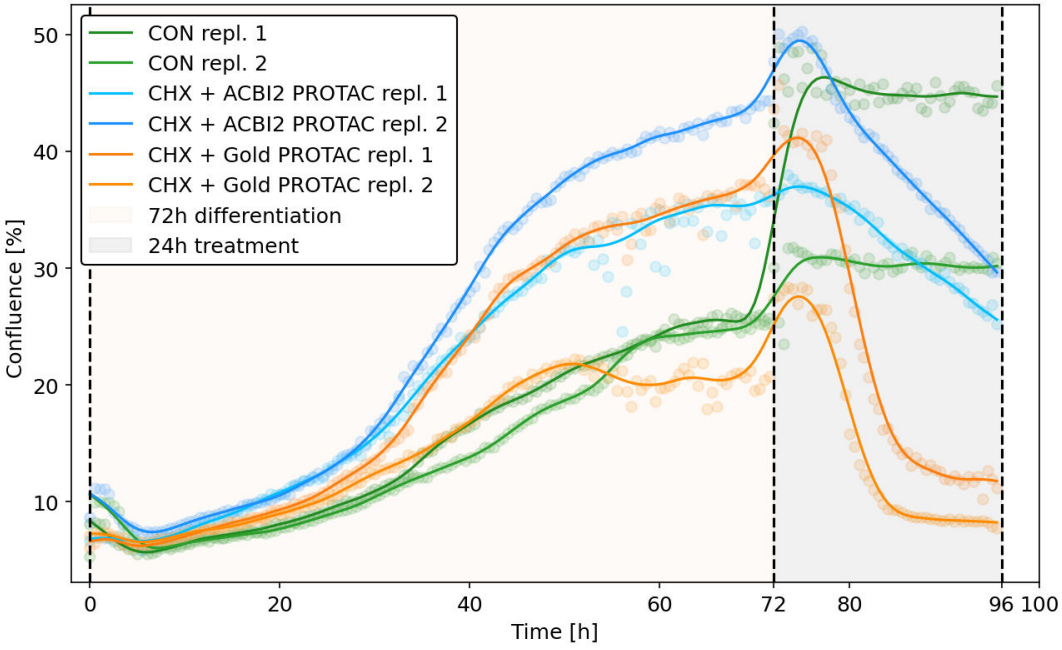

Figure 29: Continuous confluence tracking allowed by the Cellwatcher module showed different progression patterns for the duplicates of different conditions after the start of the treatment period. Green colored lines and dots represent the solvent matched control cells, blue markers show the CHX + ACBI2 PROTAC condition, while orange markers show the CHX + gold PROTAC conditions.

All replicates start at a low confluence, probably due to the fact that the cells are suspension cells and are out of the focus plane of the microscope unit. As time progresses confluence increases steadily up to the 50 hour mark, where confluence starts to reach a plateau. Confluence spikes shortly after the treatment, possibly because fresh medium was added to the wells containing DMSO, which is also known to differentiate HL-60 cells. The confluence progression differs drastically between conditions after the 75 hour mark. Control cells show no increase or decrease until the end of the assay, which confirms that the cells have been differentiated into a steady state where proliferation no longer takes place on a detectable scale. The two CHX + ACBI2 PROTAC replicates are characterized by a continuous decrease in confluence, while the two CHX + gold PROTAC samples feature a steep drop in confluence with progressing assay length. The strong decrease in the CHX + gold PROTAC samples can be explained by the gold PROTAC treatment at EC_{50} concentration combined with the high DMSO percentage in the sixwell of 0.54% that inevitably caused the death of a big fraction of the present cells. The death of a significant number of cells was visually confirmed by the presence of great amounts of cell debris compared to the other conditions when checking the cells in the microscope after the experiment was concluded. Images taken after completion of the assay are shown in figure 41a, 41b and 41c of the appendix.

The confluence was also monitored to understand whether the medium used for the BONCAT experiment affected the proliferation of differentiating HL-60 cells over the course of a 72 hour timeframe. The main difference between the two employed RPMI-1640 media was that the BONCAT RPMI-1640 medium contained L-Azidohomoalanine as a surrogate for L-Methionine, which is present in the standard RPMI-1640 medium used for all other experiments. It is noteworthy that the final BONCAT medium definitely contained L-Methionine as it, like the standard RPMI-1640 medium, was supplemented with 10% FBS. The confluence tracking results over the course of the 72 hour differentiation period can be seen in figure 30.

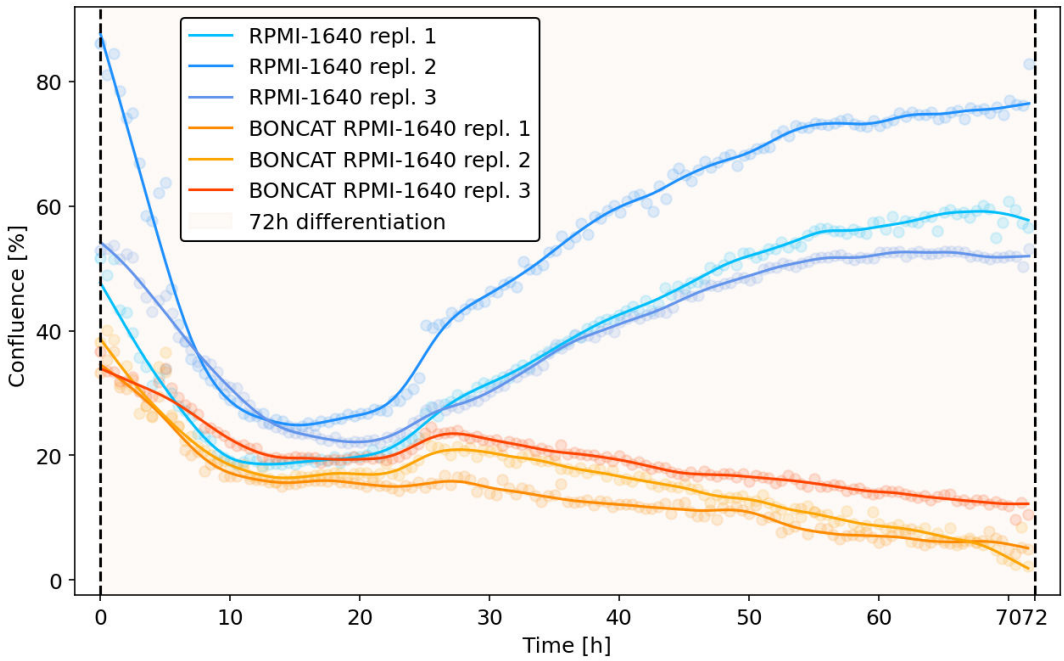

Figure 30: The confluence tracking results revealed great differences in the confluence progression over time between the standard RPMI-1640 medium, shown in blue markers, and the BONCAT medium which is shown with orange markers.

The starting confluence in all conditions was substantially higher than in figure 29, this is mainly due to the higher number of cells that were seeded into the wells. The confluence progression pattern of the standard RPMI-1640 replicates was very similar to the one seen in figure 29, showing a good reproducibility of the differentiation in the employed model system. The BONCAT medium on the other hand led to a steady decrease of confluence after the 27 hour mark, which was probably caused by the death of a significant number of HL-60 cells. A snapshot of the cells taken after assay completion showed a great amount of debris caused by death cells. The picture can be seen in figure 41d.

4.7 Evaluation of signature apoptosis marker proteins

The progression patterns of the continuous proliferation tracking by means of the Cellwatcher did hint toward the death of a significant amount of cells in certain conditions. The not negligibly small amount of cell debris in the pictures of figure 41 corroborated the expectation to find an up-regulation of proteins that play important roles in apoptotic cell death signaling. The data matrix resulting from the MaxQuant search was processed as described in section 3.5 and was additionally filtered to contain only proteins that were present in at least 70% of all the timeseries samples. Then, profiles of known apoptosis markers were aggregated and plotted in figure 31 in form of two separate profile plots for improved readability.

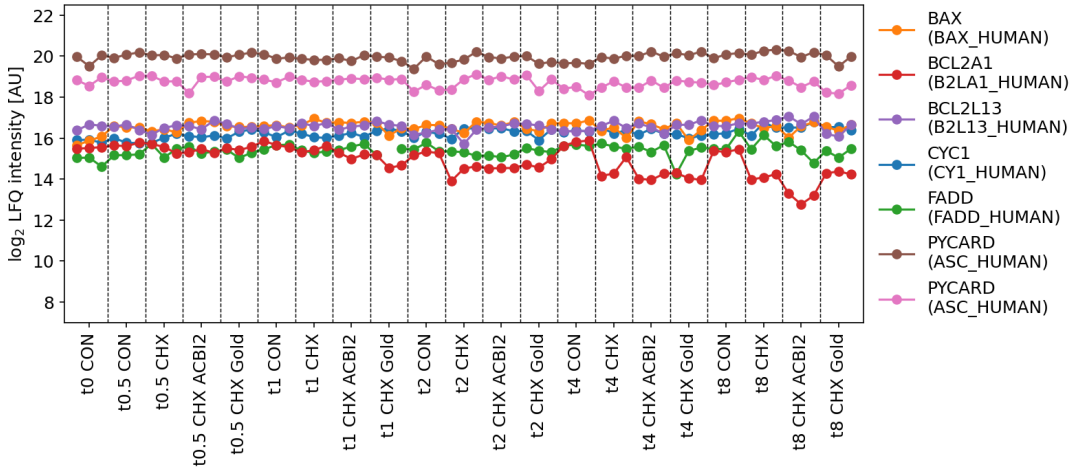

(a) General apoptosis marker proteins present in the timeseries samples.

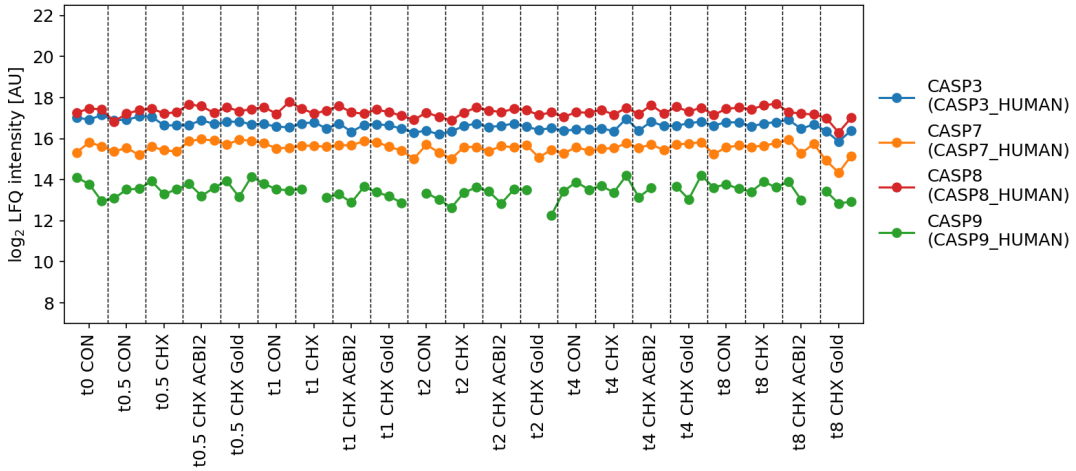

(b) Caspases as apoptosis markers in the measured timeseries samples.

Figure 31: Profile plots showing the $\log_2$ transformed LFQ values for known apoptosis marker proteins present in timeseries samples used for the determination of protein turnover rates in PMA differentiated HL-60 cells. Proteins included in the data matrix used for plotting needed to be present in at least 70% of the all samples.

The great expression stability of the different apoptosis marker proteins shown in figure 31 suggests that apoptosis did not significantly interfere with the timeseries experiment in the experimentally relevant timeframe.

4.8 Evaluation of PROTAC treatment effects on experimentally relevant proteins

In order to get a rough overview of the treatment effects, $\log_2$ transformed intensities of experimentally relevant proteins were visualized in form of profile plots. The data matrix resulting from the MaxQuant search was pre-processed using standard parameters, the stringency of applied additional filtering parameters was then changed according to find as many experimentally relevant proteins as possible. The resulting profile plots are shown below in figure 32c.

Figure 32a is not extremely relevant to the actual protein turnover experiment, as is figure 32b. Both plots show that it is possible to robustly detect experimentally relevant proteins also employing a whole-cell lysate workup, which compared to sub-cellular fractionation employed when profiling the cell lines, yields more complex sample as both cytoplasmic and nuclear fractions are present in one single sample. The intensity range of CRBN and VHL is approximately equal to the proteomic profiling samples (figure 23a), proteins relevant for PROTAC function were found to be of slightly lower intensity when compared to profiling samples in figure 23b.

The profile plot for PROTAC targets shown in 32c is much more interesting. TXNRD1 appears to be present at a high abundance in all timeseries replicates even though it was mostly present in high abundance in cytoplasmic samples. This is in contrast to the intensity values of the other known PROTAC targets, which generally appear to settle between the CYT and NE values of the profiling samples from figure 23c. As already mentioned, TXNRD1 was detected in high intensities in every sample, hence TXNRD1 was not affected by the gold PROTAC. Also SMARCA4 was detected in almost all conditions, which confirms that ACBI2 does not lead to degradation of said protein. SMARCA2, a SMARCA4 paralogue, and a known target for the ACBI2 PROTAC was not found to be present in any sample of the CHX + ACBI2 condition, which speaks for a very fast effect of the PROTAC. The SMARCA2 absence in two of the three t_0 CON samples is quite puzzling, however since the protein was robustly detected in almost all other samples detection issues were dismissed. PBRM1, a second reported ACBI2 target, was detected in all but the CHX + ACBI2 condition, which again speaks for a very fast effect of the ACBI2 PROTAC.

Several MDM2 substrate proteins and functional partners were identified both with a literature research and a STRING database search because of literature-reported effects of Cycloheximide treatments on MDM2 substrate proteins. (section 1.2.2).[88] No noticeable regulations could be detected in the profile plots.

4.9 Evaluation of the effects on experimentally relevant proteins upon Bortezomib rescue

As was done in section 4.8 for the timeseries samples, profile plots were used to get a general overview of the treatment effects in the Bortezomib rescue experiments. The resulting profile plots are shown in figure 33.

Like in section 4.8 the profile plots in figures 33a and 33b are not extremely relevant for the PROTAC effect as they only show that the detection of the proteins of interest is robust in the samples. Figure 33c shows that the expected effect of PROTAC target rescue upon incubation of the cells does not occur on the known ACBI2 protein targets. As in the timeseries samples, TXNRD1 was expressed in high levels in the six samples, a further confirmation that the gold PROTAC did not degrade the protein as expected. The four hour incubation with Bortezomib prior to the treatment with ACBI2 did not prevent SMARCA2 and PBRM1 to be degraded by the PROTAC. The rescue of the known ACBI2 targets with Bortezomib treatment therefore failed.

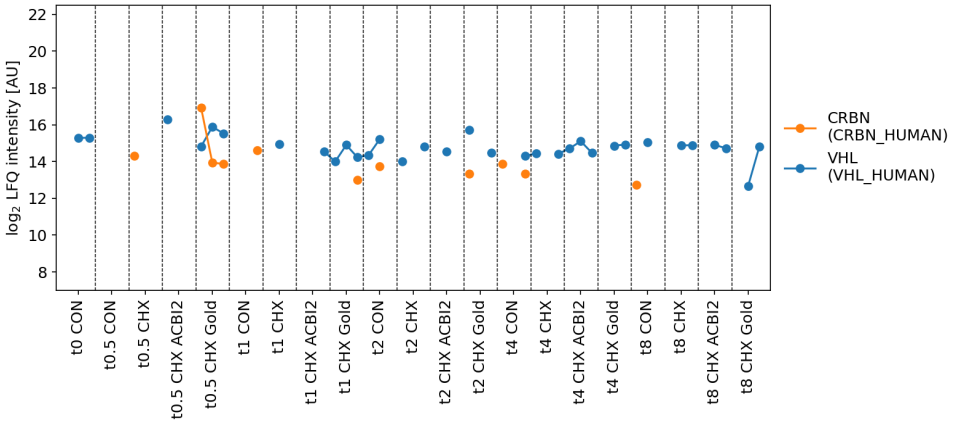

(a) Profile plot showing the presence of VHL and CRBN in the timeseries samples used for the determination of protein turnover. A very lenient filtering was applied to the data. To be included in the final data matrix used for plotting, proteins needed to be present in at least one of the samples.

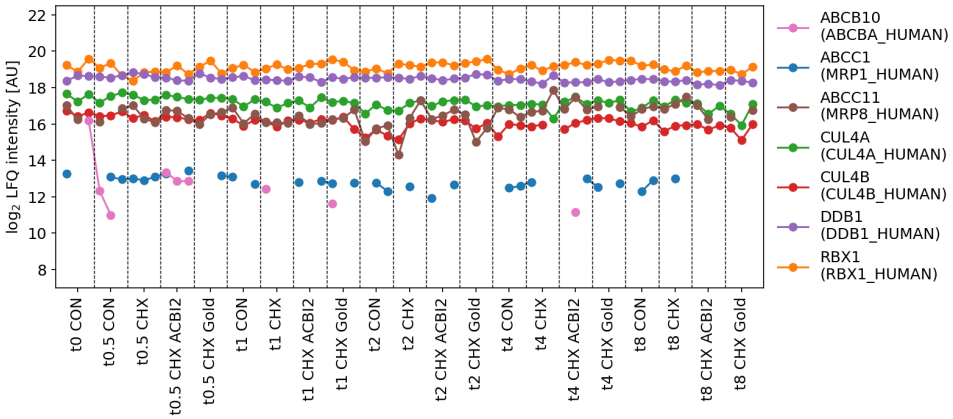

(b) This profile plot shows several proteins that are relevant for successful PROTAC function as well as drug exporters, which play a role in the removal of the PROTAC from the cell. The filtering employed on the data matrix was not stringent, only proteins present in at last one group e.g. t_{2h} CON were kept in the data used for plotting.

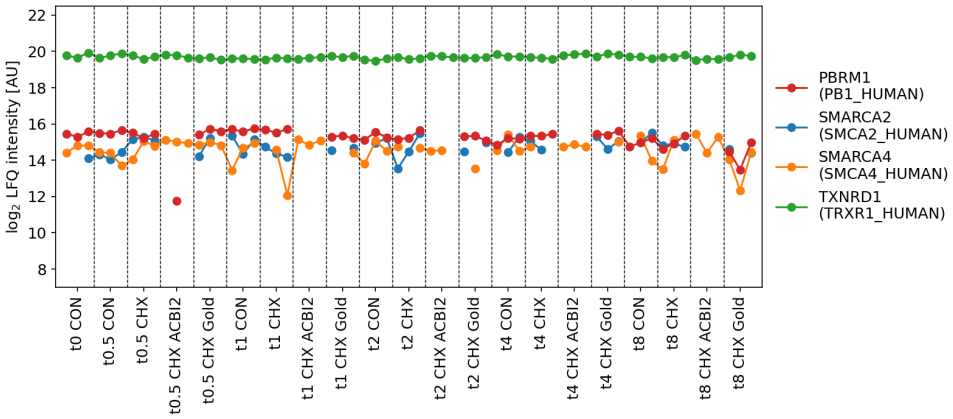

(c) Literature known PROTAC targets of the employed gold PROTAC and ACBI2 PROTAC in the different conditions. The final data matrix used for plotting was filtered to contain only proteins that were present in at least one group.

Figure 32: Profile plots showing the $\log_2$ transformed LFQ values for proteins of interest present in the different conditions of the timeseries experiment. The applied additional filtering steps are stated in the caption below the corresponding plot.

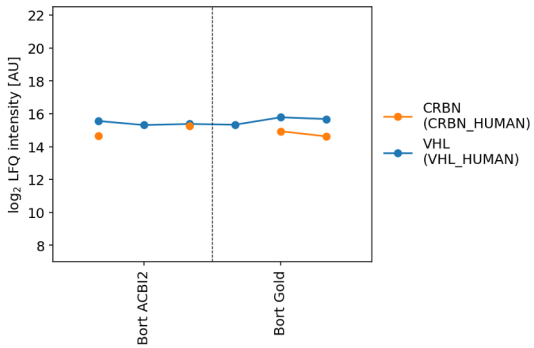

(a) The profile plot shows the presence of VHL and CRBN in the Bortezomib rescue samples. This plot was created by filtering the data matrix to contain only proteins that were present in at least one sample.

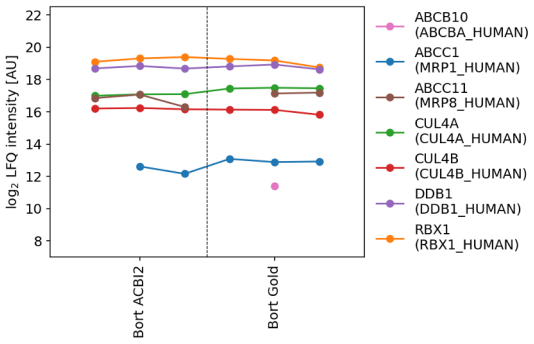

(b) Proteins relevant for PROTAc function and known drug exporters are shown in this profile plot. Proteins not fulfilling the filtering threshold of one protein in at least one group were removed from the data matrix.

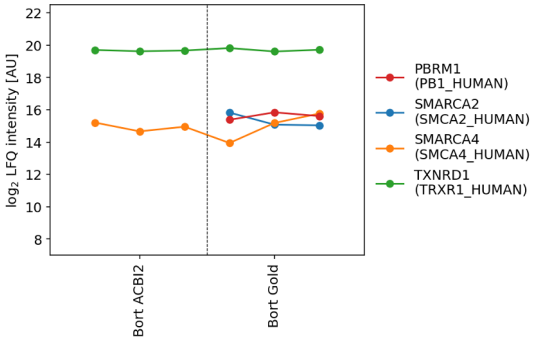

(c) Known ACBI2 and gold PROTAC targets are shown in the profile plot. The filtering applied to the data matrix was very lenient, proteins present at least one in one group were kept in the matrix as stricter filtering would have removed SMARCA2 from the matrix.

Figure 33: Log_2 transformed LFQ values of experimentally relevant proteins of interest that were present in the Bortezomib rescue experiments performed on PMA differentiated HL-60 cells. The different filtering thresholds applied to the data matrices are mentioned below the corresponding plot.

4.10 Global qualification of the timeseries dataset

While profile plots can provide a qualitative overview on a small amount of proteins, they are hardly suited for unraveling biological data from time resolved high sample number experiments. As previously mentioned, the raw data matrix from the MaxQuant search was pre-processed using the standard procedure described in section 3.5.

The data matrix resulting from the standard processing procedure was additionally filtered to only contain proteins that were present in at least 70% of the samples. A correlation heatmap was created to assess the similarity between the different timeseries experiment samples. The pearson correlation coefficient colorbar of the heatmap 42 suggests a high degree of similarity across all samples. This demonstrates that both the CHX and CHX + PROTAC treatments did not significantly affect the PMA differentiated HL-60 cell model system on a proteome-wide scale during the experimental timeframe. Low pearson similarity coefficients between samples as when comparing the different cell lines (figure 21) would not have been expected as, in this case, all samples stem from the same model system. The high similarity between samples suggests that the treatments exerted effects on a small subset of proteins instead of causing changes on the whole proteome level, as would be expected for targeted protein degradation.

To evaluate the timeseries data LFQ values in $\log_2$ space of the whole data matrix were transformed to LFQ values. These LFQ values from each protein were then normalized to the averaged LFQ value from the t_0 CON condition triplicate of the corresponding protein. This yielded the protein fraction remaining (PFR), expressed in percentages, in each sample. A strict filtering threshold was applied to the resulting data matrix in order to keep only proteins that were robustly detected in three of three replicates throughout the data matrix. Subsequently, averages and standard deviations of the protein fraction remaining values were calculated for each triplicate. Proteins were then analyzed based on the PFR data matrix.

Since protein synthesis was expected to be inhibited by CHX, proteins from samples treated with CHX (CHX, CHX + ACBI2 PROTAC and CHX + gold PROTAC conditions) were generally expected to display decreasing fraction remaining values in increasing timepoints. On the other hand, proteins from CON samples would technically be expected to keep a steady over the course of the experiment. This is because degraded proteins should be replaced without issues as *de-novo* protein synthesis is not inhibited by CHX treatment.

In an effort to understand the complex data matrix that resulted from the timeseries experiment. A subgroup of proteins from both the control (CON) and Cycloheximide (CHX) conditions was classified as stable proteins. The arbitrary requirement for classification as a stable protein was a PFR between 80% and 120% of the over all (0, 0.5, 1, 2, 4 and 8 hour) timepoints of the timeseries experiment.

This classification allows to understand a subset of the proteins from the data matrix better than before. Proteins from the stable Cycloheximide subset probably do possess half-lives, that are higher than the timeframe investigated in this experiment as their PFR does not drop below the 80% fraction remaining threshold within the eight hour mark.

Proteins were additionally classified by their degradation patterns over the course of the timeseries experiment. Proteins were classified based on several patterns. Proteins needed to exhibit decreasing PFR values only between the $t_{0.5h}$ treated condition and a t_{1h} treatment condition to be classified in the "forced reduction pattern $t_{0.5h}$ t_{1h} group" of the corresponding treatment. Data points of $t_{0.5h}$ were taken as a starting point for all non-CON samples, while t_{0h} was used as starting point for CON samples.

Inclusion stringency to further groups was gradually increased with increasing number of timepoints over which the PFR remaining needed to be lower than the previous timepoint. The number of proteins present in these groups decreased with the increasing number of timepoints,

as was generally expected.

Combining these two classification types allows the visualization of the number of stable and decreasing protein IDs with the inclusion of different numbers of timepoints in form of barplots. The pie charts above the associated barplots in figure 34 show the percentage distribution of the different classifications.

A clear trend does appear in figure 34 for both the CON and CHX conditions. The number of stable CON and stable CHX proteins is equal over all the decrease patterns as they were arbitrarily defined this way. In both the CON (figure 34a) and CHX (figure 34b) condition stable proteins make up for 33% and 36% of all proteins respectively. As the number of considered timepoints is increased, the number of proteins featuring robustly decreasing PFR values over the considered timepoints is reduced. The number of proteins with the most robust LFQ decrease pattern is much smaller in the CON condition compared to the CHX condition (44 vs 133 IDs), which suggests that the CHX treatment did indeed induce a robust *de-novo* protein synthesis inhibition. The overall number of proteins that show a robust LFQ reduction pattern over all experimental timepoints is not very big, which suggests that a steady state was achieved as CHX would have affected a proliferating model system to a higher degree.

An alternative overview of the mentioned effect can be achieved by means of Venn diagrams. A venn diagram made from both stable and decreasing protein IDs from the CON and CHX conditions can provide additional information as it shows the number of overlapping protein IDs between groups. Again, figure 35 shows very clearly how the number of proteins displaying a continuous decrease in the PFR plummets when including more timepoints.

The Venn diagrams from figure 35 generally show the same patterns as the bar graphs and pie charts from figure 34. The number of overlapping protein IDs between the different conditions decrease with the increasing number of considered timepoints because less proteins get classified as "decreasing" in both CON and CHX conditions. Proteins can be classified both as stable proteins and decreasing proteins, because they fit both the corresponding LFQ decrease pattern over the different timepoints and do not go lower than the lower PFR limit of 80% used to classify stable proteins. What stands out, however, is the steadily increasing overlap between stable CON (purple oval) and CHX (red oval) protein IDs that can be seen when looking at diagrams with an increased number of timepoints. As already mentioned, the number of decreasing CHX proteins is low, which suggests that the protein synthesis inhibition with CHX does affect certain proteins more than others.

It can be assumed that some protein IDs classified as "stable CHX" proteins, will be from proteins that have high half-lives. Thus, their PFR did not decrease below the 80% PFR threshold over the eight hour time window of the experiment.

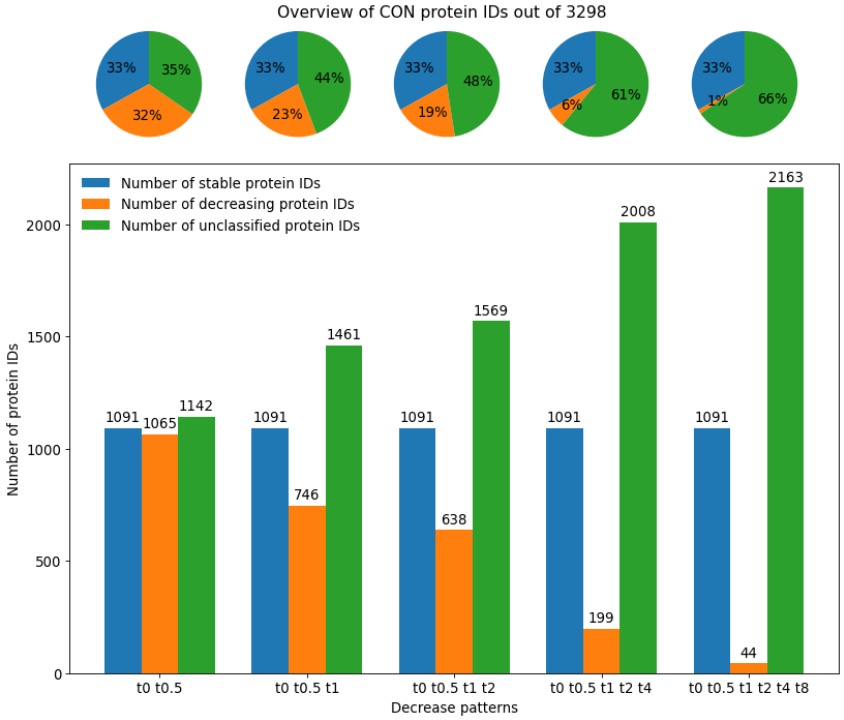

(a) Barplot and corresponding pie chart respectively showing the number and percentage of protein ID classifications in the CON condition.

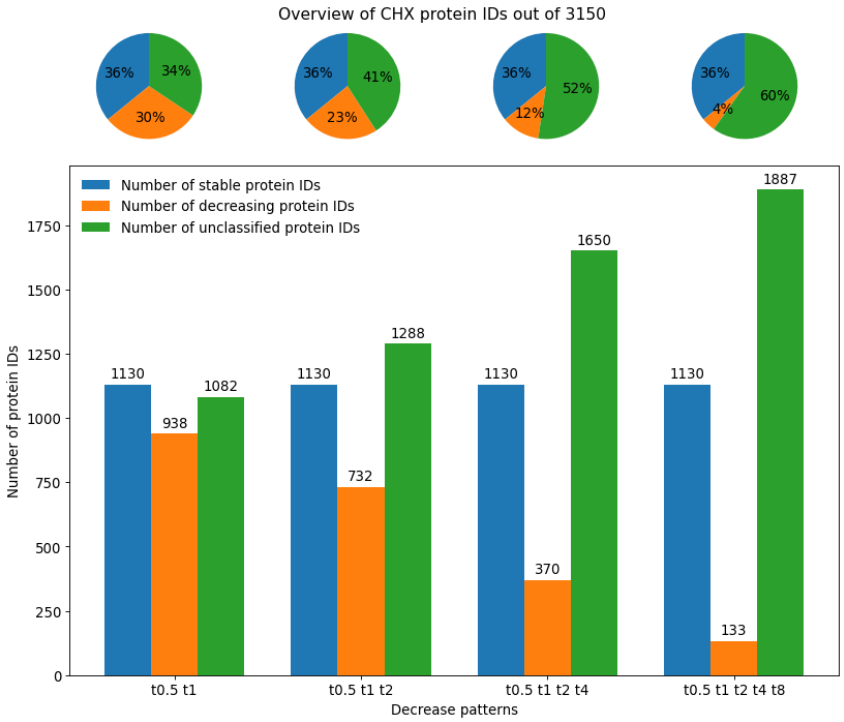

(b) Protein ID classifications in the CHX condition are shown in absolute numbers and percentages in the in the plot.

Figure 34: Barplots combined with pie charts display the absolute number and percentage of protein IDs assigned to the three possible classifications. Stable protein IDs have PFR values between 80% and 120% and are therefore stable. The number of decreasing CON proteins changes in dependence of the timepoints considered in the decrease patterns. The number of unclassified proteins is calculated by subtraction of stable and decreasing protein IDs from the total protein number specified in each plot.

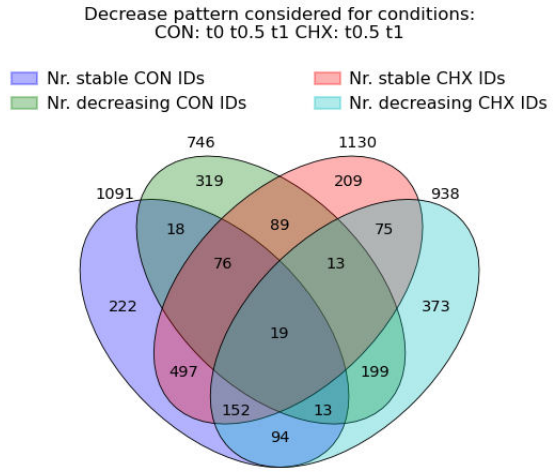

(a) Unique and overlapping protein IDs between stable proteins and proteins with continuously decreasing PFR values to the one hour timepoint of CON and CHX samples.

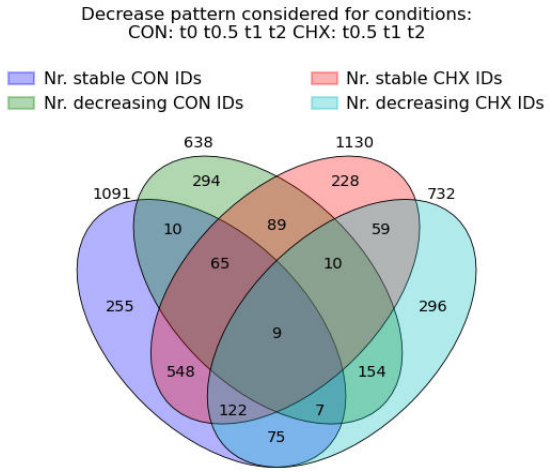

(b) Unique and overlapping protein IDs between stable proteins and proteins with continuously decreasing PFR values to the two hour timepoint of CON and CHX samples.

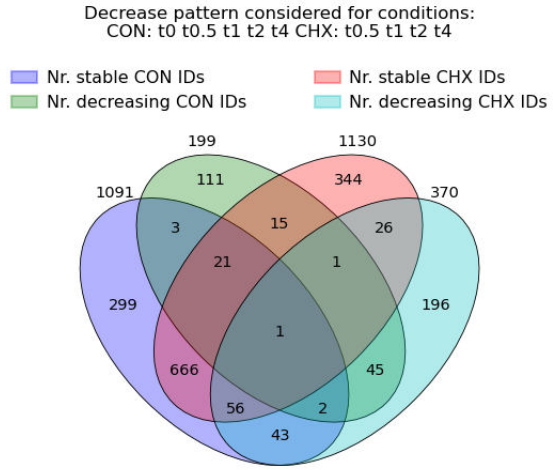

(c) Unique and overlapping protein IDs between stable proteins and proteins with continuously decreasing PFR values to the four hour timepoint of CON and CHX samples.

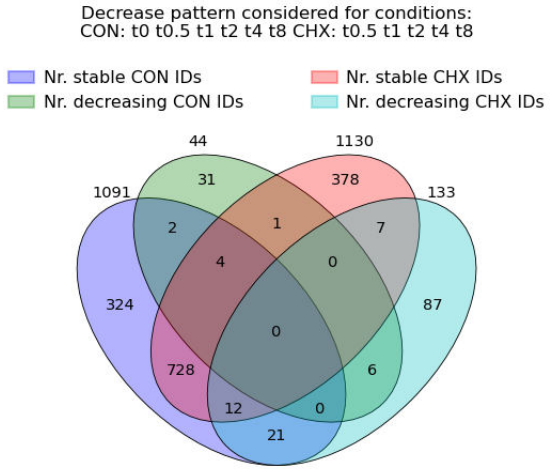

(d) Unique and overlapping protein IDs between stable proteins and proteins with continuously decreasing PFR values to the eight hour timepoint of CON and CHX samples.

Figure 35: Venn diagram showing the unique and overlapping protein IDs between the different conditions. Stable CON and CHX proteins needed to possess PFR values between 80% and 120% over all the experimental timepoints, hence the overall number is stable in all four diagrams. The number of decreasing proteins in the CON and CHX condition is due to the increased classification stringency, as proteins needed to always exhibit gradually lower PFR values from timepoint to timepoint.

4.11 Global protein half-life calculation

The classification of protein IDs introduced in the previous section was extended to all experimental conditions of the timeseries dataset to find protein IDs that exhibit similar decrease patterns in two and/or all three CHX, CHX + ACBI2 PROTAc and CHX + Gold PROTAC conditions. The goal was to identify shared regulations between the CHX and the CHX + PROTAC conditions to assess the treatment effect on a smaller pool of proteins. No PFR reduction trends were forced in the CON condition, as PFR values were expected to be relatively stable during the experiment. This was experimentally confirmed by the low number of 44 protein IDs (1% of the total proteins) that showed robustly decreasing LFQ values over all the CON timepoints. A Venn diagram showing the number of unique protein IDs and those shared between the the three experimental treatment conditions is displayed in figure 36. The timeseries data matrix was filtered in a stringent manner to contain only proteins that were detected in all three replicates of each treatment condition in the experimental timepoints ranging from $t_{0.5h}$ to t_{8h}. This stringent filtering was pursued to only account for proteins that were found to be robustly degraded in the three conditions.

The stringent filtering process did yield a data matrix containing 2807 proteins that fulfill the filtering thresholds (out of 5834) described in the paragraph above. The high number of proteins detected in all replicates suggests a high quality data matrix, which was achieved by the reproducible cell culture and sample preparation procedures as well as robust LC-MS/MS measurements.

The entries unique to one treatment condition indicate, that those proteins are solely affected by the corresponding treatment, whereas IDs shared between conditions are affected by multiple treatment conditions. The entries shared between the CHX and CHX + PROTAC conditions can then be used to assess the PROTAC share to the overall protein degradation. The data generally shows that the employed experimental design was well suited for the purpose.

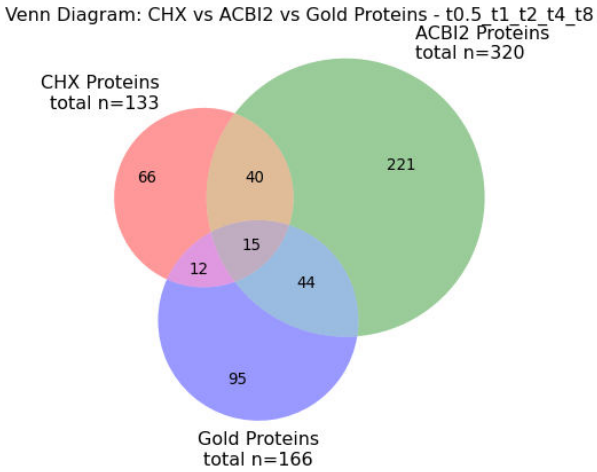

Figure 36: Venn diagram showing the number of protein IDs, unique to each condition and shared between treatment conditions, with PFR values that continuously decrease over all the timepoints from $t_{0.5h}$ to t_{8h}. Only IDs that fulfill the stringent filtering criteria of a 100% detection rate in every treatment condition and experimental timepoint were used to create the diagram.

One protein from the 15 IDs shared between all conditions was selected and the average PFR values as well as the standard deviation of the three samples was plotted for the corresponding timepoints. Additionally, the original LFQ value matrix was ln(LFQ) transformed. The resulting ln(LFQ) values of each condition of the selected protein were then plotted against the corresponding timepoints. A linear fit was calculated for each for CON from timepoint t_{0h} to t_{8h}, while treatment condition fits were calculated from $t_{0.5h}$ to t_{8h}. The slope yielded by the fit was then used for the half-life calculation of the protein in the corresponding condition by means of equation (4). The PFR plot and the corresponding semi-ln plot for the example protein is shown in figure 37.

As can be seen in figure 37, t_{0h} CON values were used as t_{0h} values for treatment conditions in the left plot as the LFQ values would have been the same for all conditions. t_{0h} data points for the treatment conditions are also present in the right plot, however they were not regarded for

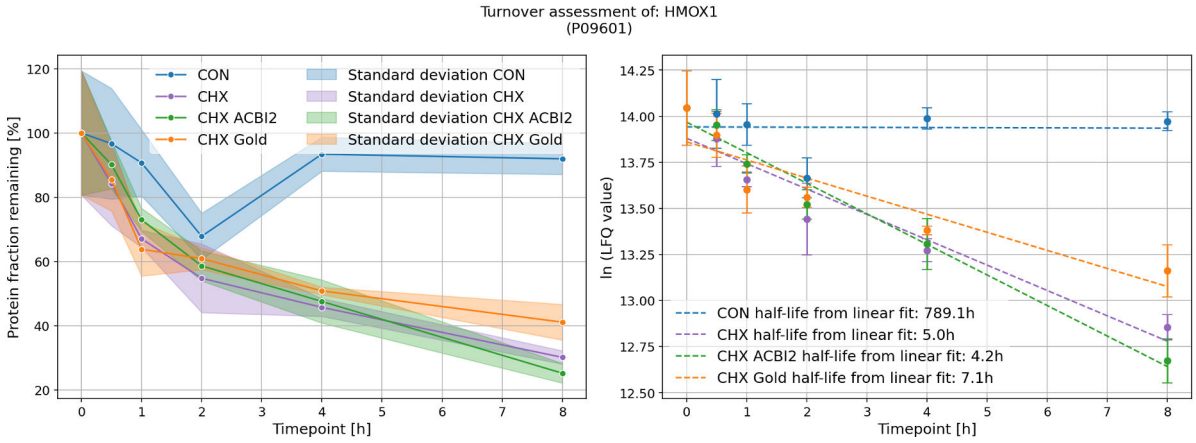

Figure 37: Combined scatter plots for the HMOX1 protein. The plot on the left shows the protein fraction remaining values over time, while the plot on the right shows the linear fits over the ln(LFQ) values of the different conditions and the half-lives calculated from the slope.

the linear fit used for the half-life calculation in the different conditions.

The PFR values below 50% for the treatment conditions in the left plot of figure 37 indicate that the employed CHX concentration was sufficient to inhibit *de-novo* protein synthesis in the PMA differentiated HL-60 cell model system. The semi-ln plot on the right hand side of the figure supports the validity of the assumptions that were made for the protein half-life calculation. The assumption of a first-order decay kinetics for proteins in steady state HL-60 cells holds up to the experimental data. This is because the ln(LFQ) values of the different timepoints do not skew far from the linear fit in all experimental timepoints. Hence, the method for half-life calculation is well suited for the project. Consequently, half-life calculation *via* this method was pursued for all proteins showing robust PFR decrease patterns over the course of all timepoints of all conditions. Relative changes in the half-lives of the different treatment conditions compared to CHX alone, would indicate PROTAC-specific effects.

The distribution of the calculated protein half-lives was visualized by means of violin plots for each experimental condition. The different plots can be found in figure 38. An attempt was made to correlate the fitted half-lives to the average LFQ values of the protein IDs of each condition. The average LFQ values was calculated by averaging the LFQ values of all replicates in all experimental timepoints for each protein ID. No correlation was observed.

Additionally, an other attempt was made to correlate the fitted half-lives with the molecular weight of the corresponding protein. The molecular weights of the relevant protein IDs were retrieved from the MaxQuant search matrix. No correlation was found between the average LFQ values and the molecular weight of the protein IDs as can be seen from the absolute lack of a trend in figure 43 and 44.

The violin plots do allow an overview on the protein half-lives of each condition. The median half-life values range from 15.00 hours in the CON condition down to 10.54 hours in the CHX + Gold PROTAC condition, with the median half-life of proteins in the CHX and CHX + ACBI2 PROTAC conditions laying between those two values. This would hint that CHX and CHX + PROTAC treatments did reduce the protein half-lives in the experimental setting compared to the CON condition.

A confirmation of this fact would, however, only be possible by a direct comparison of fitted half-lives of protein IDs shared between the different experimental conditions. This deeper insight into PROTAC treatment effects can be gained by identifying shared protein ID entries between experimental conditions and scattering the fitted half-lives of the corresponding conditions against each other. The calculation of a linear fit through the calculated half-life data allows to visualize which experimental condition yielded lower protein half-lives and therefore

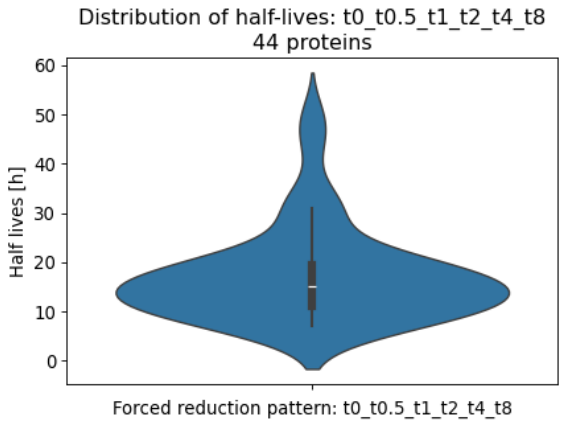

(a) Half-life distribution of CON condition proteins with robustly decreasing PFR values over time. Median half-life: 15.00 hours.

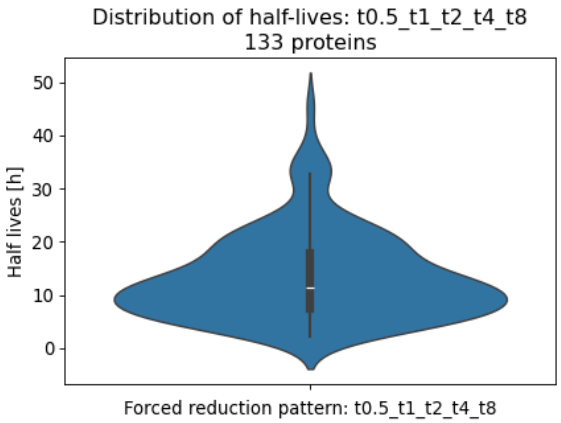

(b) Half-life distribution of CHX condition proteins with robustly decreasing PFR values over time. Median half-life: 11.53 hours.

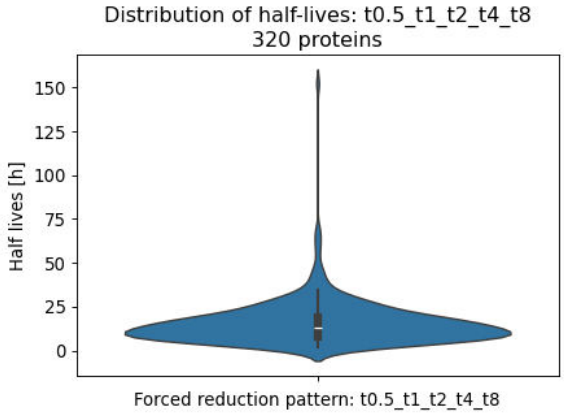

(c) Half-life distribution of CHX + ACBI2 PROTAC condition proteins with robustly decreasing PFR values over time. Median half-life: 13.32 hours.

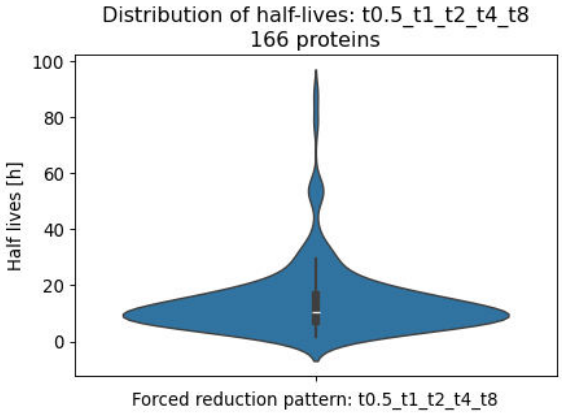

(d) Half-life distribution of CHX + gold PROTAC condition proteins with robustly decreasing PFR values over time. Median half-life: 10.54 hours.

Figure 38: Violin plots displaying the half-life distribution as well as the number of protein IDs exhibiting continuously decreasing PFR values over the experimental timepoints indicated in each plot as "forced reduction pattern". The box plot inside each violin plot shows the inter quartile distribution as well as the median protein half-life.

exhibits a higher protein degradation rate compared to the other condition. Calculating the difference of shared protein ID half-lives between two conditions allows to rank the different protein IDs based on their half-life difference in form of a rank plot. The half-lives are displayed in table 18 for six IDs shared between the CON (average half-life: 13.72 ± 4.48h) and CHX (average half-life: 13.72 ± 4.48h) conditions, in table 19 for 55 IDs shared between the CHX (average half-life: 13.12 ± 9.13h) and CHX + ACBI2 PROTAC (average half-life: 10.38 ± 7.40h) conditions, in table 20 for 27 IDs shared between the CHX (average half-life: 12.54 ± 8.13h) and CHX + gold PROTAC (average half-life: 8.14 ± 4.23h) conditions and in table 21 for 59 IDs shared between the CHX + ACBI2 PROTAC (average half-life: 13.03 ± 10.01h) and CHX + gold PROTAC (average half-life: 10.82 ± 6.80h) condition. The scatter plots and the corresponding rank plots generated by the comparison of shared protein IDs between the experimental conditions can be seen in figure 39.

The combined plots shown in figure 39 do highlight important differences in the protein half-lives shared between two experimental conditions. The comparison of the protein IDs shared between the CHX with the CHX + PROTAC condition in figure 39a shows that the majority of the IDs

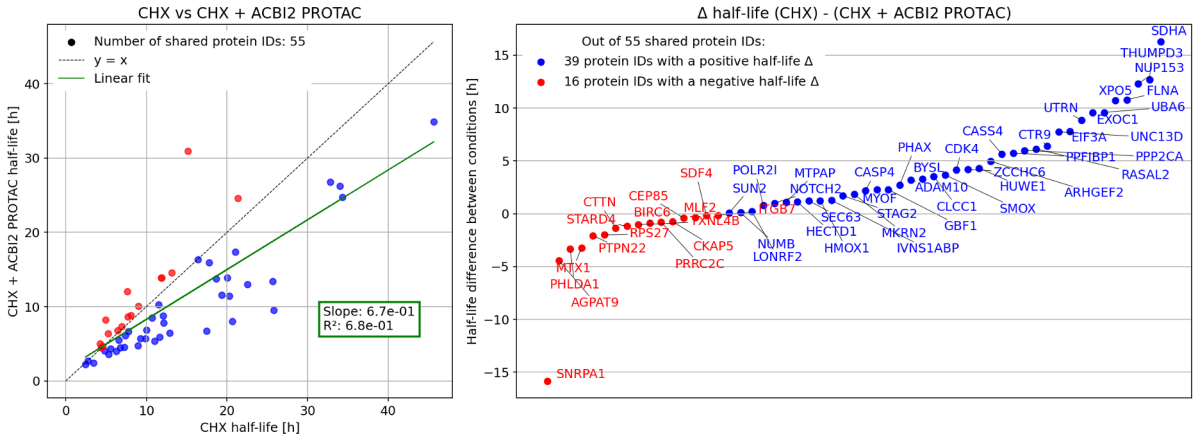

(a) Half-life analysis of protein IDs shared between the CHX and CHX + ACBI2 PROTAC condition. The half-lives of the protein IDs displayed in the plot can be found in table 19 ranked by decreasing half-life difference.

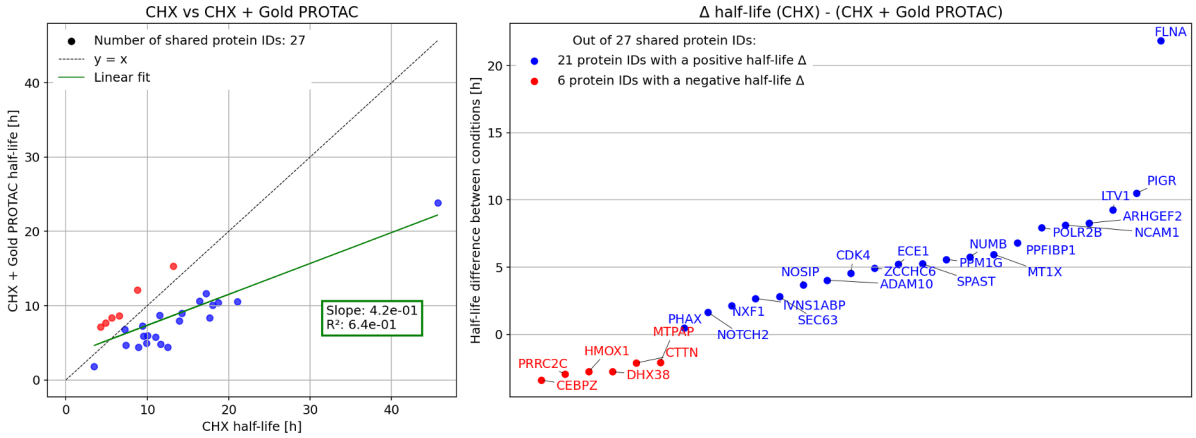

(b) Half-life analysis of protein IDs shared between the CHX and CHX + gold PROTAC condition. The half-lives of the protein IDs displayed in the plot can be found in table 20 ranked by decreasing half-life difference.

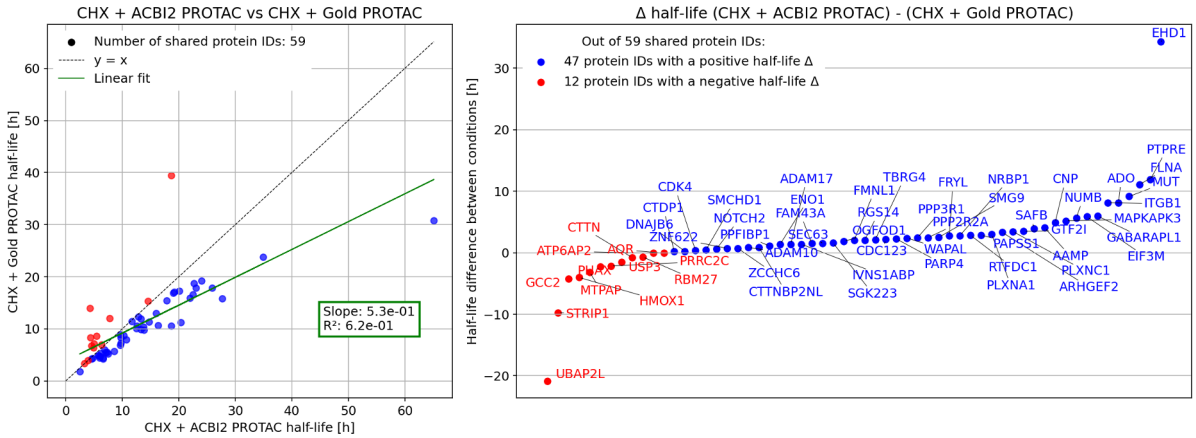

(c) Half-life analysis of protein IDs shared between the CHX + ACBI2 PROTAC and CHX + gold PROTAC condition. The half-lives of the protein IDs displayed in the plot can be found in table 21 ranked by decreasing half-life difference.

Figure 39: Scatter and rank plots resulting from the shared protein ID half-life analysis between the different experimental conditions.

(71%) undergoes a faster degradation, leading to a lower half-life, in the presence of the ACBI2 PROTAC. A similar observation was made with protein IDs shared between the CHX and CHX + gold PROTAC conditions in figure 39b, where the PROTAC presence did lead to shorter half-lives in 78% of shared entries. This supports the assumption that PROTACs do indeed affect the degradation of more than the explicit target protein they were designed to degrade. Finding these regulations would not have been possible by employing any other experimental setup. In both cases the bulk of the calculated half-life differences settle in a similar range between -5 hours to approximately + 10 hours, which shows that changes in half-lives induced by the PROTAC treatments are quite substantial. What is interesting, however, is the fact that a smaller number of proteins (27) is shared between CHX + gold and CHX compared to the number of shared IDs (55) between the CHX and CHX + ACBI2 condition. This can be seen, not only on ID regulations shared between conditions, but also on the overall number of regulations. The higher number of proteins showing a robust degradation in the CHX + ACBI2 condition in figure 36 is far higher than in the gold PROTAC condition. This was unexpected as, due to the optimized structure of the ACBI2 PROTAC, less regulations/off-target effects were expected in the CHX + ACBI2 PROTAC condition compared to the CHX + gold PROTAC equivalent. A clear trend can also be observed in the calculated half-lives of protein IDs shared between the two PROTAC conditions, where the majority (79.7%) of the half-lives are higher in the CHX + ACBI2 PROTAC compared to the CHX + gold PROTAC condition. This would suggest, that the gold PROTAC reduces the half-lives of protein IDs to a higher extent than the ACBI2 PROTAC. These combined findings could therefore indicate, that the ACBI2 PROTAC indeed affects the half-lives of a higher number of proteins, but to a lesser extent than the gold PROTAC.

The comparison of the protein half-lives detected in this experiment with previously published protein half-lives was difficult as the PMA differentiated HL-60 cell model system was, to our best knowledge, never used in literature. Generally, steady state model systems are rarely used in experiments, hence we resorted to a comparison with half-life data reported by Zecha et al.[13]. The authors relied on proliferating HeLa cells as model system, while a SILAC-TMT method was employed to determine the kinetics of protein synthesis and degradation. Since no treatment was performed on the HeLa cells, only protein IDs classified as "reducing CON" (44) were searched against the reported, 7029 entry long list of non-"inf" half-life proteins. A total of 16 overlapping protein IDs were found in the two datasets. The data summarizing the protein half-lives is shown in table 17.

The half-life comparison performed in table 17 should be interpreted with caution as, as explained in a previous paragraph, the authors investigated a completely different model system and employed a different method to assess the half-lives. What is inherently associated with SILAC-TMT experiments, is the quantification on peptide level, compared to the quantification on a protein level in label-free proteomics experiments. Additionally, the authors employed a non-linear fit to their experimental data to calculate the protein half-lives as it performed better on their data. Hence, the table mostly shows significant differences in the protein half-lives. There are, however, three proteins involved in the transcription machinery, which exhibit relatively close half-lives and are therefore highlighted in yellow in the table. It is plausible to find proteins involved in transcription processes with similar half-lives in two different model systems as those processes will be continuously going on both in proliferating and differentiated cells to keep the available cellular protein pool functional.

Table 17: Table showcasing protein name, the corresponding UniProt identifier and half-lives of proteins both detected by Zecha et al.[13] and in the "reducing CON" ID subset of this work. Rows with a yellow background color highlight proteins where the calculated half-lives are very close to one another.

Protein name(s)	UniProt identifier(s)	Half-life Zecha et al.[13] [h]	Half-Life this work [h]
Actin-related protein 2/3 complex subunit 2	O15144	76.51	29.43
Density-regulated protein	O43583	40.16	13.55
Protein phosphatase 1 regulatory subunit 11	O60927	50.03	7.11
DNA-directed RNA polymerases I; II; and III subunit RPABC1	P19388	17.67	18.38
Superkiller viralicidic activity 2-like 2	P42285	23.86	15.06
40S ribosomal protein S27	P42677	35.24	13.27
Tumor necrosis factor alpha-induced protein 2	Q03169	42.55	10.08
Bystin	Q13895	17.83	9.36
Guanine nucleotide-binding protein subunit alpha-13	Q14344; Q14344-2	85.36	20.43
Dedicator of cytokinesis protein 11	Q5JSL3	43.7	10.42
Peptidase M20 domain-containing protein 2	Q8IYS1	55.31	8.4
Ubiquitin-like domain-containing CTD phosphatase 1	Q8WVY7	64.96	17.29
Gamma-tubulin complex component 2	Q9BSJ2; Q9BSJ2-4	34.27	22.88
Ubiquitin-like protein 5	Q9BZL1	6.18	21.98
Probable ATP-dependent RNA helicase DDX41	Q9UJV9	10.88	11.6
RNA-binding protein NOB1	Q9ULX3	16.79	16.47

4.12 Global evaluation of Bortezomib rescue experiments

The rescue experiment yielded a data matrix with 5349 entries after the standard processing procedure. As with other data matrices, only proteins detected with high confidence in all three out of three replicates were used for further analysis. This reduced the number of IDs to 3880, 72.5% of the original data set. Protein IDs with continuously decreasing LFQ values from t_{0h} to t_{4h} in the Bortezomib rescue experiment were identified in both ACBI2 PROTAC (145 IDs) and gold PROTAC (72 IDs) conditions. The LFQ values at the t_{4h} timepoint were averaged separately for every single protein ID. This procedure was repeated for IDs with a continuous LFQ value reduction from $t_{0.5h}$ to t_{4h} of the regular timeseries. The rescue *via* Bortezomib was then deemed successful if the average LFQ value at the t_{4h} timepoint was higher in the Bortezomib rescue experiment compared to the regular timeseries experiment.

A successful rescue was detected for 106 IDs in the ACBI2 PROTAC condition (73%) and in 61 IDs of the gold PROTAC condition (85%). Generally the experiment worked as expected. The rescue was substantial in both rescue experiments with a median increase of LFQ values

in the ACBI2 PROTAC rescue condition of 18.88% compared to the timeseries experiment. The median increase in LFQ values in the gold PROTAC rescue was quantified to 29.33%. The protein IDs with a LFQ value increase of above 50% in the Bortezomib rescue experiment compared to the timeseries data are shown in table 22 for the Bortezomib + ACBI2 PROTAC condition (23 IDs) and in table 23 for the Bortezomib + gold PROTAC condition (20 IDs) respectively.

One detail worth nothing for the comparison of the Bortezomib rescue experiment with the regular timeseries experiment, is the absence of CHX in the former experiment. The timeseries experiment showed the presence of 44 protein IDs with robustly decreasing LFQ values in the control condition, whereas the Cycloheximide condition did lead to a robust degradation of 133 protein IDs over the course of the experiment (refer to figure 38 in section 4.11). The lack of the translational inhibitor undoubtedly inflated the number of protein IDs that feature lower LFQ values in the regular timeseries because of *de-novo* protein synthesis still going on in the Bortezomib rescue experiment.

Indeed, 24 of 106 (22.64%) of the rescued protein IDs in the Bortezomib + ACBI2 PROTAC conditions are found to be robustly decreasing in LFQ values from the $t_{0.5h}$ to t_{8h} timepoints in the CHX only condition. This number increases to 40 of 106 (37.74%) when the filtering stringency for a robust decrease is reduced to the $t_{0.5h}$ to t_{4h} timepoints. An overlap of the rescued protein IDs in the Bortezomib + gold PROTAC condition with proteins showing a robust decrease in the CHX condition of the timeseries experiment was found for 11 out of 61 (18.03%) entries and 23 out of 61 (37.70%) entries for the $t_{0.5h}$ to t_{8h} and $t_{0.5h}$ to t_{4h} timepoints respectively. The protein IDs can be found in table 24.

Thirteen shared entries between proteins with LFQ values decreasing robustly from $t_{0.5h}$ to t_{4h} and IDs that were shown to be strongly rescued ($\geq 50\%$ increase of the average LFQ value in the rescue experiment compared to the timeseries experiment) in the Bortezomib + ACBI2 PROTAC experiment were identified, which hints that the experimentally described rescue was probably caused by the absence of CHX and not by the presence of Bortezomib. Those entries were highlighted in yellow in table 22. Similarly, six entries were found to be overlapping in the Bortezomib + gold PROTAC experiment. Those IDs were highlighted in yellow in table 23.

Overall the data suggests that approximately 60% of the rescued protein IDs were probably rescued by the inhibition of the proteasome with Bortezomib.

4.13 BONCAT and comparison to timeseries results

The BONCAT experiment consisted of replacing Methionine in the culture medium with an Azidohomoalanine (AHA) surrogate over the course of the 72 hour differentiation timeframe to label newly synthesized proteins. The labelled proteins would then be covalently bound to alkyne modified beads by means of copper catalyzed click chemistry. This step allows the selective enrichment of newly synthesized protein and stringent washing steps to remove background proteins. The enrichment of AHA containing proteins potentially allows the detection of significantly lower-abundant proteins and a more robust detection of relevant proteins due to the reduced background, making a BONCAT experiment well suited to confirm targets identified in the timeseries experiment.

The BONCAT experiment, however, did not yield the expected results. An issue arose, where the intensity of one replicate of the t_{8h} timepoint of the timeseries exhibited significantly higher intensity values throughout the entirety of the total ion chromatogram compared to all other samples. This can be seen in the very low similarity to all other samples in the correlation heatmap shown in figure 45. This, did not affect the database search as the overall protein median $\log_2$ LFQ value was in similar ranges across all samples. The data matrix was additionally filtered after standard processing to contain only protein IDs that were robustly detected in three out of three replicates over all timepoints, reducing the original matrix from 3283 IDs to 749 proteins. The main problem became apparent in the progression of the protein LFQ values. Most proteins showed a spike in LFQ values in the t_{8h} timepoint, rendering a

filtering of the data matrix based on LFQ reduction patterns from t_{8h} onward useless. Therefore, protein IDs showing a steady reduction from t_{0h} to including t_{4h} were identified (164 IDs), their half-lives were calculated and their distribution plotted in form of a violin plot shown in figure 40.

Only a relatively small number of 749 proteins fulfilled the additional stringent filtering requirement (22.8% of the original matrix). This hints toward a lower data quality especially compared to the regular timeseries experiment, where 48.1% of proteins fulfilled the same 100% in all replicates filtering criterion over four separate conditions, compared to just one condition in the BONCAT experiment. The protein half-life calculation was successful and the median protein half-life of 9.6 hours was in a lower range to median values in the regular timeseries experiment. Shared regulations between the regular timeseries CHX condition ($t_{0.5h}$ to t_{8h}) and the BONCAT CHX (t_{0h} to t_{4h}) condition were scarce with only three shared protein IDs: RPL9 (P32969), NCBP1 (Q09161), RPL4 (P36578).

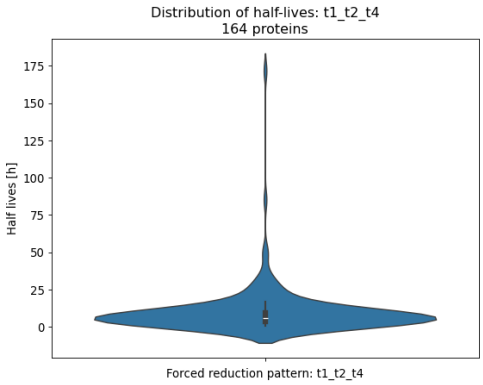

Figure 40: Violin plot showing the half-life distribution of protein IDs showing a continuous reduction of $\log_2$ LFQ values from t_{0h} to t_{4h}.

A possible reason for the inconsistent results of the BONCAT timeseries might be caused by a systematic error that was made during sample preparation. Azidohomoalanine used as Methionine surrogate in the BONCAT experiment was not only incorporated in proteins but also metabolites and was present in the medium. Cells were thoroughly washed with PBS, which probably almost quantitatively removed the Azidohomoalanine containing excess medium. Cell lysates, on the other hand, may have contained non-negligible amounts of Azidohomoalanine from e.g. metabolites which may have competed for bead binding sites against the AHA containing proteins. A protein precipitation step will be incorporated in the next attempt prior to the on-bead enrichment to quantitatively remove the non-protein fraction. This will be performed in a future experiment.

5 Conclusion

We set out to establish a method that allows the reproducible and robust measurement of protein turnover on a proteome-wide scale. This was crucial to address the question of selectivity of protein degradation by PROTACs. An optimized SMARCA2-targeting PROTAC and an investigative putative TXNRD1-targeting metallo-PROTAC were studied.

A handful of model systems were profiled on a sub-cellular protein level to identify the optimal model system for protein turnover assessments in a cellular steady state condition. The steady state condition is a crucial criterion for the protein half-life calculation based on first order degradation kinetics. The lack of a steady state would require more complex models for half-life calculation to account for anabolism, cell-cycle dependent changes in protein expression patterns and among others a way to account for the non-synchronized cell cycles in the cell population. The fulfillment of the steady state condition allows the calculation of protein half-lives *via* linear fits of decreasing experimental abundance data versus time in semi-ln plots.

Proteomic method parameters were optimized, including LC gradient length and database search settings, to allow robust proteome measurements. Finally, PMA differentiated HL-60 cells were selected, because of the presence of the majority of experimentally relevant proteins of the ubiquitin-proteasome system, as well as the robust and reproducible differentiation. The differentiation conditions of the model system were optimized, as well as the Cycloheximide (CHX) treatment concentration to inhibit *de-novo* protein synthesis to a sufficient magnitude.

A timeseries experiment was specifically designed to differentiate normal protein degradation over time from the PROTAC share to the degradation as well as to identify PROTAC-induced down-regulations of proteins from physiological degradation processes. These experiments yielded robust proteome-wide data. A significant amount of proteins of the CON condition were, as we expected, shown to be stable throughout the experiment. The Cycloheximide condition of the timeseries experiment showed that there were more (133 IDs) proteins with robustly decreasing LFQ values than in the CON condition (44 IDs), a hint toward a successful protein synthesis inhibition.

The Cellwatcher module confirmed steady state conditions after 72 hours of differentiation with respect to proliferation. The successful chemical differentiation of HL-60 cells with PMA paired with the optimized experimental design successfully allowed the identification of proteins that are regulated by PROTACs. The validity of the underlying assumptions and the presence of a steady state model system were confirmed by the low deviation of experimental data points to the linear fit used for half-life calculation in semi-ln plots.

The median protein half-life of the solvent-matched control (CON) condition of the timeseries experiment was 15.00 hours. All the treated conditions showed lower median half-lives. The CHX condition, with a 10µM concentration of the global translation inhibitor, was used as baseline in order to be able to assess the PROTAC effects and had a median half-life of 11.53 hours. The CHX + 1 nM ACBI2 PROTAC condition was used to validate the experiment as ACBI2 is fully characterized and optimized PROTAC and showed a median protein half-life of 13.33 hours. The experimental covalent gold PROTAC was employed in the CHX + gold PROTAC condition with a 60 µM concentration and yielded a median half-life of 10.54 hours. The half-life distribution in the different experimental conditions were relatively close around the 10-15 hour mark, which reflected the experimental timeframe of eight hours. The use of CHX to inhibit *de-novo* protein synthesis restricted the accessible period of time for the investigation of protein turnover due to its dose- and time-dependent cytotoxicity.

The literature reported degradation of SMARCA2 and PBRM1 by the ACBI2 PROTAC was confirmed in our experimental setup. Both proteins were fully degraded or below the detection limit already at the first timepoint of $t_{0.5h}$, which was unexpected. A four-hour incubation period with Bortezomib, an efficient proteasome inhibitor, prior to a four hour incubation period with the ACBI2 PROTAC did not prevent both proteins to be degraded. This experiment was conducted in parallel to the timeseries experiment to understand the degree to which the PROTAC degradation can be prevented by inhibition of the proteasome. The gold PROTAC,

on the other hand, did not exhibit the expected effect of degrading the putative target protein TXNRD1. Overall, the proteasomal inhibition with Bortezomib led to the rescue of 66 protein IDs (45.52%) in the ACBI2 PROTAC condition and 38 IDs (52.78%) in the gold PROTAC condition compared to the same time range in the timeseries experiment.

This shows that the employed method is suited, not only to assess protein half-lives on a proteome-wide level, but also evaluate the specific effects of PROTAC treatments as well as the effect of simultaneous proteasomal inhibition on protein half-lives.

The experimental setup allowed to detect several shared protein IDs that exhibited lower half-lives in the CHX + PROTAC condition compared to the CHX condition alone for both the gold as well as for the ACBI2 PROTAC. These findings strongly suggest that PROTACs might be affecting the half-lives of a higher number of proteins, but with varying degree of degradation efficiency. The number of affected half-lives in turn imply that PROTACs do indeed degrade more than a small number of proteins. In the experiments we identified 39 proteins that possessed shorter half-lives in the combined CHX + ACBI2 PROTAC condition compared to the CHX condition. Similarly, 21 protein IDs with lower half-lives than in the CHX condition were identified in the CHX + gold PROTAC condition. Follow-up experiments and more research is necessary to confirm these findings as they might hint to unwanted off-target effects of PROTAC treatments. These effects, if confirmed, would undeniably contribute to a better understanding of PROTAC mode of action.

The BONCAT experiment was a promising alternative, but should be repeated in a future study due to the presumed intracellular presence of Azidohomoalanine, which may have competed for binding sites on the enrichment beads. This issue can be effectively circumvented by incorporating a protein precipitation step before the affinity reaction on the beads. The method itself is well suited for the integration in the LC-MS/MS protein digestion workflow and might be helpful in unraveling specific questions in future cell culture experiments.

Overall, the development of a mass spectrometric method to determine protein turnover was successful and can be used as a starting point for future experiments revolving around the assessment of protein half-lives in complex systems. It may enable a proteome-wide view on the dynamics of protein degradation in the context of drug modes of action and will complement existing perturbation studies.

6 Acknowledgements

I am very grateful to Ass.-Prof. Dr. Samuel Matthias Meier-Menches for allowing me to conduct the research in his group, for supervising me, for sharing his deep knowledge and for his motivational can-do attitude shown throughout every step of this thesis. I would also like to express my gratitude to him for believing in my capabilities to come up with experimental design suggestions and to perform the experiments and data analysis for such a project. This allowed me to understand how many details need to be taken into account when doing these kind of experiments and helped me gain a deeper understanding on how science works.

Furthermore I would like to thank Lukas Skos and Yasmin Borutzki for (re)introducing me to cell culture procedures and for sharing their invaluable tips on how to perform reproducible experiments. Moreover, i would like to thank Johanna Mader and Günter Plessl-Walder for sharing their knowledge for sample preparation procedures, as well as Andrea Bileck for reliable LC-MS/MS measurements. Without them, none of this would have been possible in the first place.

I would like to generally thank all members of the Gerner and Meier-Menches group and fellow master students for the warm welcome, for creating a comfortable atmosphere and for their shared passion for bioanalytical chemistry that widened my knowledge in the field.

I am also deeply grateful to Anna for her patience, support and motivation. Finally, I would like to thank my parents who have always supported me, my education and made my chemistry studies possible in the first place.

Ad maiora

7 References

1. Toyama, B. H. & Hetzer, M. W. Protein homeostasis: Live long, won't prosper. *Nature Reviews Molecular Cell Biology* **14,** 55–61. ISSN: 14710072 (2013).
2. Toyama, B. H. *et al.* Identification of long-lived proteins reveals exceptional stability of essential cellular structures. *Cell* **154,** 971–982. ISSN: 10974172 (2013).
3. Fornasiero, E. F. & Savas, J. N. Determining and interpreting protein lifetimes in mammalian tissues. *Trends in Biochemical Sciences* **48,** 106–118. ISSN: 0968-0004 (2023).
4. Ross, A. B., Langer, J. D. & Jovanovic, M. Proteome turnover in the spotlight: Approaches, applications, and perspectives. *Molecular and Cellular Proteomics* **20,** 1–17. ISSN: 15359484 (2021).
5. Eden, E. *et al.* Proteome half-life dynamics in living human cells. *Science* **331,** 764–768. ISSN: 00368075 (2011).
6. Rusilowicz-Jones, E. V., Urbé, S. & Clague, M. J. Protein degradation on the global scale. *Molecular Cell* **82,** 1414–1423. ISSN: 1097-2765 (2022).
7. Ciechanover, A. Proteolysis: from the lysosome to ubiquitin and the proteasome. *Nature Reviews Molecular Cell Biology* **6,** 79–87. ISSN: 1471-0080 (2005).
8. Tai, H. C. & Schuman, E. M. Ubiquitin, the proteasome and protein degradation in neuronal function and dysfunction. *Nature Reviews Neuroscience* **9,** 826–838. ISSN: 1471-0048 (2008).
9. Eldeeb, M. A. *et al.* A molecular toolbox for studying protein degradation in mammalian cells. *Journal of Neurochemistry* **151,** 520–533. ISSN: 1471-4159 (2019).
10. Miyawaki, A. Development of probes for cellular functions using fluorescent proteins and fluorescence resonance energy transfer. *Annual Review of Biochemistry* **80,** 357–373. ISSN: 00664154 (2011).
11. Sha, Z., Zhao, J. & Goldberg, A. L. in *Methods in Molecular Biology* 261–276 (2018).
12. Rowlinson, B., Crublet, E., Kerfah, R. & Plevin, M. J. Specific isotopic labelling and reverse labelling for protein NMR spectroscopy: using metabolic precursors in sample preparation. *Biochemical Society Transactions* **50,** 1555–1567. ISSN: 14708752 (2022).
13. Zecha, J. *et al.* Peptide level turnover measurements enable the study of proteoform dynamics. *Molecular and Cellular Proteomics* **17,** 974–992 (2018).
14. Boisvert, F. M. *et al.* A quantitative spatial proteomics analysis of proteome turnover in human cells. *Molecular and Cellular Proteomics* **11,** 1–15. ISSN: 15359476 (2012).
15. Grandi, P. & Bantscheff, M. Advanced proteomics approaches to unravel protein homeostasis. *Drug Discovery Today: Technologies* **31,** 99–108. ISSN: 1740-6749 (2019).
16. Zecha, J. *et al.* Linking post-translational modifications and protein turnover by site-resolved protein turnover profiling. *Nature Communications* **13,** 1–14 (2022).
17. Obrig, T. G., Culp, W. J., Mckeehan, W. L. & Hardesty, B. The mechanism by which Cycloheximide and related Glutarimide antibiotics inhibit peptide synthesis on reticulocyte ribosomes. *Journal of Biological Chemistry* **246,** 174–181 (1971).
18. Schneider-Poetsch, T. *et al.* Inhibition of eukaryotic translation elongation by cycloheximide and lactimidomycin. *Nature Chemical Biology* **6,** 209–217. ISSN: 1552-4469 (2010).
19. Li, J. *et al.* Proteome-wide mapping of short-lived proteins in human cells. *Molecular Cell* **81,** 4722–4735. ISSN: 1097-2765 (2021).
20. Miao, Y. *et al.* Cycloheximide (CHX) chase assay to examine protein half-life. *Bio Protocol* **13,** 1–11. ISSN: 23318325 (2023).

21. Dai, C. L. *et al.* Inhibition of protein synthesis alters protein degradation through activation of protein kinase B (AKT). *The Journal of Biological Chemistry* **288,** 23875–23883. ISSN: 00219258 (2013).

22. Mcshane, E. *et al.* Kinetic analysis of protein stability reveals age-dependent degradation. *Cell* **167,** 803–815 (2016).

23. Dieterich, D. C., Link, A. J., Graumann, J., Tirrell, D. A. & Schumann, E. M. Selective identification of newly synthesized proteins in mammalian cells using bioorthogonal noncanonical amino acid tagging (BONCAT). *Proceedings of the National Academy of Sciences of the United States of America* **103,** 9482–9487. ISSN: 00278424 (2006).

24. Bagert, J. D. *et al.* Quantitative, time-resolved proteomic analysis by combining bioorthogonal noncanonical amino acid tagging and pulsed stable isotope labeling by amino acids in cell culture. *Molecular and Cellular Proteomics* **13,** 1352–1358. ISSN: 15359484 (2014).

25. Kiick, K. L., Saxon, E., Tirrell, D. A. & Bertozzi, C. R. Incorporation of azides into recombinant proteins for chemoselective modification by the Staudinger ligation. *Proceedings of the National Academy of Sciences of the United States of America* **99,** 19–24. ISSN: 00278424 (2001).

26. Ma, Y., McClatchy, D. B., Barkallah, S., Wood, W. W. & Yates, J. R. Quantitative analysis of newly synthesized proteins. *Nature Protocols* **13,** 1744–1762. ISSN: 1750-2799 (2018).

27. Zhao, L., Zhao, J., Zhong, K., Tong, A. & Jia, D. Targeted protein degradation: mechanisms, strategies and application. *Signal Transduction and Targeted Therapy* **7,** 1–13 (2022).

28. Sathe, G. & Sapkota, G. P. Targeted protein degradation proteomic approaches advancing targeted protein degradation. *Trends in Pharmacological Sciences* **44,** 786–801 (2023).

29. Cecchini, C., Pannilunghi, S., Tardy, S. & Scapozza, L. From conception to development: Investigating PROTACs features for improved cell permeability and successful protein degradation. *Frontiers in Chemistry* **9,** 1–23. ISSN: 22962646 (2021).

30. Fang, Y. *et al.* Progress and challenges in targeted protein degradation for neurodegenerative disease therapy. *Journal of Medicinal Chemistry* **65,** 11454–11477 (2022).

31. Cao, C., He, M., Wang, L., He, Y. & Rao, Y. Chemistries of bifunctional PROTAC degraders. *Chemical Society Reviews* **51,** 7066–7114. ISSN: 1460-4744 (2022).

32. Sakamoto, K. M. *et al.* Protacs: chimeric molecules that target proteins to the Skp1-Cullin-F box complex for ubiquitination and degradation. *Proceedings of the National Academy of Sciences of the United States of America* **98,** 8554–8559. ISSN: 0027-8424 (2001).

33. Garber, K. The PROTAC gold rush. *Nature Biotechnology* **40,** 12–16. ISSN: 15461696 (2022).

34. Paiva, S. L. & Crews, C. M. Targeted protein degradation: Elements of PROTAC design. *Current Opinion in Chemical Biology* **50,** 111–119. ISSN: 1367-5931 (2019).

35. Troup, R. I., Fallan, C. & Baud, M. G. Current strategies for the design of PROTAC linkers: A critical review. *Exploration of Targeted Anti-tumor Therapy* **1,** 273–312. ISSN: 26923114 (2020).

36. Min, J. *et al.* Phenyl-Glutarimides: Alternative Cereblon binders for the design of PROTACs. *Angewandte Chemie International Edition* **60,** 26663–26670. ISSN: 15213773 (2021).

37. Jarusiewicz, J. A. *et al.* Phenyl Dihydrouracil: An alternative Cereblon binder for PROTAC design. *ACS Medicinal Chemistry Letters* **14,** 141–145 (2023).

38. Kofink, C. *et al.* A selective and orally bioavailable VHL-recruiting PROTAC achieves SMARCA2 degradation in vivo. *Nature Communications* **13,** 1–15. ISSN: 20411723 (2022).

39. Farnaby, W. *et al.* BAF complex vulnerabilities in cancer demonstrated via structure-based PROTAC design. *Nature Chemical Biology* **15,** 672–680. ISSN: 1552-4469 (2019).

40. Skos, L. *et al.* Gold-templated covalent targeting of the CysSec-dyad of thioredoxin reductase 1 in cancer cells. *Cell Reports Physical Science* **5,** 1–16. ISSN: 26663864 (2024).

41. Ito, T. *et al.* Identification of a primary target of Thalidomide teratogenicity. *Science* **327,** 1345–1350. ISSN: 0036-8075 (2010).

42. O'Dowd, P. D., Sullivan, G. P., Rodrigues, D. A., Chonghaile, T. N. & Griffith, D. M. First-in-class metallo-PROTAC as an effective degrader of select Pt-binding proteins. *Chemical Communications* **59,** 12641–12644. ISSN: 1364-548X (2023).

43. Iwai, K. *et al.* Identification of the von Hippel-Lindau tumor-suppressor protein as part of an active E3 ubiquitin ligase complex. *Proceedings of the National Academy of Sciences of the United States of America* **96,** 12436–12441. ISSN: 00278424 (1999).

44. Diehl, C. J. & Ciulli, A. Discovery of small molecule ligands for the von Hippel-Lindau (VHL) E3 ligase and their use as inhibitors and PROTAC degraders. *Chemical Society Reviews* **51,** 8216–8257. ISSN: 1460-4744 (2022).

45. Nguyen, T. V. *et al.* Glutamine triggers acetylation-dependent degradation of Glutamine Synthetase via the Thalidomide receptor Cereblon. *Molecular Cell* **61,** 809–820. ISSN: 10974164 (2016).

46. Kadoch, C. & Crabtree, G. R. Mammalian SWI/SNF chromatin remodeling complexes and cancer: Mechanistic insights gained from human genomics. *Science Advances* **1,** 1–17. ISSN: 23752548 (2015).

47. Hoffman, G. R. *et al.* Functional epigenetics approach identifies BRM/SMARCA2 as a critical synthetic lethal target in BRG1-deficient cancers. *Proceedings of the National Academy of Sciences of the United States of America* **111,** 3128–3133. ISSN: 00278424 (2014).

48. Varela, I. *et al.* Exome sequencing identifies frequent mutation of the SWI/SNF complex gene PBRM1 in renal carcinoma. *Nature* **469,** 539–542. ISSN: 1476-4687 (2011).

49. Thompson, M. Polybromo-1: The chromatin targeting subunit of the PBAF complex. *Biochimie* **91,** 309–319. ISSN: 0300-9084 (2009).

50. Zhong, L. & Holmgren, A. Essential role of selenium in the catalytic activities of mammalian thioredoxin reductase revealed by characterization of recombinant enzymes with selenocysteine mutations. *Journal of Biological Chemistry* **275,** 18121–18128. ISSN: 00219258 (2000).

51. Fan, C. *et al.* Enhancement of auranofin-induced lung cancer cell apoptosis by selenocystine, a natural inhibitor of TrxR1 in vitro and in vivo. *Cell Death & Disease* **5,** 1–11. ISSN: 2041-4889 (2014).

52. Senga, T. *et al.* PCNA is a cofactor for CDT1 degradation by CUL4/DDB1-mediated N-terminal ubiquitination. *Journal of Biological Chemistry* **281,** 6246–6252. ISSN: 00219258 (2006).

53. Wertz, I. E. *et al.* Human De-Etiolated-1 regulates c-Jun by assembling a CUL4A Ubiquitin ligase. *Science* **303,** 1371–1374 (2004).

54. Conseil, G., Deeley, R. G. & Cole, S. P. Functional importance of three basic residues clustered at the cytosolic interface of transmembrane helix 15 in the multidrug and organic anion transporter MRP1 (ABCC1). *Journal of Biological Chemistry* **281,** 43–50. ISSN: 1083351X (2006).

55. Hogan, B., Fellous, M., Jacob, F. & Avner, P. Isolation of a human teratoma cell line which expresses F9 antigen. *Nature* **270,** 515–518. ISSN: 0028-0836 (1977).

56. Usanova, S. *et al.* Cisplatin sensitivity of testis tumour cells is due to deficiency in interstrand-crosslink repair and low ERCC1-XPF expression. *Molecular Cancer* **9,** 1–11. ISSN: 14764598 (2010).

57. Drexler, H. G. & Matsuo, Y. Malignant hematopoietic cell lines: In vitro models for the study of multiple myeloma and plasma cell leukemia. *Leukemia Research* **24,** 681–703. ISSN: 0145-2126 (2000).

58. Duperray, C. *et al.* Phenotypic analysis of human myeloma cell lines. *Blood* **73,** 566–572. ISSN: 0006-4971 (1989).

59. Collins, S. J. The HL-60 promyelocytic leukemia cell line: Proliferation, differentiation, and cellular oncogene expression. *Blood* **70,** 1233–1244. ISSN: 0006-4971 (1987).

60. Dalton, W. J. *et al.* HL-60 cell line was derived from a patient with FAB-M2 and not FAB-M3. *Blood* **71,** 242–247. ISSN: 0006-4971 (1988).

61. Newburger, P. E., Baker, R. D., Hansen, S. L., Duncan, R. A. & Greenberger, J. S. Functionally deficient differentiation of HL-60 promyelocytic leukemia cells induced by Phorbol Myristate Acetate. *Cancer Research* **41,** 1861–1865 (1981).

62. Rovera, G., Santoli, D. & Damsky, C. Human promyelocytic leukemia cells in culture differentiate into macrophage-like cells when treated with a phorbol diester. *Proceedings of the National Academy of Sciences of the United States of America* **76,** 2779–2783. ISSN: 00278424 (1979).

63. Zhang, Y., Fonslow, B. R., Shan, B., Baek, M. C. & Yates, J. R. Protein analysis by shotgun/bottom-up proteomics. *Chemical Reviews* **113,** 2343–2394. ISSN: 00092665 (2013).

64. Conesa, A. & Beck, S. Making multi-omics data accessible to researchers. *Scientific Data* **6,** 1–4. ISSN: 2052-4463 (2019).

65. Zubarev, R. A. The challenge of the proteome dynamic range and its implications for in-depth proteomics. *Proteomics* **13,** 723–726. ISSN: 1615-9861 (2013).

66. Bantscheff, M., Schirle, M., Sweetman, G., Rick, J. & Kuster, B. Quantitative mass spectrometry in proteomics: a critical review. *Analytical and Bioanalytical Chemistry* **389,** 1017–1031. ISSN: 1618-2650 (2007).

67. Ferna, C. *et al.* Impact of the identification strategy on the reproducibility of the DDA and DIA results. *Journal of Proteome Research* **19,** 3153–3161 (2020).

68. Guo, J. & Huan, T. Comparison of full-scan, data-dependent, and data-independent acquisition modes in liquid chromatographymass spectrometry based untargeted metabolomics. *Analytical Chemistry* **92,** 8072–8080 (2020).

69. Cox, J. *et al.* Accurate proteome-wide label-free quantification by delayed normalization and maximal peptide ratio extraction, termed MaxLFQ. *Molecular and Cellular Proteomics* **13,** 2513–2526. ISSN: 15359484 (2014).

70. Aebersold, R. & Mann, M. Mass spectrometry-based proteomics. *Nature* **422,** 198–207. ISSN: 1476-4687 (2003).

71. Karas, M., Bahr, U. & Dülcks, T. Nano-electrospray ionization mass spectrometry: Addressing analytical problems beyond routine. *Fresenius' Journal of Analytical Chemistry* **366,** 669–676. ISSN: 09370633 (2000).

72. Meier, F. *et al.* Parallel accumulation-serial fragmentation (PASEF): Multiplying sequencing speed and sensitivity by synchronized scans in a trapped ion mobility device. *Journal of Proteome Research* **14,** 5378–5387. ISSN: 15353907 (2015).

73. Meier, F. *et al.* Online parallel accumulation–serial fragmentation (PASEF) with a novel trapped ion mobility mass spectrometer. *Molecular and Cellular Proteomics* **17,** 2534–2545. ISSN: 15359484 (2018).

74. Meier, F., Park, M. A. & Mann, M. Trapped ion mobility spectrometry and parallel accumulation–serial fragmentation in proteomics. *Molecular and Cellular Proteomics* **20,** 1–13. ISSN: 15359484 (2021).

75. Mitulović, G. & Mechtler, K. HPLC techniques for proteomics analysis-a short overview of latest developments. *Briefings in Functional Genomics* **5,** 249–260. ISSN: 2041-2649 (2006).

76. Roberg-Larsen, H., Wilson, S. R. & Lundanes, E. Recent advances in on-line upfront devices for sensitive bioanalytical nano LC methods. *Trends in Analytical Chemistry* **136,** 1–10. ISSN: 0165-9936 (2021).

77. Shan, L. & Jones, B. R. Nano-LC: An updated review. *Biomedical Chromatography* **36,** 1–21. ISSN: 1099-0801 (2022).

78. Boehringer Ingelheim. *opnMe.com Boehringer Ingelheim open innovation portal* 2017. `https://www.opnme.com/`.

79. Mosmann, T. Rapid colorimetric assay for cellular growth and survival: application to proliferation and cytotoxicity assays. *Journal of Immunological Methods* **65,** 55–63. ISSN: 0022-1759 (1983).

80. Stockert, J. C., Horobin, R. W., Colombo, L. L. & Blázquez-Castro, A. Tetrazolium salts and formazan products in cell biology: Viability assessment, fluorescence imaging, and labeling perspectives. *Acta Histochemica* **120,** 159–167. ISSN: 16180372 (2018).

81. Smith, P. K. *et al.* Measurement of protein using bicinchoninic acid. *Analytical Biochemistry* **150,** 76–85. ISSN: 0003-2697 (1985).

82. Cox, J. & Mann, M. MaxQuant enables high peptide identification rates, individualized p.p.b.-range mass accuracies and proteome-wide protein quantification. *Nature Biotechnology* **26,** 1367–1372. ISSN: 1546-1696 (2008).

83. Tyanova, S. *et al.* The Perseus computational platform for comprehensive analysis of (prote)omics data. *Nature Methods* **13,** 731–740. ISSN: 1548-7105 (2016).

84. Mckinney, W. *Data structures for statistical computing in Python* in *Proceedings of the 9th Python in Science Conference* (2010), 56–61.

85. Hunter, J. D. Matplotlib: A 2D graphics environment. *Computing in Science and Engineering* **9,** 90–95. ISSN: 15219615 (2007).

86. Waskom, M. L. seaborn: Statistical data visualization. *Journal of Open Source Software* **6,** 1–4. ISSN: 2475-9066 (2021).

87. Meier-Menches, S. M. *et al.* A proteomic platform enables to test for AML normalization in vitro. *Frontiers in Chemistry* **10,** 1–12. ISSN: 22962646 (2022).

88. Marine, J. C. & Lozano, G. Mdm2-mediated ubiquitylation: p53 and beyond. *Cell Death & Differentiation* **17,** 93–102. ISSN: 1476-5403 (2009).

8 Appendix

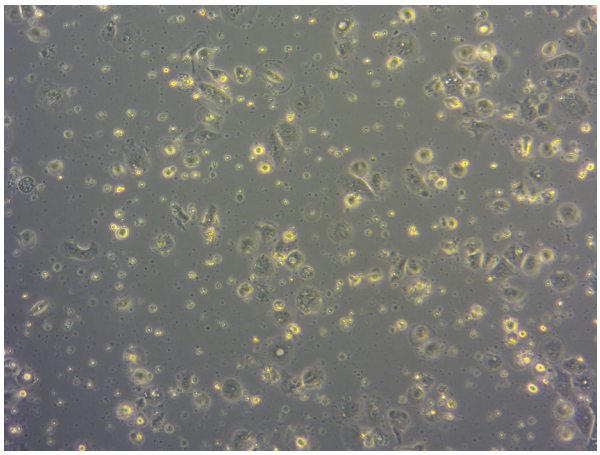

(a) PMA differentiated HL-60 cells after 72 hours of differentiation and 24 hours of incubation with DMSO as solvent control condition. 10x magnification

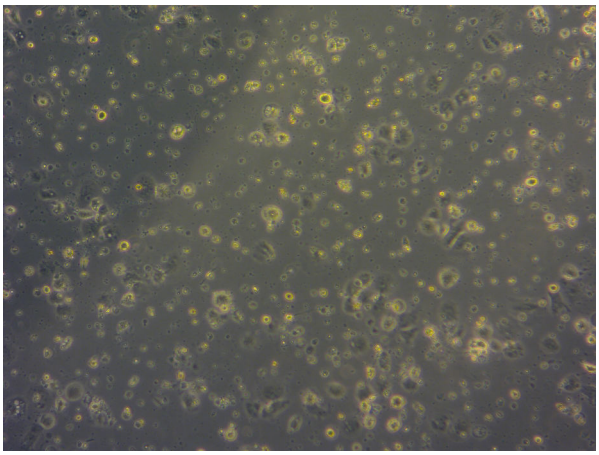

(b) PMA differentiated HL-60 cells after 72 hours of differentiation and 24 hours of incubation with 10 µM CHX and 1 nM ACBI2 PROTAC. 10x magnification

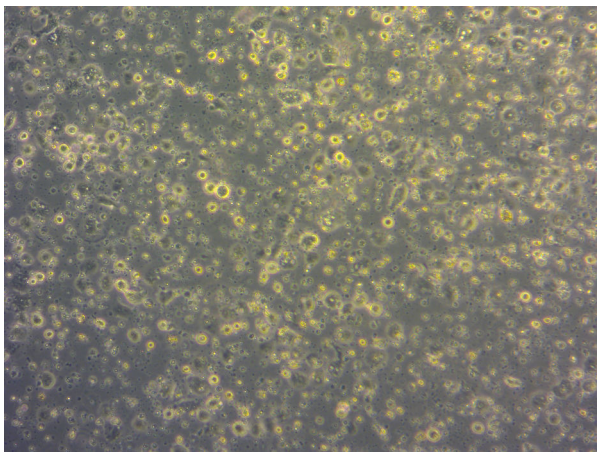

(c) PMA differentiated HL-60 cells after 72 hours of differentiation and 24 hours of incubation with 10 µM CHX and 60 µM Gold PROTAC. 10x magnification

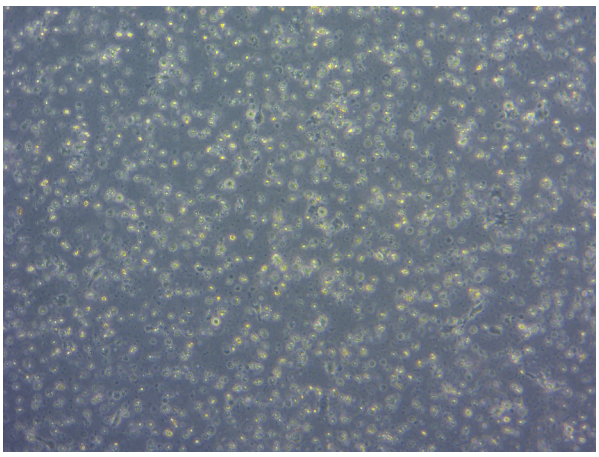

(d) PMA differentiated HL-60 cells in BONCAT medium after a 72 hour differentiation timeframe. 10x magnification

Figure 41: Snapshots of different conditions after completion of the continuous confluence tracking by means of the Cellwatcher module.

Table 18: Half-lives of protein IDs shared between the CON and CHX conditions ranked by decreasing half-life difference. The half-life difference was calculated by subtracting CHX half-lives from the corresponding counterpart in the CON condition. (CON - CHX)

	Half-lives [h]	
Protein	CON	CHX
NOB1	16.47	11.07
CASS4	18.39	11.00
RPS27L	17.31	12.98
BYSL	9.36	12.09
RPS27	13.27	11.88
CLTA	7.49	10.52

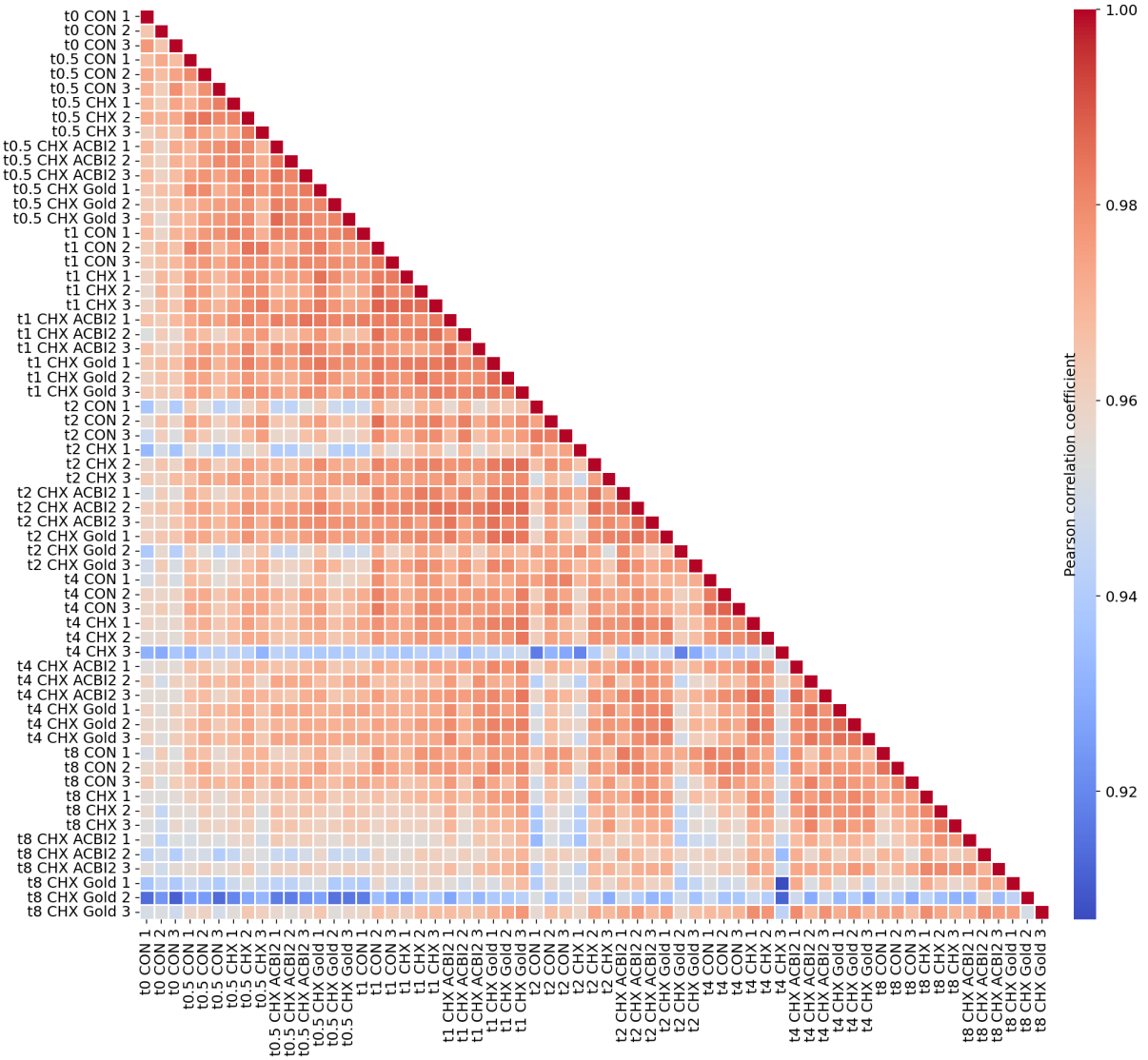

Figure 42: Correlation heatmap of the timeseries dataset. Proteins included in the data matrix for similarity calculation needed to be present in at least 70% of all samples.

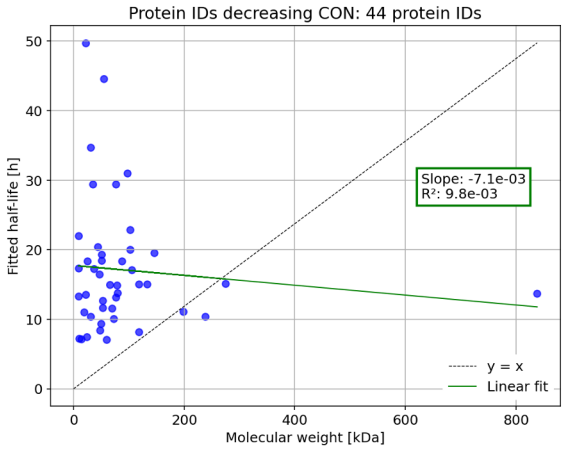

(a) Half-life vs. molecular weight scatter plot for protein IDs with steadily decreasing PFR values in the CON condition.

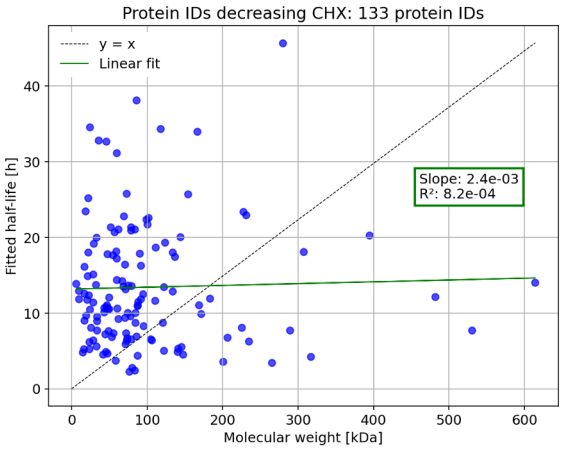

(b) Half-life vs. molecular weight scatter plot for protein IDs with steadily decreasing PFR values in the CHX condition.

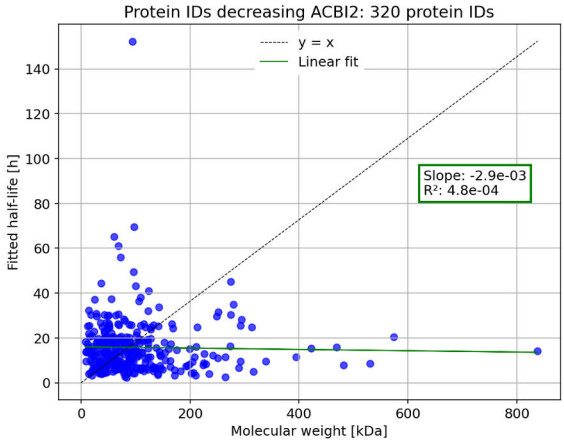

(c) Half-life vs. molecular weight scatter plot for protein IDs with steadily decreasing PFR values in the CHX + ACBI2 PROTAC condition.

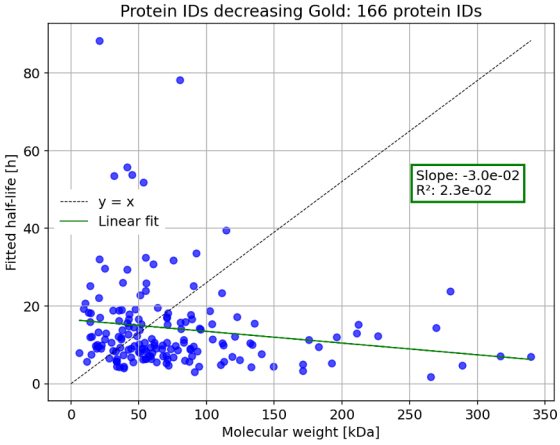

(d) Half-life vs. molecular weight scatter plot for protein IDs with steadily decreasing PFR values in the CHX + gold PROTAC condition.

Figure 43: Scatter plots showing the lack of correlation between the fitted half-lives of the protein IDs and their reported molecular weight in the different experimental conditions. Exclusively protein IDs with steadily decreasing PFR values over the course of all experimental timepoints were used for the corresponding conditions.

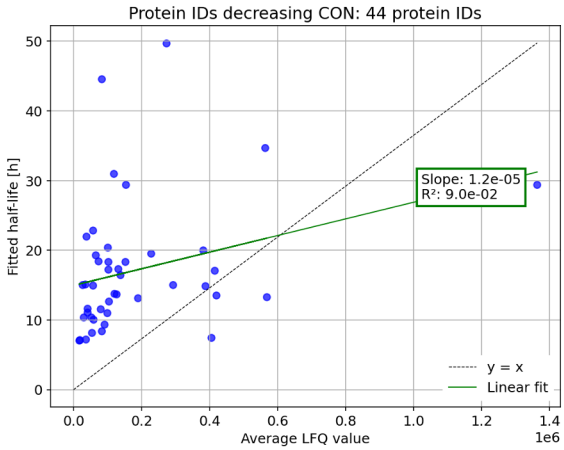

(a) Half-life vs. average LFQ value scatter plot for protein IDs with steadily decreasing PFR values in the CON condition.

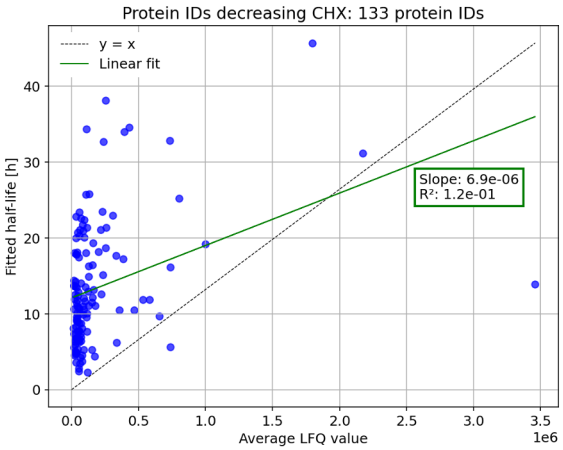

(b) Half-life vs. average LFQ value scatter plot for protein IDs with steadily decreasing PFR values in the CHX condition.

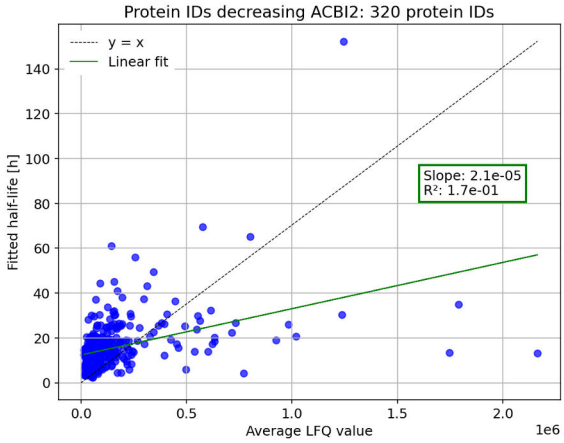

(c) Half-life vs. average LFQ value scatter plot for protein IDs with steadily decreasing PFR values in the CHX + ACBI2 PROTAC condition.

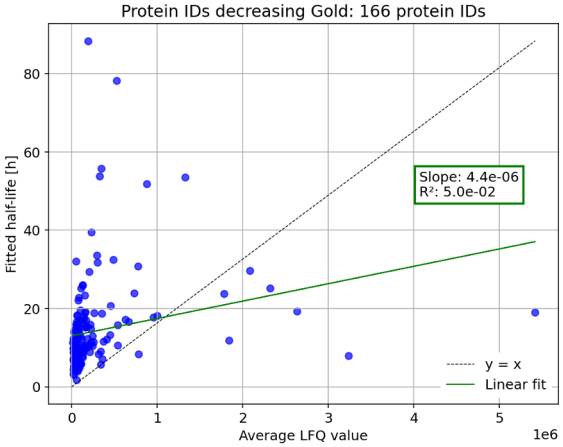

(d) Half-life vs. average LFQ value scatter plot for protein IDs with steadily decreasing PFR values in the CHX + gold PROTAC condition.

Figure 44: Scatter plots showing the lack of correlation between the fitted half-lives of the protein IDs and their average LFQ values in the different experimental conditions. The average LFQ values were calculated by averaging the LFQ values of each protein ID over all timepoints and replicates. Exclusively protein IDs with steadily decreasing PFR values over the course of all timepoints were used for the corresponding conditions.

Table 19: Half-lives of protein IDs shared between the CHX and CHX + ACBI2 PROTAC conditions ranked by decreasing half-life difference. The half-life difference was calculated by subtracting CHX + ACBI2 PROTAC half-lives from the corresponding counterpart in the CHX condition. ((CHX) - (CHX + ACBI2 PROTAC))

(a) Shared protein IDs half-lives ranked by decreasing half-life differences. Part 1

	Half-lives [h]	
Protein	CHX	CHX+ACBI2
SDHA	25.79	9.50
THUMPD3	20.67	8.00
NUP153	25.69	13.39
FLNA	45.68	34.89
XPO5	17.45	6.73
UBA6	34.34	24.75
EXOC1	22.56	12.99
UTRN	20.30	11.44
EIF3A	33.99	26.20
UNC13D	19.32	11.58
CTR9	12.89	6.47
RASAL2	20.04	13.90
PPP2CA	32.80	26.80
PPFIBP1	11.66	5.92
CASS4	11.00	5.33
ARHGEF2	18.69	13.72
HUWE1	12.13	7.82
ZCCHC6	9.88	5.67
CDK4	8.93	4.76
SMOX	21.07	17.39
CLCC1	9.27	5.72
BYSL	12.09	8.80
ADAM10	10.03	6.84
PHAX	7.23	4.52
GBF1	6.78	4.48
MYOF	6.25	3.98
CASP4	10.70	8.49

(b) Shared protein IDs half-lives ranked by decreasing half-life differences. Part 2

	Half-lives [h]	
Protein	CHX	CHX+ACBI2
MKRN2	17.81	15.96
STAG2	5.31	3.59
IVNS1ABP	7.37	6.09
HMOX1	5.59	4.35
SEC63	11.53	10.30
HECTD1	7.74	6.63
MTPAP	6.55	5.47
NOTCH2	3.46	2.46
POLR2I	4.84	4.06
LONRF2	2.42	2.20
NUMB	16.42	16.31
SUN2	2.77	2.70
ITGB7	4.36	4.51
SDF4	4.54	4.71
MLF2	6.45	6.82
CEP85	6.96	7.37
CKAP5	8.11	8.84
PRRC2C	4.22	5.00
BIRC6	7.72	8.62
TXNL4B	9.02	10.06
STARD4	5.25	6.42
CTTN	13.17	14.54
RPS27	11.88	13.88
PTPN22	11.85	13.92
MTX1	21.35	24.57
PHLDA1	4.91	8.24
AGPAT9	7.64	12.07
SNRPA1	15.13	30.95

Table 20: Half-lives of protein IDs shared between the CHX and CHX + gold PROTAC conditions ranked by decreasing half-life difference. The half-life difference was calculated by subtracting CHX + gold PROTAC half-lives from the corresponding counterpart in the CHX condition. ((CHX) - (CHX + gold PROTAC))

	Half-lives [h]	
Protein	CHX	CHX+gold
FLNA	45.68	23.82
PIGR	21.05	10.54
LTV1	17.65	8.40
ARHGEF2	18.69	10.41
NCAM1	12.52	4.39
POLR2B	18.02	10.09
PPFIBP1	11.66	4.84
MT1X	13.92	7.96
NUMB	16.42	10.65
PPM1G	17.20	11.62
SPAST	14.22	8.96
ECE1	11.01	5.76
ZCCHC6	9.88	4.95
CDK4	8.93	4.37
ADAM10	10.03	6.00
NOSIP	9.55	5.88
SEC63	11.53	8.73
IVNS1ABP	7.37	4.70
NXF1	9.40	7.28
NOTCH2	3.46	1.81
PHAX	7.23	6.77
MTPAP	6.55	8.63
CTTN	13.17	15.30
DHX38	4.89	7.66
HMOX1	5.59	8.36
PRRC2C	4.22	7.16
CEBPZ	8.75	12.14

Table 21: Half-lives of protein IDs shared between the CHX + ACBI2 PROTAC and CHX + gold PROTAC conditions ranked by decreasing half-life difference. The half-life difference was calculated by subtracting CHX + gold PROTAC half-lives from the corresponding counterpart in the CHX + ACBI2 PROTAC condition. ((CHX + ACBI2 PROTAC) - (CHX + gold PROTAC))

(a) Shared protein IDs half-lives ranked by decreasing half-life differences. Part 1

	Half-lives [h]	
Protein	CHX+ACBI2	CHX+gold
EHD1	65.13	30.82
PTPRE	27.72	15.84
FLNA	34.89	23.82
MUT	20.39	11.24
ADO	18.68	10.54
ITGB1	25.94	17.81
GABARAPL1	21.94	15.96
EIF3M	22.50	16.64
NUMB	16.31	10.65
MAPKAPK3	23.05	17.86
CNP	24.05	19.18
AAMP	13.85	9.79
SAFB	22.68	18.72
GTF2I	13.34	9.87
PLXNC1	14.77	11.32
ARHGEF2	13.72	10.41
PLXNA1	16.02	13.01
PAPSS1	20.09	17.23
RTFDC1	8.53	5.68
NRBP1	10.74	7.94
FRYL	9.63	6.89
SMG9	9.72	7.21
PPP2R2A	17.87	15.39
PPP3R1	12.53	10.07
WAPAL	6.63	4.23
PARP4	7.47	5.23
CDC123	6.61	4.43
TBRG4	19.04	16.90
RGS14	12.60	10.54
FMNL1	19.16	17.13

(b) Shared protein IDs half-lives ranked by decreasing half-life differences. Part 2

	Half-lives [h]	
Protein	CHX+ACBI2	CHX+gold
OGFOD1	7.32	5.49
SGK223	6.01	4.40
SEC63	10.30	8.73
FAM43A	7.04	5.54
IVNS1ABP	6.09	4.70
ADAM17	9.70	8.34
ENO1	13.29	11.93
PPFIBP1	5.92	4.84
CTTNBP2NL	6.21	5.33
ADAM10	6.84	6.00
ZCCHC6	5.67	4.95
ZNF622	9.63	8.91
NOTCH2	2.46	1.81
SMCHD1	12.84	12.35
CDK4	4.76	4.37
DNAJB6	4.51	4.28
CTDP1	11.66	11.46
AQR	3.29	3.34
ATP6AP2	3.91	3.97
RBM27	6.33	7.01
CTTN	14.54	15.30
USP3	4.89	6.43
PRRC2C	5.00	7.16
PHAX	4.52	6.77
MTPAP	5.47	8.63
HMOX1	4.35	8.36
GCC2	7.72	11.98
STRIP1	4.25	13.99
UBAP2L	18.65	39.49

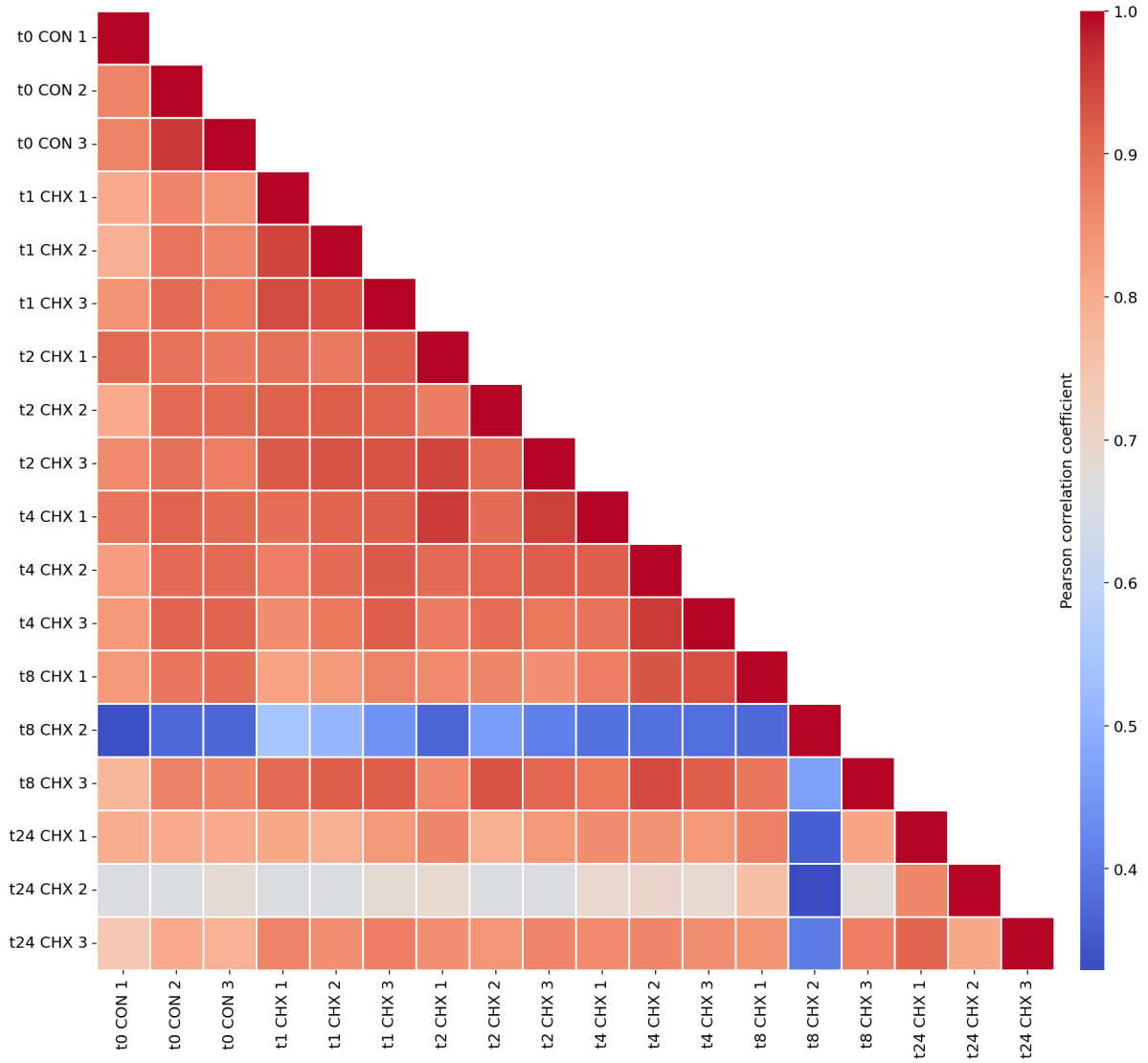

Figure 45: Correlation heatmap of the BONCAT CHX timeseries experiment. Proteins included for the correlation coefficient calculation required to be present in at least one sample in total. The t_{8h} CHX 2 sample, which shows extremely low similarity to all other samples exhibited a significantly higher total ion chromatogram than all other samples.

Table 22: Protein IDs rescued by the four hour Bortezomib incubation prior to the four hour ACBI2 PROTAC treatment compared to the corresponding four hour timepoint in the timeseries experiment. Average LFQ values of the triplicates at the 4h timepoint in the two conditions as well as the absolute LFQ difference are shown in the table. The achieved LFQ value increase with the Bortezomib rescue is also reported in percent for the different proteins. Proteins with at least a 50% LFQ value increase in the Bortezomib rescue experiment compared to the ACBI2 timeseries are found to be in the table. Hence only 23 protein IDs out of the 106 IDs with a successful rescue are shown. Protein IDs highlighted in yellow were found to show robustly decreasing LFQ values between the $t_{0.5h}$ to t_{4h} timepoints in the CHX condition of the timeseries experiment. Their rescue is therefore probably due to the absence of CHX in the rescue experiment and not the inhibition of the proteasome with Bortezomib.

Protein ID	Average LFQ ACBI2 rescue	Average LFQ ACBI2 timeseries	LFQ difference (Rescue - Timeseries Exp.)	LFQ increase compared to timeseries experiment [%]
APLP2	3.12E+05	1.75E+04	2.95E+05	1689.82
HMOX1	4.37E+06	6.05E+05	3.77E+06	622.04
MLF2	2.06E+05	3.48E+04	1.72E+05	493.31
BCL2A1	7.08E+04	1.74E+04	5.34E+04	306.5
MMP9	6.65E+05	1.75E+05	4.89E+05	279.63
STARD4	2.60E+05	7.36E+04	1.87E+05	253.54
BAG3	2.48E+05	7.57E+04	1.72E+05	227.85
PHLDA1	7.22E+04	2.78E+04	4.44E+04	159.72
SUN2	8.60E+04	3.46E+04	5.14E+04	148.35
FNDC3B	8.43E+04	3.47E+04	4.96E+04	142.93
SCOC	8.97E+04	4.12E+04	4.85E+04	117.87
RTFDC1	1.54E+05	7.39E+04	7.97E+04	107.92
GTF2E1	6.22E+04	3.01E+04	3.21E+04	106.54
IVNS1ABP	1.08E+05	5.44E+04	5.37E+04	98.74
SDF4	1.15E+05	6.25E+04	5.21E+04	83.44
TNIP1	1.30E+05	7.43E+04	5.54E+04	74.5
SERPINA1	2.98E+05	1.71E+05	1.27E+05	74.28
CASS4	1.24E+05	7.17E+04	5.21E+04	72.7
NRP1	2.37E+05	1.41E+05	9.61E+04	68.1
ADAM9	1.92E+04	1.16E+04	7.59E+03	65.31
NDRG1	2.14E+05	1.37E+05	7.63E+04	55.52
MKL2	3.22E+04	2.12E+04	1.10E+04	51.69
MKRN2	4.83E+04	3.22E+04	1.61E+04	50.11

Table 23: Protein IDs rescued by the four hour Bortezomib incubation prior to the four hour Gold PROTAC treatment compared to the corresponding four hour timepoint in the timeseries experiment. Average LFQ values of the triplicates at the 4h timepoint in the two conditions as well as the absolute LFQ difference are shown in the table. The achieved LFQ value increase with the Bortezomib rescue is also reported in percent for the different proteins. Proteins with at least a 50% LFQ value increase in the Bortezomib rescue experiment compared to the Gold timeseries are found to be in the table. Hence only 20 protein IDs out of the 61 IDs with a successful rescue are shown. Highlighted IDs were shown to have robustly decreasing LFQ values between the $t_{0.5h}$ to t_{4h} timepoints in the CHX condition of the timeseries experiment. Hence, the rescue is probably due to the absence of CHX in the rescue experiment and not the inhibition of the proteasome with Bortezomib.

Protein ID	Average LFQ Gold rescue	Average LFQ Gold timeseries	LFQ difference (Rescue - Timeseries Exp.)	LFQ increase compared to timeseries experiment [%]
ATP6AP2	3.03E+05	3.86E+04	2.64E+05	684.72
HMOX1	4.78E+06	6.47E+05	4.14E+06	639.4
TIMP1	7.53E+05	1.68E+05	5.85E+05	347.86
BCL2A1	7.30E+04	1.77E+04	5.53E+04	313.25
CHI3L1	6.45E+05	1.97E+05	4.47E+05	226.55
UTP3	6.81E+04	2.70E+04	4.11E+04	152.1
ATP6AP1	7.27E+04	3.00E+04	4.28E+04	142.57
RTFDC1	1.70E+05	7.33E+04	9.64E+04	131.61
SCOC	9.23E+04	4.22E+04	5.01E+04	118.81
IVNS1ABP	1.20E+05	6.03E+04	5.95E+04	98.76
USP47	1.59E+04	8.21E+03	7.72E+03	94.06
EYA3	6.18E+04	3.30E+04	2.87E+04	86.98
NCAM1	4.03E+04	2.20E+04	1.83E+04	83.25
LTV1	5.40E+05	3.01E+05	2.39E+05	79.37
SERPINA1	2.89E+05	1.62E+05	1.27E+05	78.05
PPP1R8	5.93E+04	3.34E+04	2.59E+04	77.69
EMR2	1.80E+05	1.09E+05	7.14E+04	65.81
ADAM10	1.59E+05	9.96E+04	5.92E+04	59.51
G3BP2	8.07E+05	5.19E+05	2.88E+05	55.58
ECE1	5.55E+04	3.66E+04	1.89E+04	51.75

Table 24: List of overlapping protein IDs between the proteins rescued by Bortezomib in the two separate rescue experiments and the protein IDs showing a robust LFQ value decrease in the timeseries CHX condition.

ACBI2 PROTAC rescue CHX decrease pattern		Gold PROTAC rescue CHX decrease pattern	
$t_{0.5h}$ to t_{4h}	$t_{0.5h}$ to t_{8h}	$t_{0.5h}$ to t_{4h}	$t_{0.5h}$ to t_{8h}
HMOX1	HMOX1	HMOX1	HMOX1
MLF2	MLF2	TIMP1	TIMP1
MMP9	STARD4	CHI3L1	IVNS1ABP
STARD4	PHLDA1	UTP3	NCAM1
BAG3	SUN2	SCOC	LTV1
PHLDA1	IVNS1ABP	IVNS1ABP	ADAM10
SUN2	SDF4	NCAM1	ECE1
SCOC	CASS4	LTV1	POLR2B
IVNS1ABP	MKRN2	SERPINA1	CEBPZ
SDF4	NUMB	ADAM10	NUMB
SERPINA1	ECE1	G3BP2	MT1X
CASS4	ADAM10	ECE1	
MKRN2	HECTD1	NDUFV1	
NUMB	AGPAT9	POLR2B	
ECE1	GBF1	CEBPZ	
ADAM10	EXOC1	SNX17	
HECTD1	NUP153	NUMB	
AGPAT9	CKAP5	NOL11	
SLC30A9	FSD1L	BAG5	
GBF1	MTX1	MT1X	
TNRC6B	MACF1	NDUFB7	
EXOC1	HUWE1	EEF1B2	
DHX29	BYSL	EIF3M	
NDUFV1	EIF3A		
NUP153			
TMX4			
YTHDF1			
CKAP5			
PPP1R12A			
FSD1L			
SLC4A7			
PFDN2			
MTX1			
SEH1L			
MACF1			
ICAM3			
HUWE1			
BYSL			
EIF3A			
AP3M1			